SUB-GAP ABSORPTION AND POTENTIAL FLUCTUATIONS IN HYDROGENATED AMORPHOUS SILICON AND ITS ALLOYS

A Thesis Submitted
in Partial Fulfilment of the Requirements
for the degree of
DOCTOR OF PHILOSOPHY

By
ANIL KUMAR SINHA

to the
DEPARTMENT OF PHYSICS
INDIAN INSTITUTE OF TECHNOLOGY, KANPUR
MAY, 1998

CERTIFICATE

It is certified that the work contained in the thesis entitled "*Sub-gap absorption and potential fluctuations in hydrogenated amorphous silicon and its alloys*", by Shri Anil Kumar Sinha, has been carried out under my supervision and that this work has not been submitted elsewhere for a degree.

(S.C. Agarwal)
Professor
Department of Physics
I. I. T. Kanpur

May, 1998.

Synopsis

Hydrogenated amorphous silicon(a-Si:H) is the most widely studied material amor
disordered semiconductors. a-Si:H thin films made by the glow discharge of silane(
have a low ($10^{15} - 10^{16} cm^{-3} eV^{-1}$) density of localised states(DOS) at the Fermi
This allows the material to be doped n-type or p-type at will. This is usually dor
mixing SiH_4 with phosphine(for n-type) or diborane(for p-type) during the prepar
by glow discharge. a-Si:H can also be doped interstitially by in diffusion of lith
Thus, the material finds use in many devices like photovoltaic cells, photoconduc
thin film transistors etc.

DOS in the mobility gap of the bulk of a-Si:H is the most significant param
that decides its suitability for device applications. Also, the density of surface state
important. Various experiments like field effect, thermally stimulated currents, ca
citance, deep level transient spectroscopy, space charge limited currents and sub
absorption etc have been used for the determination of DOS in a-Si:H. Each meth
has its advantages and limitations. Optical absorption in the sub gap region[$\alpha(h\nu)$] h
been used for the determination of bulk states with the advantage that the informati
about the shallow as well as the deep states can be obtained.

Two techniques, namely, constant photocurrent measurements(CPM) and phot
thermal deflection spectroscopy(PDS) are used to measure the sub gap absorption
a-Si:H. One generally finds, however, that the two techniques yield different values
$\alpha(h\nu)$, on the same sample. This is expected, since CPM is a photocurrent measur
ment and is not sensitive to the surface states. In a-Si:H, the surface states are lar
in number and the carriers generated in the surface region recombine quickly witho
contributing to the photocurrent. In addition, some of the bulk states may also nc

contribute to CPM if the transitions they participate in, have localised states as the final states. On the other hand, PDS is a thermal effect and is sensitive to all the transitions involving the bulk as well as the surface states.

In the literature, the density of surface states has been obtained by measuring $\alpha(h\nu)$ on identical a-Si:H films of varying thicknesses, using PDS. However, making such samples is practically difficult and gives large uncertainty in the measured density of surface states.

In the present work, α measured by CPM and PDS on a given sample of given thickness is analysed to obtain the distribution and density of bulk states in the entire mobility gap as well as surface states. This method obviates the difficulties associated with the preparation of identical samples of varying thicknesses. In addition, the dual beam constant photocurrent measurements(DBCPM), are used to obtain the correlation energy between electrons. Further, using DBCPM we also obtain the shape of the mid-gap states, which is not possible using CPM or PDS. We have applied this technique of measuring the bulk and surface states in undoped a-Si:H and a-Si:H doped with various amounts of phosphorous(P). Our results are in qualitative agreement with the literature. We also report the measurements of $\alpha(h\nu)$ on lithium(Li) doped samples. This is interesting because Li is interstitial dopant in a-Si:H, unlike P which is substitutional. Since, the shape of the surface states in a-Si:H is not known, various shapes of surface states like a delta function, a rectangular and a Gaussian are tried. We find that the calculated density of surface states is not very sensitive to the shape chosen. Further, the density of bulk and surface states in P and Li doped a-Si:H are found to be similar.

For device fabrication, a-Si:H may be subjected to various surface treatments like oxidation, etching with hydrofluoric acid and exposure to various plasma. These may change the density of states in the bulk and at the surface. These changes can give useful information for device fabrication and have not been studied in detail, so far. We have measured changes in the density of bulk and surface states after various surface treatments, and light soaking using sub-gap absorption measurements. We find that light soaking(Staebler Wronski effect) is mainly a bulk effect and does not change the density of surface states much. Native oxide etching, using hydrofluoric acid, is found to increase the density of surface states, whereas, treatment with hydrogen plasma at

room temperature decreases the density of surface states. This might explain why treating a-Si:H with hydrogen plasma, in device fabrication, yields better results.

The potential fluctuations play an important role in determining the electronic properties of a-Si:H. Several experiments like NMR, show that hydrogen is distributed non-uniformly in a-Si:H. A non-uniform distribution of hydrogen is likely to give rise to potential fluctuations in a-Si:H. In addition, presence of charge centers, charged and neutral dangling bonds and the dopants, if present, may also contribute to them. Overhof and Beyer have used transport measurements(conductivity and thermopower) to obtain the width of these potential fluctuations in a-Si:H. We have estimated the width of potential fluctuations using sub-gap absorption measurements, on P doped a-Si:H. We find that the width of potential fluctuations increases with the increasing doping concentrations. In addition, we have also measured the width of long range potential fluctuations by transport measurements on the same samples, using the analysis of Overhof and Beyer. The width of the potential fluctuations, estimated using optical absorption measurements, is found to be about a factor of 20 more than that of the long range potential fluctuations, estimated using transport measurements. These results are explained qualitatively, by arguing that in transport measurements, carriers are likely to overlook the sharp fluctuations in the potential because of quantum mechanical tunneling of carriers, as these fluctuations are short ranged. On the other hand, sub gap absorption measurements are local processes and are likely to be sensitive to the short range potential fluctuations, which may have a larger width. We also explain qualitatively the difference in α measured by CPM and PDS using potential fluctuations.

Organisation of the thesis

The present thesis has seven Chapters. Chapter 1 gives a brief introduction to the sub gap absorption and the potential fluctuations in a-Si:H and the motivation behind the present work. The sample preparation, doping and initial characterisation of the films are given in Chapter 2. Details of the constant photocurrent measurement(CPM) and photothermal deflection spectroscopy(PDS) set ups are also contained in this Chapter.

In Chapter 3, we describe the determination of bulk density of states in the entire mobility gap using CPM and PDS measurements. The dual beam CPM results used to determine the shape of the mid gap states, are also discussed in this Chapter.

$\alpha(h\nu)$ measured by CPM and PDS have been used to determine the surface states in Chapter 4. Results on undoped a-Si:H and a-Si:H doped with varying phosphorous and lithium concentrations are also presented in this Chapter. Chapter 5 gives the results on the determination of density of surface states after various surface treatments. In Chapter 6, we explain the difference in $\alpha(h\nu)$ as measured by CPM and PDS, in terms of the potential fluctuations present in a-Si:H. The width of the potential fluctuations estimated by transport measurements is compared with those estimated by the optical absorption measurements. Finally, Chapter 7 summarises our results and lists the major conclusions of the thesis. Some unanswered questions and directions for further research are suggested.

ACKNOWLEDGMENTS

I am extremely grateful to Prof. S. C. Agarwal, my thesis supervisor, for his valuable guidance, inspiration and encouragement during all stages of the work reported in this thesis. I am also thankful to him for patiently going through this manuscript and for his suggestions during its preparation.

I thank Prof. V. A. singh for his keen interest and valuable suggestions through out this work. I am also grateful to him for his interest in my professional growth. I also thank Dr Y. N. Mohapatra for his suggestions and encouragements.

I take this opportunity to thank Dr. E. Bhattacharya of Department of Electrical Engineering, I. I. T. Madras and Dr. Satyendra Kumar of this department for their suggestions and help during the initial phase of this work.

I am indebted to Dr. R. Bhattacharya, Dr. P. N. Dixit and Dr. T. Seth of national Physical Laboratory, New Delhi, for providing with some of the samples used in this work.

Discussions with Prof. A. Mookerjee of Bose Institute, Calcutta was very fruitful and has helped in improving a part of the thesis considerably. His help and encouragement are acknowledged with gratitude.

It gives me great pleasure to acknowledge the contributions of my colleagues Dr. S. K. Tripathi, Dr. G. S. Narayana, Dr. Pratima Agarwal, Dr. P. K. Dwivedi, Dr. Santosh Kumar, Shri Alok Srivastava and Shri Dinesh Deva for their help, encouragement and suggestions. They have also made my stay in the campus pleasant.

Technical support from Dr. Ram Bilas and Mr. Rajendra Kumar are being acknowledged with pleasure. Help from the staff from Physics Workshop and Central Workshop, I. I. T. Kanpur, are acknowledged with pleasure. I also express my sincere thanks to the office staff of Physics department for their cooperation. I express my sincere thanks to shri A. K. Rajpal and shri P. S. Chauhan for their help in computer automation of the measurements.

Finally, I acknowledge the help and encouragement of my colleagues, Dr. R. V. Nandedkar, Dr G. S. Lodha, Dr. K. J. S. Sawhney, shri M. H. Modi, shri M. K. Tiwari and Miss Pragya Tripathi at Center for Advance Technology, Indore.

Finally, I express my sincere gratitude for my wife, Bharati, and my daughters, Shruti and Shrishti for their love and affection, which went a long way in smooth progress of this work.

Last but not the least, I would like to convey my sincere thanks to one and all who were helpful during my stay at IIT Kanpur.

To

My Parents

&
Parents in-law

Contents

List of Figures

List of Tables

Chapter 1

Introduction

Hydrogenated amorphous silicon (a-Si:H) is the most promising tetrahedrally bonded amorphous semiconductor, being used for many devices like photovoltaic cells [1], photoconductors, thin film transistors [2] and many more [3]. There are many proposed applications of the material [3] and therefore it is important to study and solve the persisting problems and issues.

The difference between the amorphous semiconductors and their crystalline counterpart is the lack of long range periodicity of atomic structure in the former. But the short range periodicity is preserved even in the amorphous semiconductors [4]. This results in a similar electronic structure like the band gap, as in the crystalline semiconductors. Thus, amorphous semiconductors have bands consisting of extended states separated by a mobility gap which may have localised states coming from disorder [5]. This disorder is the result of variation in the bond angle and the bond lengths. This results in the tailing of the band edges giving rise to the localised states in the tail region. This is known as the Anderson localisation [5]. In addition, amorphous semiconductors may also have coordination defects (like dangling bonds) resulting in some more localised states in the middle of the mobility gap. The density of localised states in the gap is usually large ($\approx 10^{20} cm^{-3}$) [6] in an amorphous semiconductor.

Because of the high density of localised states (DOS) near the Fermi level (E_F), the effect of doping in most amorphous semiconductors can not be observed, as their Fermi level is pinned. Spear and LeComber [7] discovered in 1972 that unlike other

amorphous semiconductors, a-Si:H prepared by the glow discharge of silane has a low density of localised states at E_F. Also, the dark conductivity can be changed by several orders of magnitude by gas phase doping either n type or p type [8,9]. It is believed that hydrogen in a-Si:H is crucial in achieving low density of states at E_F. Further studies revealed that hydrogen not only act as the bond terminators, reducing the density of dangling bond states, but also releases the strain in the network, reducing the bond length and bond angle fluctuations.

1.1 Bulk and Surface States

Presence of disorder and defects in a-Si:H give rise to the localised electronic states in the mobility gap. These states significantly affect the properties of the material. Also, doping changes the density, nature and the energy levels of these states. Therefore, the information about the localised states is of great importance.

The mobility gap in a-Si:H, contains a continuum of states. We get exponentially decreasing shallow states near the band edges, and deep states arising from the coordination defects. Fig. 1.1 shows the schematic of the standard model of bulk localised states in undoped a-Si:H, as proposed by Street et al [10]. Doping changes the distribution and density of gap states [11].

It increases the bond distortions and also increases the deep gap states. The nature and the position of the deep gap states also change. On n-type doping, the singly occupied neutral dangling bond states (D°) change to doubly occupied states D^-, and we get only one Gaussian peak for the deep states as compared to two peaks in the case of undoped a-Si:H [10].

Localised states in the band gap have been extensively studied by Luminescence [10], electron spin resonance [12], field effect measurements [13], thermally stimulated currents [14], space charge limited currents [15], capacitance techniques [16] and sub gap absorption measurements [17-20] etc. Sub-gap absorption is a fundamental process that measures the density and the energy position of all the states in the band gap, thus providing a convenient tool for DOS characterisation. However, certain assumptions are necessary to obtain information of DOS from the sub gap absorption data. The matrix

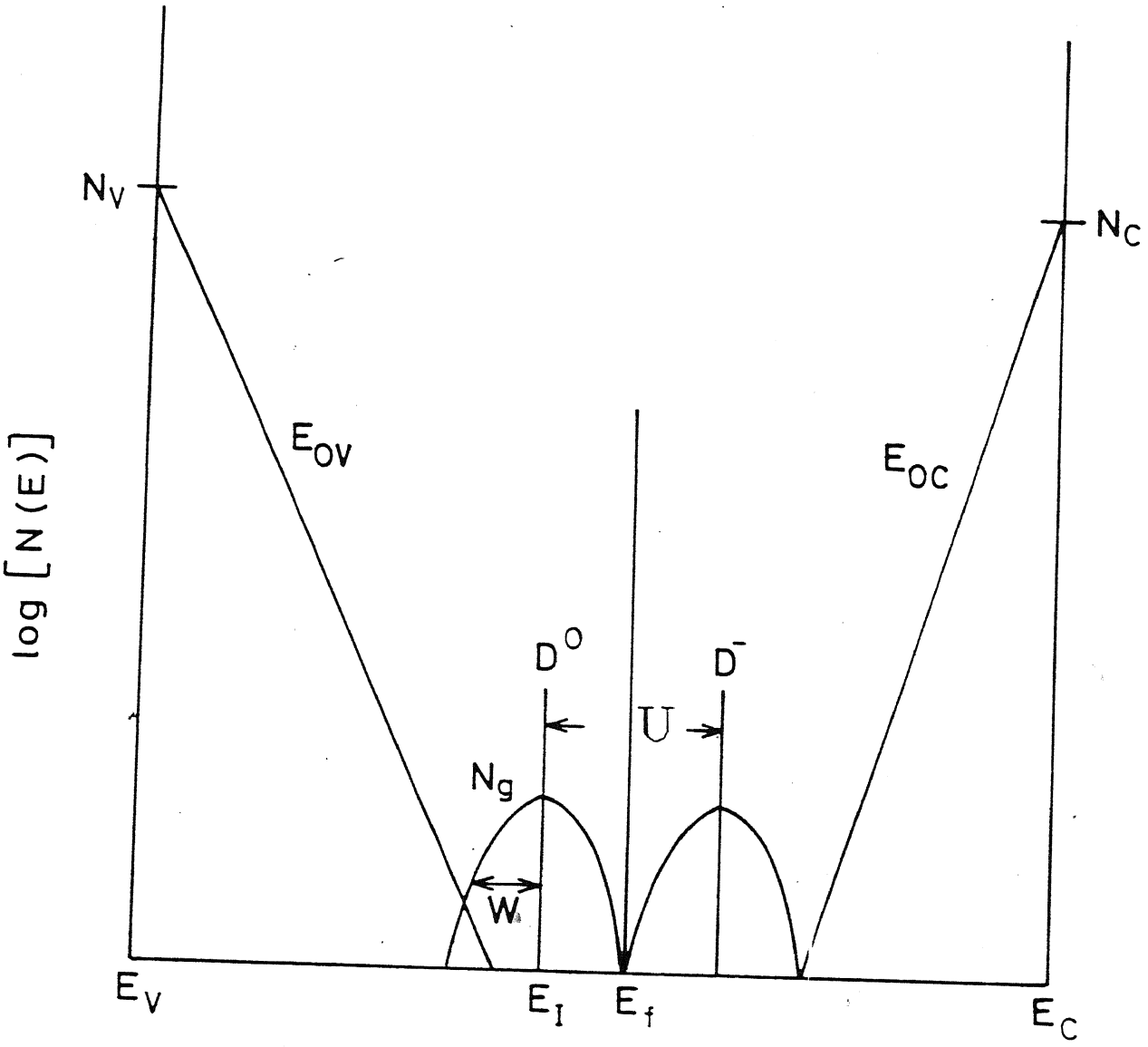

Figure 1.1: Bulk localised states consisting of exponential Urbach edges and Gaussian mid-gap states. E_v and E_c are band edges. E_F is the Fermi level. D^o and D^- are neutral and charged dangling bond states. U is the correlation energy [after reference 10].

elements of the optical transitions are not known. These are generally assumed to be independent of the photon energy, i.e. the matrix element for the transitions between the localised to the extended states are assumed to be the same as that from extended to extended states. Also, in order to get DOS from sub-gap absorption, the shape of the distribution of DOS has to be known, in advance, and has to be guessed. Various shapes of DOS have been suggested [10,21]. So far, the issue has not been resolved.

The smallest absorption coefficient (α) that can be measured comfortably using the conventional transmission and reflection techniques is 50-100 cm^{-1} for a 1 μm thick a-Si:H film. The α associated with the transitions involving the deep states in a-Si:H can be smaller by a factor of about 100. In an attempt to measure extremely small α, two techniques, namely, constant photocurrent measurement (CPM) [17,18] and photothermal deflection spectroscopy (PDS) [19,20] are employed. We describe the CPM and PDS set ups in Chapter 2.

$\alpha(h\nu)$ measured by the CPM and PDS on the same sample, are usually not equal, α_{pds} being larger than α_{cpm}. Fig. 1.2 illustrates this for an undoped a-Si:H sample (#18). The difference arises because CPM is not sensitive to the optical transitions involving a part of the bulk states and full surface states [22,23], whereas, PDS is sensitive to all the transitions.

We analyse $\alpha_{cpm}(h\nu)$ and $\alpha_{pds}(h\nu)$ data to get the bulk states in the entire mobility gap (Chapter 3), and surface states (Chapter 4), for undoped and doped a-Si:H. This method of measuring the density of surface states (N_s), has the advantage, that it needs only one sample. The usual method for measuring N_s needs a number of identical samples of varying thicknesses [22,24,25]. This is difficult to achieve practically.

In addition to phosphorous (P) incorporation, a-Si:H can also be doped n-type by the in-diffusion of lithium (Li). However, Li is interstitial donor [27], whereas, P is substitutional. Also, because Li doping is done at 100-150°C, the hydrogen concentration is likely to remain the same as in undoped a-Si:H. Therefore, one can study the effect of the dopant alone. It is interesting to compare the DOS in P doped a-Si:H [a-Si:H(P)] and Li doped a-Si:H [a-Si:H(Li)].

Also, it is worthwhile to see if some of the issues that remain unresolved for a-Si:H(P) remain unanswered for a-Si:H(Li) also. One such controversy is about the position of

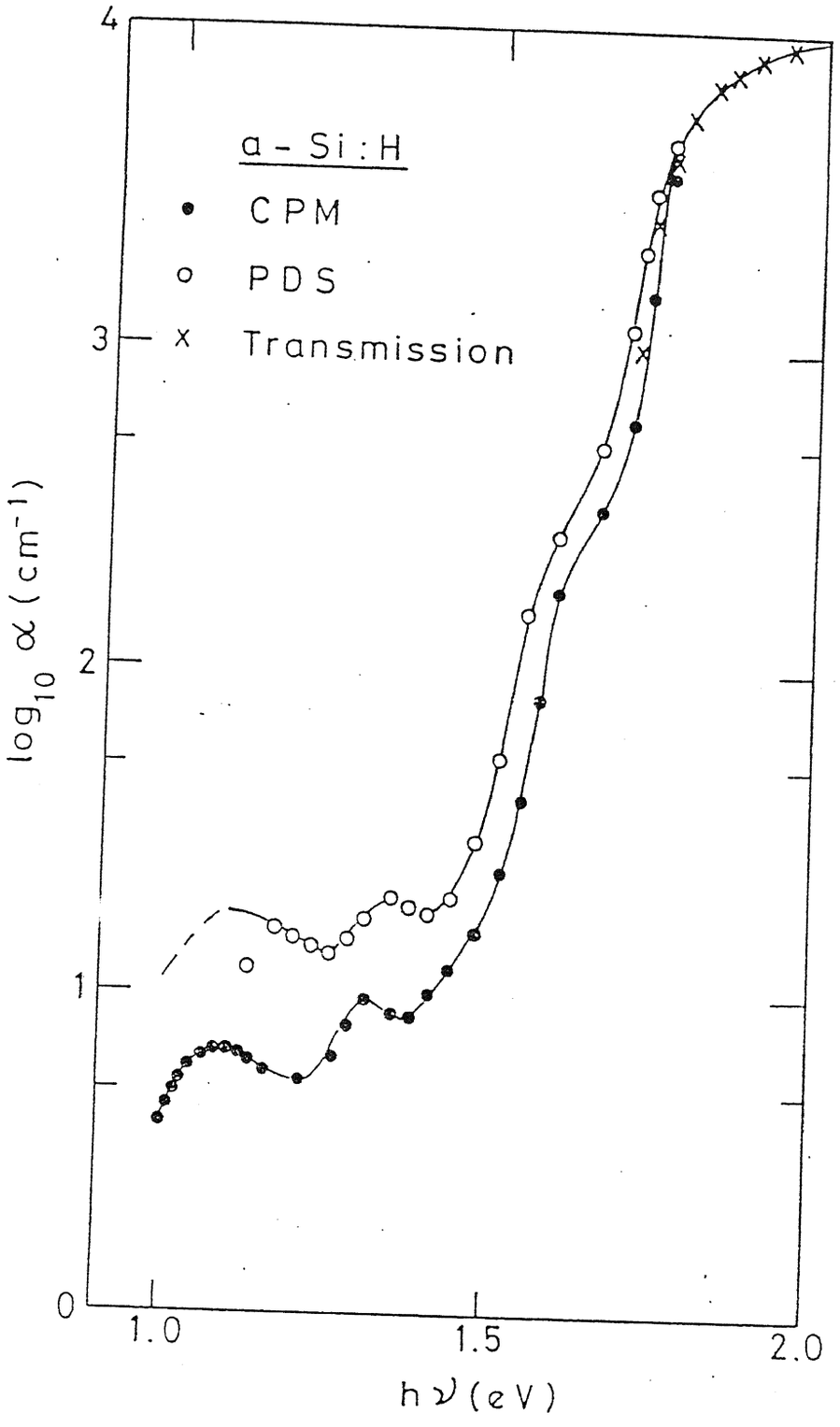

Figure 1.2: Sub-gap absorption coefficient measured as a function of photon energy ($h\nu$) using CPM (solid circle), PDS (open circles) and transmission (crosses) [after reference 21].

D^- in a-Si:H(P). Street et al [10] suggest that the position of D^- in undoped and in P doped a-Si:H are the same. This is called the "Basic Model". On the other hand, Kocka et al [27], based on sub-gap absorption measurements, suggest that on doping, the dangling bonds form intimate pair with the dopants, resulting in the shift of the energy position of D^- away from the conduction band edge. Now, Li may or may not form the intimate pair with dangling bonds. Therefore, it is interesting to study the position of dangling bond states in a-Si:H(Li).

In a-Si:H based device fabrication, a-Si:H has to undergo various surface treatments. It has been found that treatment with hydrogen plasma improves the quality of devices having a number of interfaces, like solar cells. A possible reason for this may be that the treatment decreases the number of surface states. However, in the literature the density of surface states have not been measured before and after these surface treatments. We report estimation of N_s after light soaking and various surface treatments like etching, oxidation and exposure to various plasma etc (Chapter 5).

1.2 Potential Fluctuations

a-Si:H grown by glow discharge is heterogeneous [28-30]. Structural investigations of the a-Si:H films show that the bonded hydrogen is distributed non-uniformly in clusters, even in the best quality material [31]. The heterogeneities give rise to potential fluctuations. In addition, potential fluctuations in a-Si:H may also arise because of the variations in the bond angle and bond length, non-uniform distribution of the neutral and charged dangling bonds as well as the dopants (if present). It is difficult to handle the problem of potential fluctuations, in a fundamental way. Nevertheless, they are important as they must influence the electronic properties of a-Si:H in a profound manner [32]. One such property is the degradation of electronic properties of a-Si:H on light soaking (Staebler-Wronski effect) [33]. It is found that additional dangling bonds are created [34], on light soaking. Other photo induced structural changes have also been suggested [32]. Also, there are reports of increase in the width of potential fluctuations [35-37], on light soaking.

In a-Si:H, the range of potential fluctuations from structural disorder, is likely to

be of the order of inter-atomic distances [38] ($\approx 3\mathring{A}$). In transport measurements, carriers are required to move through the potential fluctuations. Therefore, carriers can't see the sharp changes in the potential, because they can tunnel through them. quantum mechanically. therefore, the transport measurements are sensitive to the long range potential fluctuations [35,36]. Fig 1.3 shows the in phase part of the long range potential fluctuations, associated with non uniform distribution of charged centers or region which may be related to impurity and structural disorder [28]. Local density fluctuations or compositional variations are expected to produce spatial variations of the mobility gap and have not been shown in the figure, for clarity. It should be noted that the lines drawn represent the local potential average over a region of the order of coherence length of the electron and not the true local potential. In such fluctuating mobility edges, spatial average of conductivity is dominated by highest energy regions of the potential fluctuations where the conductivity is lowest. On the other hand, the thermopower measures the average energy over the complete transport path and the low and high energy regions of the potential fluctuations contribute more equally. The difference (E_Q) in the conductivity and thermopower activation energies is, therefore, a rough measure of the magnitude of potential fluctuations.

Overhof and Beyer [35,36] have done model calculations and have related to the width of long range potential fluctuations to E_Q quantitatively.

Whereas, transport measurements are sensitive to the long range potential fluctuations, optical absorption measurements are likely to be sensitive to the short range potential fluctuations, of the order of interatomic distances. This is because optical absorption are vertical transitions in the real space (Fig. 1.3). Therefore, an analysis of sub-gap absorption measurements using potential fluctuations, is likely to give the width of short range potential fluctuations in contrast with the transport measurements. which give the information about the long range potential fluctuations.

In a-Si:H, $\alpha(h\nu)$ has Urbach edge region (region II) and plateau region (region III. see Fig. 1.2). Absorption in the Urbach edge region is attributed to bond length and bond angle variations, whereas region II is attributed to the absorption involving the deep gap states. John et al [38] have done quantum mechanical calculations to obtain exponential Urbach edge starting from Gaussian potential fluctuations. They relate the

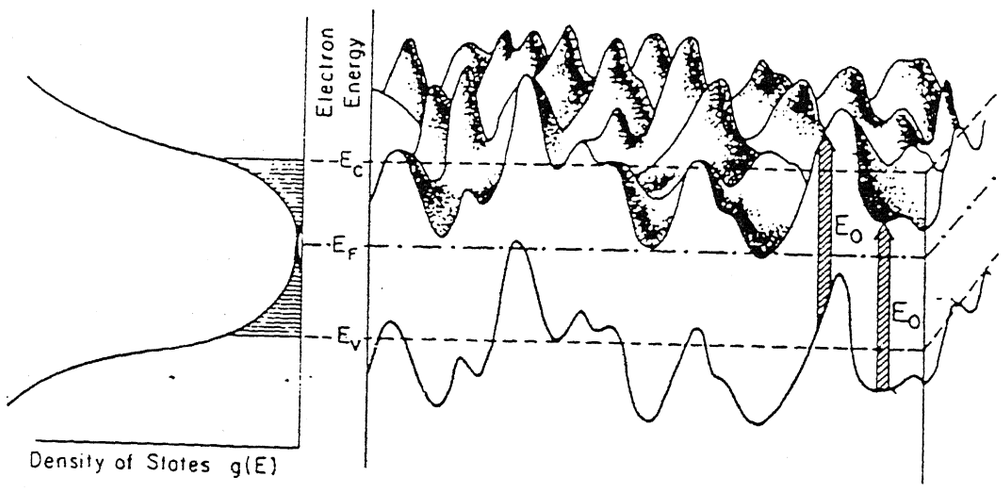

Figure 1.3: Long range potential fluctuations as might be present in a-Si:H(E_V and E_C represent the valance and conduction band percolation edges, respectively. E_F is the Fermi level. Note that short range potential wells are not shown. The part of the potential fluctuations which causes changes in E_o is also not shown (after reference 28).

width of the potential fluctuations (V_T) to slope of Urbach edge (E_o) [38].

1.3 Motivation for the Present Work

In the previous sections, we very briefly described the current status of this field and the problems and puzzles that need to be solved. We have undertaken a study of some of these issues and they are the main motivations of the present work. In the following we describe the salient features of the problems that have motivated this study.

In the literature, $\alpha_{cpm}(h\nu)$ and $\alpha_{pds}(h\nu)$ have been used to obtain the density of localised states only in a part of the mobility gap. In particular, the slope of the conduction band Urbach edge has not been obtained using sub-gap absorption measurements. Further, for the DOS determination, the shape of DOS has to be guessed in advance. Several different shapes have been proposed. We have used dual beam CPM (DBCPM) data and tried to guess the shape of DOS (Chapter 3). In addition, the value of the correlation energy (U), is not known precisely, although it is agreed that U is not negative [39]. We have attempted to measure U, using DBCPM (Section 3.1.1.4).

Li is an interstitial dopant in a-Si:H. It is observed that on doping with phosphorous from the gas phase, less hydrogen gets incorporated in the material. Since, Li diffusion is done at lower temperatures (less than 150^oC), the hydrogen concentration in the material is expected to remain the same as that in undoped samples. This allows one to study the effect of doping in a-Si:H(Li) without worrying about changing hydrogen concentration. In particular, it is interesting to compare a-Si:H(P) and a-Si:H(Li) for their bulk as well as surface states.

The existing methods of determining density of surface states using sub-gap absorption technique, presents practical difficulties of preparing a number of identical films. Other methods need perfectly uniform film and can be used only for device quality materials. Thus a technique, free from the above mentioned difficulties, is desirable which can estimate bulk states as well as the surface states. Our analysis, described in Chapter 3 and 4, obviates these difficulties.

Potential fluctuations in a-Si:H are not studied much. For example, difference

between $\alpha(h\nu)$ measured by CPM and PDS have not been explained using potential fluctuations. Also, it is observed that transport measurements see potential fluctuations, which is some kind of average of the short range potential fluctuations. Optical absorption is sensitive to the short range potential fluctuations. Therefore, width of potential fluctuations measured by transport and optical measurements on the same samples may give how the potentials, as seen by transport measurements, are averaged. These and other issues have been taken up in Chapter 6.

1.4 Organisation of the Thesis

The next Chapter describes the preparation of undoped and doped a-Si:H films by glow discharge method and doping with phosphorus and lithium. The characterisation of these films for amorphous nature, dark conductivity as a function of temperature, room temperature photoconductivity and thermopower is discussed in brief. Experimental set-up for the transmission measurement for obtaining absorption coefficient (α) in the region 2.5eV$\geq$ h$\nu \geq$ 1.6eV, thickness and band gap of a-Si:H thin films is discussed. The details of the instrumentation for computer controlled measurements of sub-gap α using constant photocurrent measurement (CPM) and photothermal deflection spectroscopy (PDS) techniques are also given in this Chapter.

Chapter 3 describes the principle and analysis of $\alpha_{pds}(h\nu)$ and $\alpha_{cpm}(h\nu)$ data. The technique adopted for the determination of the bulk states in the entire mobility gap in undoped and n type doped a-Si:H is discussed. Further, the details of dual beam constant photocurrent measurement (DBCPM) to obtain the correlation energy U and the shape of the deep gap states are discussed in this Chapter. Results on undoped a-Si:H, a-Si:H doped with various quantities of Li and P are discussed. Also, the position of D^- in a-Si:H(Li) have been discussed. Finally we give summary and conclusions of this Chapter.

In Chapter 4, we apply α_{CPM} and α_{PDS} data for the measurement of density of surface states. Again results on the samples, for which the bulk states are determined in Chapter 3, have been discussed. The effect of detailed distribution of the surface states have been discussed. Finally, we give the summary and conclusion of this Chapter.

Low density of surface states are crucial from the device point of view. In Chapter 5, we report the results on the measurement of density of surface states after various surface treatments like light soaking, oxide etching, oxidation using concentrated H_2SO_4 and annealing and treatment with room temperature nitrogen and Hydrogen plasma. These experiments also study the sensitivity of the technique for the measurement of density of surface states proposed in Chapter 4.

Chapter 6 describes how width of short range potential fluctuations (V_{rms}) and the long range potential fluctuations (Δ) can be obtained using sub-gap absorption and transport measurements respectively. Sub-gap absorption and transport measurements are performed on the same samples and V_{rms} and Δ are calculated. An empirical relation between V_{rms} and Δ is found. An attempt have been made to explain this empirical relationship. Further, a more comprehensive distribution of the potential fluctuations have been proposed, which explains both sub-gap absorption data in the entire region measured by us.

Chapter 7 summarises the results and the conclusions of the present study. The directions to carry out further work which helps in understanding the bulk and surface states and the potential fluctuations in a-Si:H are also given in the Chapter.

Bibliography

1. S. Guha, J. Non. Cryst. Solids, **198 -200**, 1076 (1996).

2. S. Tomiyama, T. Ozawa, H. Ito and T. Nakamura, J. Non. Cryst. Solids, **198 -200**, 1087 (1996).

3. R. A. Street, S. Nelson, L. Antonuk and V. Perez mendez, MRS Symp. **192** 441 (1990).

4. N. F. Mott and E. A. Davis, Electronic processes in Non-Crystalline Materials, (Clarendon Press, Oxford, 1979), Chapters 2 and 6.

5. S. R. Elliot, Physics of Amorphous Materials, (Longman, UK, 1990), Chapter 3.

6. H. Overhof and P. Thomas, Electronic Transport in Hydrogenated Amorphous Semiconductors, Volume 114, (Springer-Verlag, Berlin, 1989).

7. W. E. Spear and P. G. LeComber, J. Non. Cryst. Solids, **8-10**, 727 (1972).

8. W. E. Spear and P. G. LeComber, Solid State Comm. **17**, 1193 (1975).

9. W. E. Spear and P. G. LeComber, Phil. Mag. **33**, 935 (1976).

10. R. A. Street, J. Zesch and M. J. Thompson, Appl. Phys. Lett. **43**(7), 672 (1983).

11. J. Kocka, J.Non.Cryst. Solids, **90**, 91 (1987).

12. J. D. Cohen, J. P. Habrison and K. W. Wecht, Phys. Rev. Lett. **48**, 109 (1982).

13. W. E. Spear and P. G. LeComber J. Non. Cryst. Solids, **8-10**, 727 (1972).

14. D. S. Misra, Ph.D Thesis, "Determination of the density of localised states in well characterised thin films of hydrogenated amorphous silicon prepared by glow discharge", IIT Kanpur, (Unpublished) 1984.

15. S. Ashok and S. J. Fonash, IEEE, Electron Devices, **ED-1**, 200 (1980).

16. P. Viktorovitch and D. Moddel, J. Appl. Phys. **E1**, 4847 (1980).

17. M. Vanecek, J. Kocka, J. Stuchlik, Z. Koicek, O. Stika, and A. Triska, Solar Energy Materials **8**, 411 (1983).

18. A. K. Sinha, M. Malhotra, S. Kumar, E. Bhattacharya and S. C. Agarwal, Ind. J. Pure & Appl. Phys. **31**, 548 (1993).

19. W. B. Jackson, N. M. Amer, A. C. Boccara, and D. Fournier, Appl.Optics **20**, 1333 (1981).

20. S. C. Agarwal, J. S. Payson and S. Guha, Phys. Rev. **B 36**, 9348 (1987); A. K. Sinha and S. C. Agarwal, Ind. J. Pure & Appl. Phys. (1998) (in press).

21. M. Hack and M. Shur, J. Appl. Phys. **54**, 5858 (1983); S. Guha, J.Non.Cryst. Solids, **77&78**, 1451 (1985).

22. Z. E. Smith, V. Chu, K. Shepard, S. Aljishi, D. Slobodin, J. Kolodzey, S. Wagner, and T. L. Chu, Appl.Phys.Lett. **50**, 1521 (1987).

23. A. K. Sinha and S. C. Agarwal, Phil. Mag. B (1998), (In Press).

24. H. Curtnis, N. Wyrsch and A. V. Shah, Electronics Letters **23**, 228 (1987).

25. M. Favre, H. Curtnis and A. V. Shah, J.Non-Cryst. Solids, **97 & 98**, 731 (1987).

26. W. Beyer and R. Fischer, Appl. Phys. Lett. **31**, 850 (1977).

27. J.Kocka, M.Vanecek and A.Triska, Amorphous silicon and Related Materials (ed. H. Fritzsche), Vol. 1A, (World Scientific, Singapore, 1989), page 296.

28. H. Fritzsche, J. Non-Cryst. Solids, **6**, 49 (1971).

29. S. C. Agarwal, Ind. J. Pure and Appl. Phys., **34**, 597 (1996); S. C. Agarwal, Bull. Mater. Sci. **18**, 669 (1995).

30. E. N. Economou, C. M. Soukoulis, M. H. Cohen and A. D. Zdetsis, Phys. Rev. **B 31**, 6172 (1985); M. H. Cohen, in Random Media, IMA Vol. 7, (ed. G. Papanicolaou), Springer-Verlag New York (1987) page 89.

31. R. A. Street, Hydrogenated Amorphous Silicon (Cambridge University, 1991) Chapter 7.

32. H. Fritzsche, Solid State Comm. **94**, 953 (1995).

33. D. L. Staebler and C. R. Wronski, Appl. Phys. Lett. **31**, 32 (1977).

34. H. Derch, J. Stuke and J. Beichler, Appl. Phys. Lett. **38**, 456 (1981).

35. H. Overhof and W. Beyer, Phil. Mag. **B 43**, 433 (1981).

36. H. Overhof and W. Beyer, Phil. Mag. **B 47**, 377 (1983).

37. P. Agarwal and S. C. Agarwal, J. Appl. Phys. (1997).

38. S. John, C. M. Soukoulis, M. H. Cohen and E. N. Economou, Phys. Rev. Lett. **57**, 1777 (1986).

39. See for example, J. Z. Liu, G. Lewen, J. P. Conde and P. Roca i Cabarrocas, J. Non-Cryst. Solids **164 & 165**, 383 (1993).

Chapter 2

Experimental

This Chapter describes the preparation of both undoped and doped hydrogenated amorphous silicon (a-Si:H) thin films and their initial characterisation for quality. Further, the details of the set ups for transmission, constant photocurrent measurement (CPM), photothermal deflection spectroscopy (PDS) and dual beam constant photocurrent measurement (DBCPM) are also given.

2.1 Preparation of a-Si:H Films

Hydrogenated amorphous Silicon (a-Si:H) is prepared by the decomposition of silane (SiH_4) gas in a mixture with argon or hydrogen in rf glow discharge apparatus [1]. Many variations of the technique have been tried to tailor the film properties [2,3]. Fig. 2.1 shows the glow discharge reaction chamber made of stainless steel. A capacitor geometry is used. The substrates are loaded on the top electrode (anode), which is heated externally using a heater as shown in the figure. Prior to the deposition, the system is evacuated to the base pressure of $\approx 10^{-8}$ torr using a turbo molecular pump. The system is purged with hydrogen and substrates are cleaned using hydrogen plasma. Silane with the carrier gas is then introduced in the reaction chamber, and an electric field is applied between the cathode and the anode (Fig. 2.1). Silane molecules are dissociated through collisions with the fast electrons in the plasma, into neutral radicals, atoms and ions. These atoms and ions travel to the growing surface through a gas phase diffusion process, resulting in amorphous silicon thin films onto Corning 7059

Table 2.1: Optimum parameters for depositing undoped a-Si:H, using rf glow discharge

Gas Composition	Ratio
SiH_4 : H_2	10:90
Flow Rate	20 sccm
Power Density	$40mW/cm^2$
Deposition Rate	1 $\AA$/sec.
Substrate Temperature	300°C
Pressure of deposition	1 torr

glass substrates. More details of the deposition system are given elsewhere [4]. A multi chamber glow discharge system is described in ref. [5].

The quality of a-Si:H films depends upon the deposition conditions, like ratio of gases in the gas mixture, flow rate of gases, substrate temperature, pressure of deposition, absorbed power density etc. A combination of these parameters for obtaining good quality material varies from system to system. Table 2.1 gives the optimum deposition parameters for our system. Some of the films for this study have also been made outside optimum conditions to vary the density of defect states.

2.1.1 Substrates

Corning 7059 glass slides (25mm×25mm×0.5mm) are used as substrates for optical and electrical measurements. These are alkali free and are transparent in the region of interest (0.6eV to 4.0eV). For IR spectroscopy polished high resistivity silicon wafers are used.

The 7059 glass substrates are first washed in liquid detergent, rinsed in distilled water and then deionised water. These are then cleaned ultrasonically in acetone and finally degreased in vapours of isopropyl alcohol. Silicon substrates are degreased and then etched with 15% solution of HF. Substrates are then rinsed in deionised water and finally are exposed to the vapour of isopropyl alcohol.

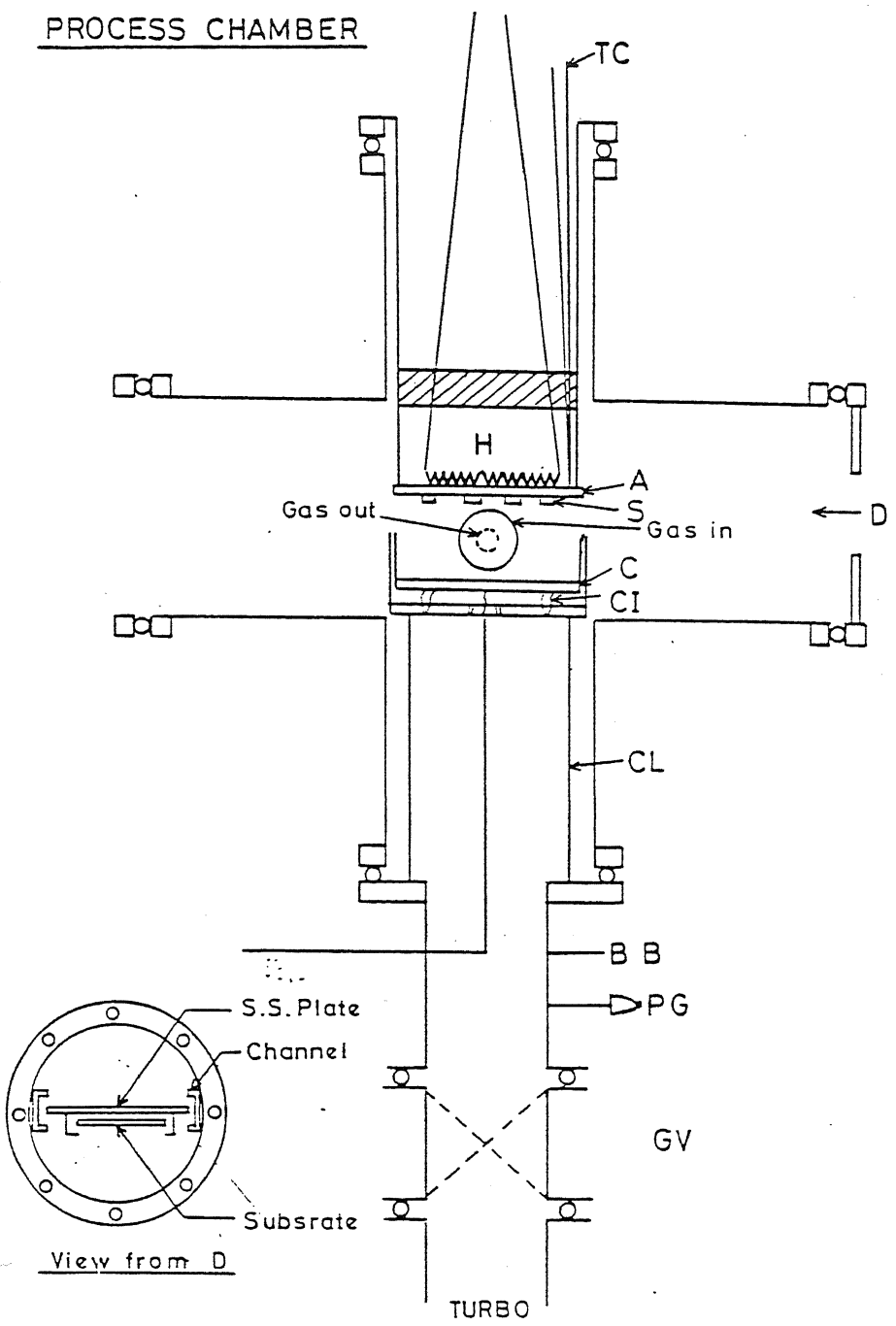

Figure 2.1: Schematic diagram of the reaction chamber used for preparation of a-Si:H. Here, GV is the gate valve, B and PG are beratron and penning gauges, A, H and S are anode, substrate heater and substrate respectively. CI and CL represent insulators and SS cylinder. D is the view port, C the cathode and TC the thermocouple (after reference 5).

2.1.2 Doping

For phosphorous (P) doping, SiH_4 is mixed with PH_3 in appropriate amounts. Phosphorus acts as a substitutional donor. For interstitial doping [6], both vacuum evaporation of lithium (Li) and ion implantation of Li have been used [7,8], with success. We have used vacuum evaporation of Li.

Li pieces, covered with methanol in a tungsten boat, are loaded in a vacuum evaporation system. Methanol is put to protect Li from air. a-Si:H thin film is kept at an elevated temperature of $100 - 150°C$ and about 100 $\AA$ thick Li is evaporated on top of it at a base pressure of about 10^{-6} torr. The sample is then annealed at a temperature $100 - 200°C$ for 1-2 hours. Higher temperature and longer times of annealing give higher concentration of diffused Li in a-Si:H. The excess Li is removed from the surface by etching the film with 10 % HF. The sample is again annealed at about 150°C for 6 hours to make the diffusion as uniform as possible. More details are given elsewhere [7,8].

2.1.3 Electrodes

Nichrome and graphite (Aqua dag) are used as electrodes. It is found that both make ohmic contacts for electric fields of interest up to 600 V/cm. About 1μm thick nichrome strips ($\approx$ 1 cm. in length and $\approx$ 2 mm apart) are evaporated through a suitable mask on a-Si:H film deposited on 7059 glass substrate.

Small drops of graphite black in an organic solvent (separation $\approx$ 2mm) are carefully put on the sample and allowed to dry for about 30 minutes.

2.1.4 Surface treatment

Various treatments are done to change the surface and the changes in the surface states are measured. These are light soaking, annealing, native oxide etching, oxide growth and treatment with nitrogen and hydrogen plasma.

Light soaking is done by white light ($\approx$ 20 mW/cm^2) from 300W tungsten-halogen lamp for 15 hours. A red filter is used to avoid heating of the sample. Etching of the native oxide is done using HF (15% in deionised water) for 10 minutes. Oxide on the

surface is re grown by treating the sample with concentrated sulfuric acid, rinsing in deionised water and exposure to isopropyl alcohol, followed by annealing (150°C, 2h). Finally, we also treated the a-Si:H sample with nitrogen plasma (300K, $40mW/cm^2$,dc plasma for 2 hours) and hydrogen plasma (300K, $40mW/cm^2$,dc plasma for 2 hours).

2.2 Characterisation of a-Si:H Films

Films are characterised structurally by x-ray, optically IR and visible-UV spectroscopy and electrically by dark conductivity (σ) as a function of temperature and voltage, room temperature photoconductivity (σ_{ph}) and thermopower as a function of temperature.

2.2.1 Structural Characterisation

a-Si:H films are characterised for their amorphous nature using x-ray diffraction. The x-ray diffractogram gives a broad peak, characteristic of amorphous material. Electron diffraction consists of diffused rings, which also shows that the films are amorphous.

2.2.2 Electrical Characterisation

All doped and undoped films are characterised by dark and photoconductivity (σ and σ_{ph}) at room temperature. For σ_{ph} measurement, light from a 300W tungsten halogen lamp (80V, 4amps) with a red filter is used. It gives about $30mW/cm^2$ of intensity on the sample. We find $\sigma \approx 10^{-10} ohm^{-1}cm^{-1}$ and $\sigma_{ph} \approx 10^{-5} ohm^{-1}cm^{-1}$, for our good quality undoped a-Si:H.

Measurement of activation energy (E_σ) Activation energy of the dark conductivity is obtained by measuring σ as a function of T between 300K and 450K in vacuum. The details of the measurement chamber are described elsewhere [6]. Fig. 2.2 shows log σ versus 1/T curve for undoped a-Si:H thin film (# X1). E_σ is found to be $\approx$ 0.75eV.

Measurement of thermopower (S): For the measurement of thermopower (S), coplanar nichrome electrodes, about 1cm long and 0.5 cm apart, are evaporated on the top surface of the film. The sample is placed on two separate copper blocks, containing two independent heaters. The temperatures of the two ends (T_1 and T_2) are monitored

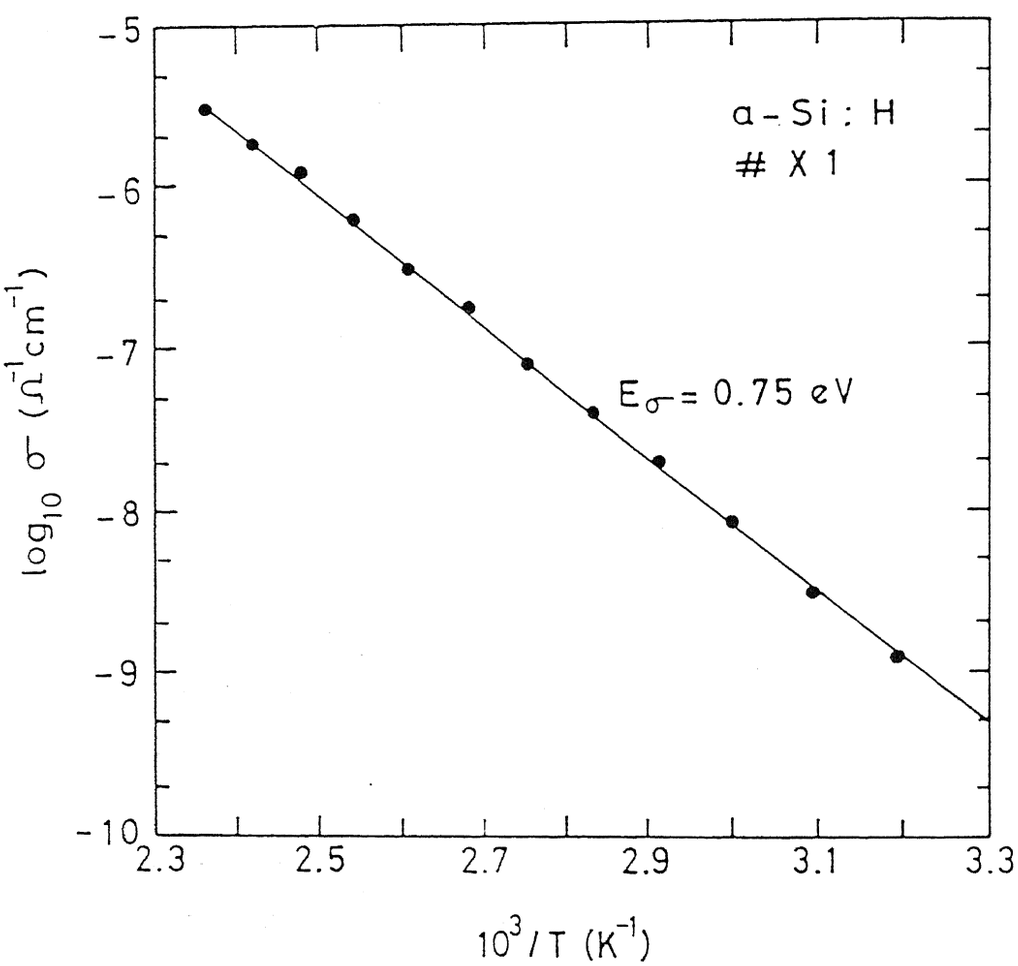

Figure 2.2: log σ plotted as a function of 1000/T for an undoped a-Si:H film. The activation energy (E_σ) is (0.75±0.05)eV.

using two copper-constatan thermocouples, placed on each electrode. By varying the heater currents, a temperature difference ΔT (= T_1 - T_2) varying between 0 and $\pm$ 5K could be achieved. Corresponding thermo emf (ΔV) is measured. Slope of the plot of ΔV as a function of ΔT gives S. These measurements are done in the partial pressure (0.5 mbar) of helium, for better thermal contact between the sample and the thermocouple. More details are given in Ref [6]. The thermopower is found to be negative and its magnitude increases with the temperature. These observations are in agreement with others [9]. Fig. 2.3 shows S as a function of 1/T for a P doped a-Si:H sample (#5). The slope is $E_s = 0.13 \pm 0.03 eV$.

2.2.3 Transmission Measurements

Optical transmission (400-1200nm) measurements are used to obtain refractive index ($n(\lambda)$), thickness(d), optical gap (E_g) and absorption coefficient ($\alpha(\lambda)$) of a-Si:H deposited on 7059 glass. An accurate determination of $\alpha(\lambda)$, d and E_g using transmission measurements is very important for our work because $\alpha(\lambda)$ values are used for fixing the α scale in the CPM. Also, d is used in obtaining α from PDS signal and E_g values are used in the DOS modeling. In the present work we have used the transmission measurements and analysis followed by Swanepoel [10], which gives an accuracy of 1% for films with good thickness uniformity as claimed by the author [10]. The analysis and formulae used, are given in Appendix A in a closed form.

Transmission spectrum is measured using a Hitachi - 2000 spectrophotometer for $400nm \leq \lambda \leq 900nm$ and a home made setup for $400nm \leq \lambda \leq 1200nm$. Similar values of transmission are obtained from the two set ups. Fig. 2.4 shows the home made set up used. It consists of a 75W quartz halogen lamp and a grating monochromator (Bausch & Lomb). The monochromatic beam is focused onto the sample using a lens. A high pass order sorting filter (Hoya-64) is used to remove the second order radiation from the monochromator output. To decrease the noise from stray light, we use a chopper (SR-540) and a lock-in amplifier (SR-510). The sample is mounted on a fixed, opaque plate with a hole of $\approx$ 5mm diameter. The transmitted intensity is measured using calibrated photodiodes as shown in Fig. 2.4. We use a Si photodiode for $400nm \leq \lambda \leq 1050nm$

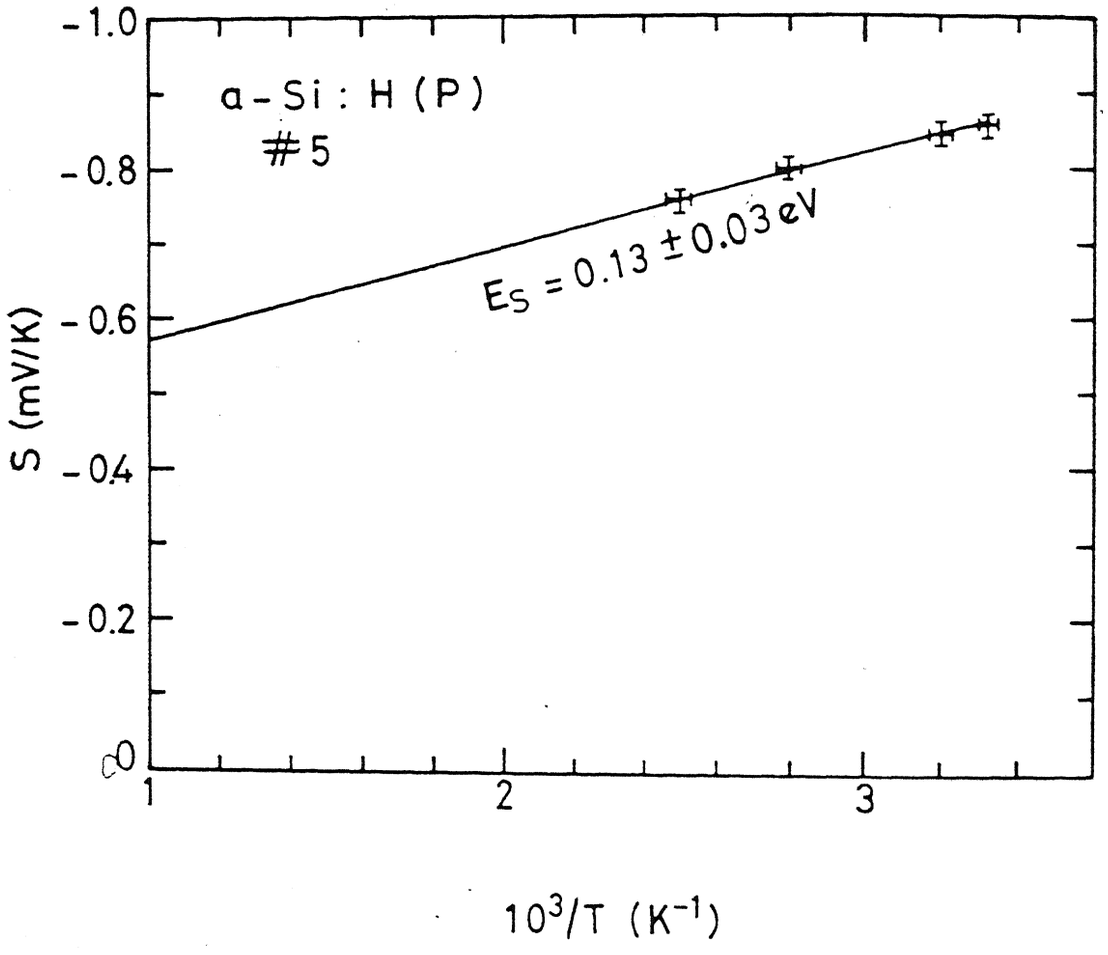

Figure 2.3: Thermopower(S) plotted as a function of 1000/T for P doped a-Si:H. E_s is found to be $\approx$ 0.13eV.

and a Ge photodiode for $\lambda > 1050nm$. After measuring the transmitted intensity through the sample, the sample is removed from the plate carefully without disturbing the setup. Intensity of the incident light is now measured.

The set up is fully automated. The automation consists of reading the lock-in amplifier data using a Personal Computer (PC) with serial port (RS 232C) communication. Also, a stepper motor controlled by the same PC is used to drive the monochromator grating as shown in Fig. 2.4. Details of the circuit used for controlling the stepper motor are given in Appendix B. The computer programme for the automation is given in Appendix C. Fig. 2.5 shows $(\alpha h\nu)^{1/2}$ as a function of $h\nu$ for an undoped a-Si:H film (No. 5/94). The Tauc's optical gap [11] is found to be $(1.75 \pm 0.10eV)$. The thickness calculated from the interference fringes is found to be $\approx$ 1080$\pm$50 nm, and is confirmed by a telestep apparatus.

2.3 Sub-Gap Absorption Measurements

The lowest α for 1 μm film that can be measured using our transmission set up described above is about 50 cm^{-1}. However, α in the sub-gap region can be smaller by a factor of 100 or smaller. Hence more sensitive techniques are required. We have measured sub-gap α using two techniques namely photothermal deflection spectroscopy (PDS) [12,13]. and constant photocurrent measurement (CPM) [14,15].

2.3.1 Photothermal Deflection Spectroscopy (PDS)

2.3.1.1 Principle

The PDS technique is based on the detection of heat produced when a sample absorbs sub band gap light called the pump light. As shown in Fig. 2.6, the pump beam (marked 1) is focused on to the sample, kept in carbon tetra chloride (CCl_4). As the sample absorbs the pump light, the probe beam (marked 2 in Fig. 2.6) is deflected by the thermally induced changes in the refractive index of CCl_4, which is in thermal contact with the sample. The deflection of the probe beam is measured using a position sensitive detector (PSD). The deflection of the probe beam results in a signal (S) in the

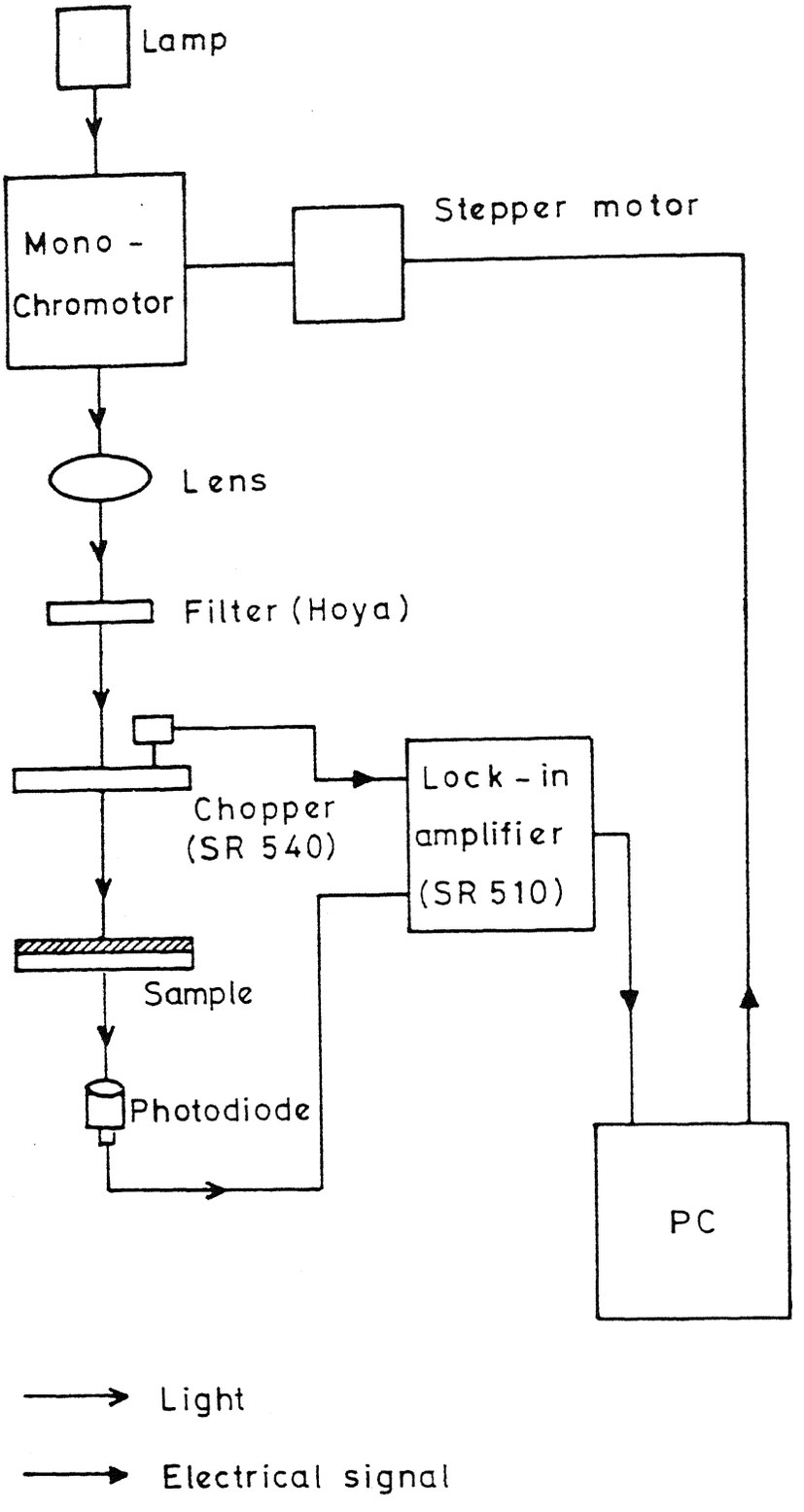

Figure 2.4: Setup for Transmission measurements in visible-near IR region. Unfilled arrows indicate the light rays, whereas, the filled arrows indicate the electrical signal.

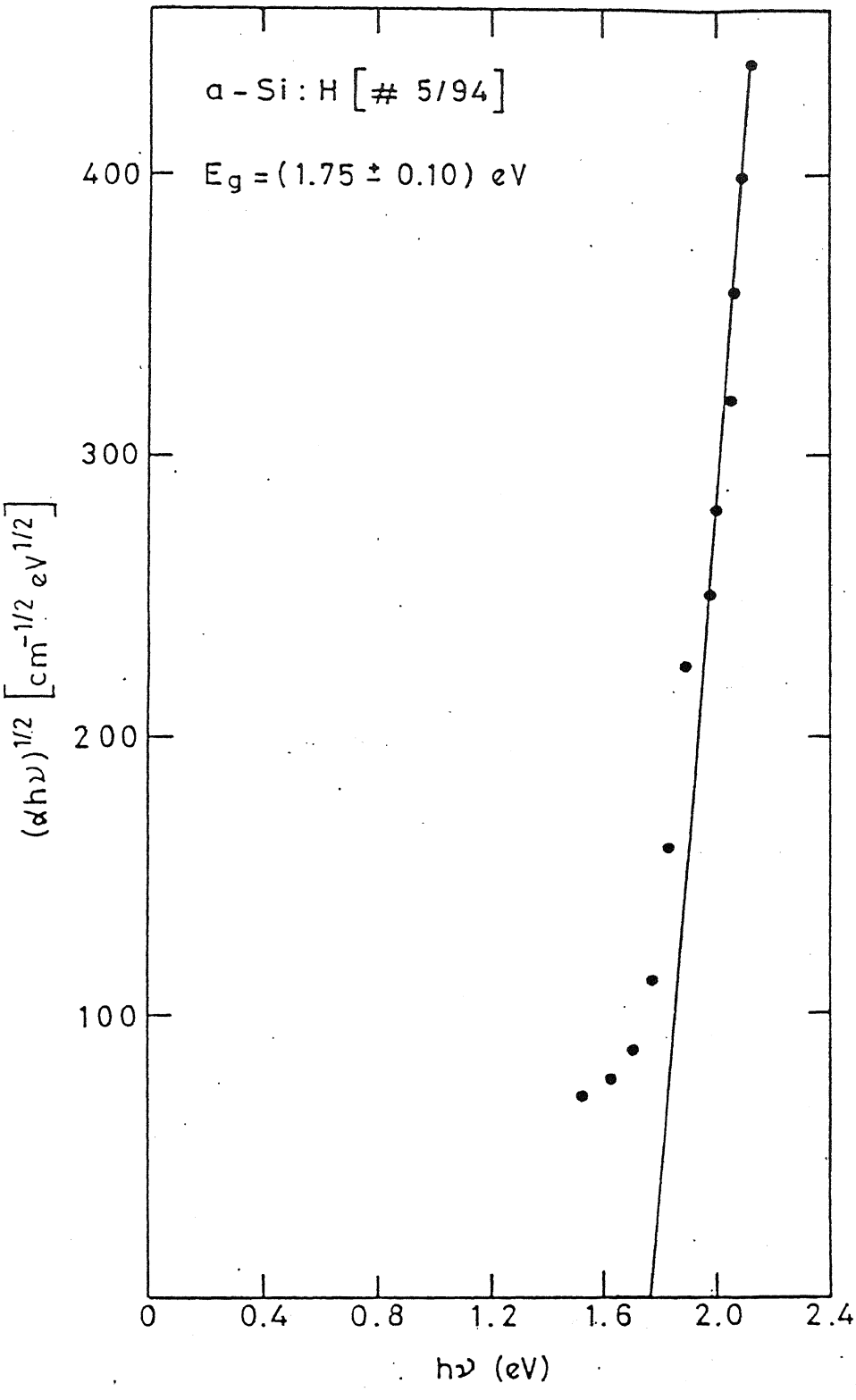

Figure 2.5: Tauc's plot for undoped a-Si:H. The optical gap is 1.75±0.1eV.

PSD and associated electronic circuit. The signal can be expressed as [12]:

$$S = S_o[1 - exp(-\alpha d)] \tag{2.1}$$

where, d is the film thickness and S_o is the PDS signal in the saturation region, since $S = S_o$ when $\alpha d >> 1$. Thus, knowing S_o from the saturated region of the PDS signal and d from the interference fringes in the transmission measurements [10], α can be obtained using Eq. (2.1). However, this leads to a larger uncertainty in the determination of absolute value of α. This can be improved by matching the value of α in a wavelength region in which the transmission measurements can also give absolute value of α, with greater precision. Details of the experimental set up [13] used in our laboratory are given below.

2.3.1.2 Instrumentation

Fig. 2.6 shows the schematic diagram of the PDS setup fabricated by us. It consists of a monochromatic sub band gap light (pump beam 1 in Fig. 2.6), a He-Ne laser probe light (probe beam 2 in Fig. 2.6), a Position Sensitive Detector (PSD), an electronic circuit to enhance the signal to noise ratio and a lock-in amplifier to measure the signal. The pump light is from a high intensity grating monochromator which uses a 75W quartz halogen lamp as a source. It is chopped at a low frequency (9Hz in our case) to reduce the thermal lag. The monochromatic beam is focused on to the sample kept in a quartz cell containing pure and triple distilled CCl_4. A long pass filter is used to filter out the second order from the grating monochromator. The probe beam (Fig. 2.6) is from a low power (2mW) He-Ne laser with good pointing stability (ours is better than 0.03 m rad/hour). The probe beam is focused using a short focal length ($\approx$ 4 cm.) lens near the center of the sample, and is allowed to pass nearly grazing the sample. The PSD is a quadrant photodiode. Since we need to detect the deflection of the probe beam only along one direction, two diodes out of the four in the PSD (which are perpendicular to this direction) are shorted together to get two diode pairs. Details of the mounting of the PSD and the equivalent circuit diagram of the PSD are given in Appendix D. Actual components used by us are shown in Fig. 2.6.

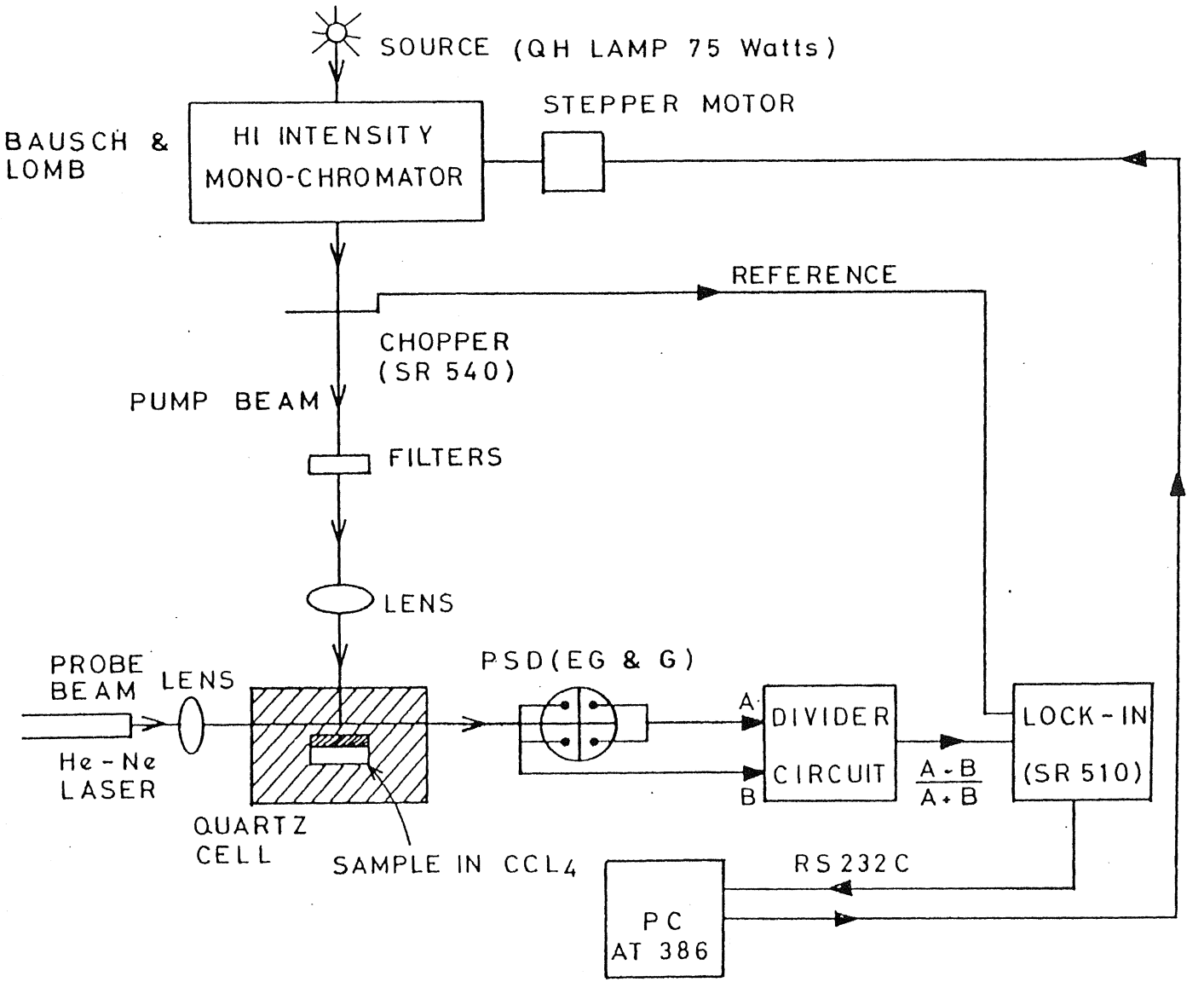

Figure 2.6: Setup for Photothermal Deflection Spectroscopy. Filled arrows are the light rays, whereas, the unfilled arrows are the electrical signal.

The difference of the two outputs from the PSD is proportional to the PDS signal. These signals (called A and B) are processed in an analog electronic circuit to get (A-B)/(A+B) and amplified. Details of the divider circuit are in Appendix E. The signal is extremely small, and utmost care is required for good performance. The following points were kept in mind while designing our PDS system:

The deflection medium (liquid) should be such that it does not react with the material under investigation. Also, it should not absorb light up to near IR and should have a large rate of change of refractive index with temperature (dn/dT). For a-Si:H films, CCl_4 satisfies all these conditions and has dn/dT $= 8 \times 10^{-4}$/K. However, special care has to be taken to handle CCl_4, because it is highly volatile and can be a health hazard upon inhalation. As an alternate, Fluorinert FC72 (3M Product) can be used. This liquid is less toxic, but has about a factor of 2 lower dn/dT (dn/dT $= 4 \times 10^{-4}$/K) compared to CCl_4 and also induces considerable change in the phases of lock-in signal [16] for photon energies h$\nu < 1.4$eV. Therefore. we have used CCl_4 in a well ventilated room. Further, dust particles in the deflecting medium can cause tremendous noise. It is found that triple distillation of CCl_4 and clean environment while handling it helps.

Finally, the mechanical vibrations can be a great source of noise. These are suppressed by keeping the experimental setup on a vibration free table having good attenuation characteristics, particularly at low frequencies (10-20 Hz) (we used a vibration free table from Newport, Model M-MST-48-8).

2.3.1.3 Automation of PDS

The PDS signal is very low and noisy. Hence long integration times (10-30 sec.) are required to reduce the noise. Also, to get a reasonable data set, one has to take readings at close intervals of wavelength. This is very tiresome and automation is desirable.

Our automated PDS set up is shown in Fig. 2.6. The main features are essentially the same as those in the manual mode described in Section 2.3.1.2. Additional arrangements for the automated measurements have been made using a computer (PC - 386). The PC has the following functions:

a) Initialisation of the monochromator at the desired initial wavelength by moving the monochromator with the help of a stepper motor, run by the PC.

b) Reading the PDS signal from the lock-in amplifier (SR 510) using the serial port of the PC and RS 232C communication.

c) Moving the monochromator by desired steps using the stepper motor.

The details of the circuit and software for running the stepper motor are given in Appendix B.

The computer programme for the automation (Appendix C) consists of the following subroutines:

i) Subroutine to read the data through Serial Port (for the lock-in amplifier SR 510).

ii) Subroutines to run the motor driver circuits.

2.3.2 Constant Photocurrent Measurement (CPM)

2.3.2.1 Principle

The real problem, when we try to estimate α from the photocurrent measurements, is that of changing life time of the electrons (τ) with the changing Fermi level split [17]. In CPM, however, the photocurrent is kept constant by changing the intensity of light as the energy of incident light ($h\nu$) is varied in the sub band gap region. Therefore, the same set of recombination centers govern the free carrier lifetime and hence τ is constant. The intensity that gives the predetermined constant value of the photocurrent, can be related to α as discussed below:

For undoped a-Si:H, the photocurrent is mainly contributed by the electron current because the $\mu\tau$ product is about 10 times larger for electrons than holes [17]. The photocurrent density (J_n) is given by [18]

$$J_n = e\, n_{ph}(1 - R)[1 - exp(-\alpha\, d)]\, \eta\, \mu\tau\, F/L. \tag{2.2}$$

Where e is the electronic charge, n_{ph} the number of incident photons per unit area per unit time, R is the reflection coefficient, d the film thickness, η the photogeneration efficiency, μ the electron mobility, τ the mean lifetime of the electrons (recombination lifetime), F the applied electric field and L is the separation between the electrodes.

In the sub gap region R is a slowly varying function and can be assumed to be a constant. $\mu\tau$ product depends upon the position of quasi Fermi level, and is a constant

in this case. The value of η is found to be ≈ 1 at 300K [17]. However, by the comparison of CPM derived α with PDS derived α, it is found that $\eta(h\nu)$ does not decrease even in the sub gap region (with an uncertainty of about a factor of 2) [17]. Thus we obtain from Eq. (2.2)

$$J_n = constant \times [1 - exp(-\alpha d)]\ n_{ph} \tag{2.3}$$

Now, for sub band gap region αd ¡¡ 1, hence [1-$exp(-\alpha$d)] reduces to αd. Thus for constant photocurrent Eq. (2.3) reduces to

$$\alpha(h\nu) = \frac{constant}{n_{ph}(h\nu)}, \tag{2.4}$$

Therefore, by measuring the intensity that keeps the photocurrent constant at a predetermined value, we can find the spectral dependence of α up to a constant using Eq. (2.4). This constant is obtained by matching the CPM curve with the α obtained by the transmission in the region of higher energy where $\alpha d \approx 1$.

2.3.2.2 Instrumentation

Fig. 2.7 shows the setup for CPM. Here the light source is the same as the pump beam part of the PDS apparatus as described already in the Section 2.3.1.2. A beam splitter (10% reflection) is used to monitor the intensity of the incoming beam using a calibrated photodiode (we used a Si photodiode, in the energy range $1.8eV > h\nu > 1.1eV$ and a Ge photodiode, in the energy range $1.2eV > h\nu > 0.8eV$). The constant value of the photocurrent is read across a $1M\Omega$ resistor using a lock-in amplifier. A bias of 10V (electrode separation 0.2cm.) is used for the measurement of photocurrent (typically $10^{-10}A$). Actual components used by us are indicated in Fig. 2.7.

2.3.2.3 Automation of CPM

In CPM, photocurrent is kept constant by controlling the power to the monochromator lamp in a feedback arrangement at every wavelength of measurement. This reduces labour and gives better accuracy, compared to the manual measurements.

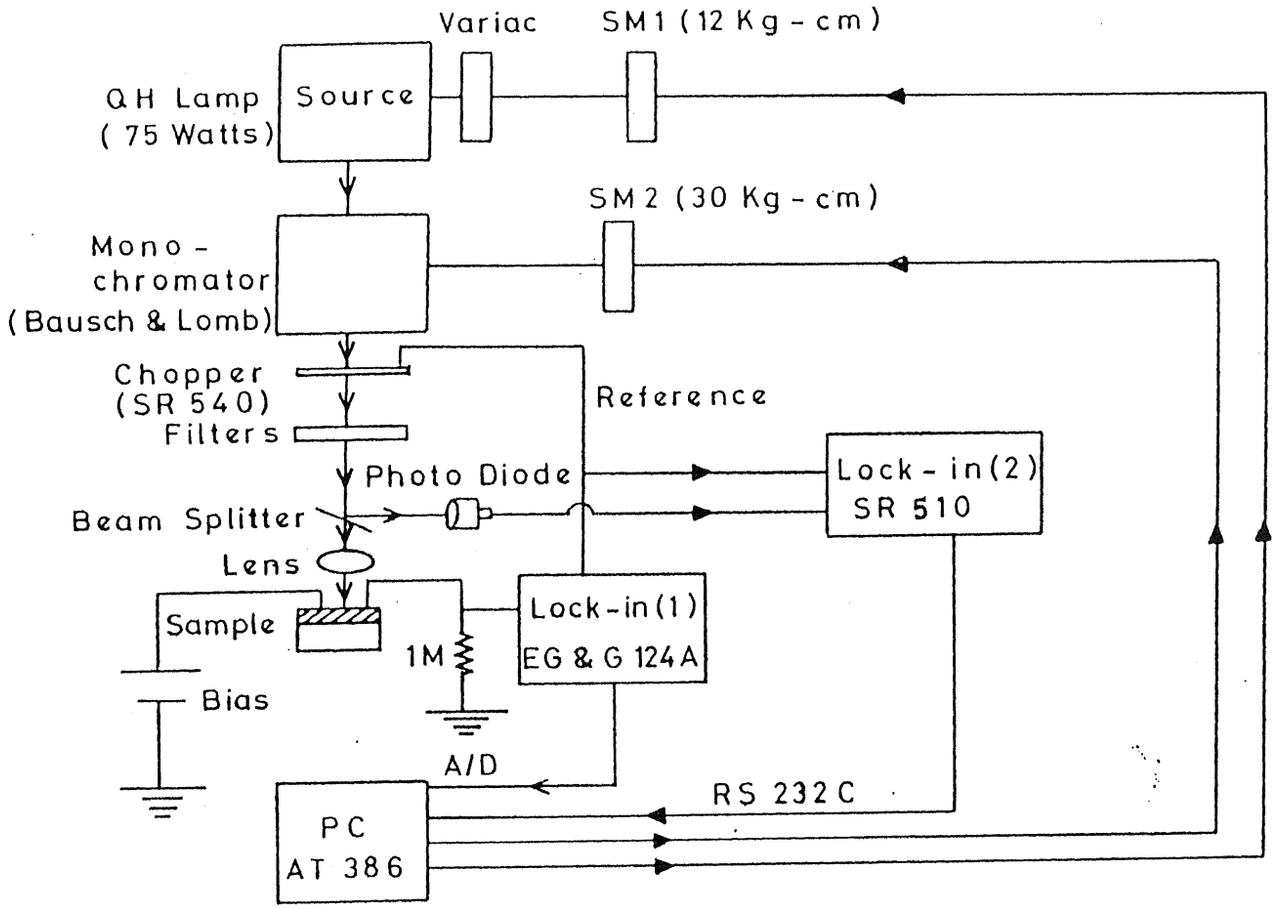

Figure 2.7: The setup for Constant Photocurrent Method. SM1 and SM2 are the stepper motors. Lock-in 1 is an analog lock-in amplifier and hence, an A/D card (PCL 812) is used to read this signal through PC. Filled arrows are the light rays, whereas, the unfilled arrows represent the electrical signal.

Our automated CPM setup is shown in Fig. 2.7. The main measurement sections are essentially the same as in the manual mode described in Section 2.3.2.2. The following are the additional arrangements for the automated measurements:

a) Initialisation of the monochromator using the stepper motor (SM2 in Fig. 2.7) used for driving the monochromator (Appendix B).

b) Reading the photocurrent across 1M *Ohm* resistance in the lock-in amplifier [lock-in (1) in Fig. 2.7] using A/D card and the PC.

c) Comparing this photocurrent with the predetermined constant value of the photocurrent, and moving the variac attached to the monochromator lamp using the stepper motor (SM1, Fig. 2.7) one step in the desired direction and comparing the new photocurrent with the predetermined value. Repeating this process step by step till the photocurrent in the sample is within 2% of the predetermined photocurrent value.

d) After reaching the predetermined photocurrent value, the intensity of the lamp is measured using calibrated photodiode and lock-in amplifier (lock-in 2 in Fig. 2.7).

e) The monochromator is moved to another wavelength using the stepper motor (SM2).

The movement of stepper motor is further discussed in Appendix B. The computer program for the automated CPM measurements (Appendix F) has the following subroutines:

i) Subroutine to read the data through Serial Port (for the lock-in amplifier SR 510).

ii) Subroutine to read the data throgh A/D card (for the analogue Lock-in Amplifier).

iii) Subroutines to run the motor driver circuits.

2.3.3 Dual Beam Constant Photocurrent Measurements (DB-CPM)

CPM is sensitive only to those optical transitions which end in the conduction band extended states. But for the determination of correlation energy (U), information about the optical transition ending in the localised states is also required. This is achieved by changing the occupancy of the localised states using a dc bias light. This can help in obtaining U and the shape of the deep gap states, as discussed later in Section 3.3.

Dual beam constant photocurrent measurements (DBCPM) [19] is ac CPM done

in the presence of a highly absorbing dc light, known as the pump light. We have used another high intensity monochromator as the source for the intense dc light. The details of the instrumentation and automation of the set up are the same as discussed in section 2.3.2. We have used a quartz halogen lamp (120 W) along with a high intensity grating monochromator (Oriel), as the pump light. The wavelength used is 650nm. The intensity of the pump light is approximately 20 times that of the chopped (probe) light. Fig. 2.7 also represents the DBCPM set up without the bias light.

Bibliography

1. A. Matsuda and N. Hata in Glow-Discharge Hydrogenated Amorphous Silicon, (KTK Scientific Publishers, Tokyo, 1989), p. 9-38.

2. C. Anandan, C. Mukherjee, T. Seth, P. N. Dixit and R. Bhattacharya, Appl. Phys. Lett. **66**, 85 (1994).

3. C. Mukherjee, C. Anandan, P. N. Dixit, and R. Bhattacharya, Appl. Phys. Lett. **68**, 835 (1996).

4. D. S. Misra and S. C. Agarwal, Bull. Mater. Sci. **3**, 347 (1981).

5. S. K. Tripathi, D. Deva, S. Kumar, P. N. Dixit and S. C. Agarwal, Ind. J. Pure & Appl. Phys. **31**, 660 (1993).

6. W. Beyer and R. Fischer, Appl. Phys. Lett. **31**, 850 (1977); K. Winer and R.A. Street, J. Appl. Phys. **65**, 2272 (1989).

7. S. K. Tripathi, A. K. Sinha, S. Kumar and S. C. Agarwal in Physics of Semiconductor Devices, ed. Krishan Lal (Narosa, New Delhi, 1994), p. 589.

8. Pratima Agarwal, Ph.D. thesis, "Thermal and Light Induced Metastabilities in Phosphorus and Lithium Doped Hydrogenated Amorphous Silicon", IIT Kanpur, (1995) unpublished.

9. D. Hauschildt, W. Fuhs and H. Mell, Phys. Stat. Sol. **111**, 171 (1982).

10. R. Swanepoel, J. Phys. **E16**, 1214 (1983).

11. J. Tauc in Amorphous and Liquid Semiconductors, ed. J. Tauc, (Plenum Press, N.Y. 1974), Chap. 4.

12. W. B. Jackson, N. M. Amer, A. C. Boccara, and D. Fournier, Appl. Optics, 20, 1333 (1981).

13. A. K. Sinha and S. C. Agarwal, Ind. J. Pure & Appl. Phys. (1998), (in press).

14. M. Vanecek, J. Kocka, J. Stuchlik, Z. Koicek, O. Stika, and A. Triska, Solar Energy Materials **8**,411 (1983).

15. A. K. Sinha, M. Malhotra, S. Kumar, E. Bhattacharya and S. C. Agarwal, Ind. J. Pure & Appl. Phys. **31**, 548 (1993).

16. H. Curtins and M. Favre, Amorphous Silicon and Related Materials, (World Scientific, Singapore, 1990) p. 329.

17. J. Kocka, M. Vanecek and A. Triska in Amorphous Silicon and Related Materials, ed. H. Fritzsche, (World Scientific, Singapore, 1988) p. 296.

18. R. S. Crandall in Semiconductors and Semimetals, Vol. 21(B), ed. Pankov, (Academic, Orlando, 1984) p. 289.

19 J. Z. Liu, G. Lewen. J. P. Conde and P. Roca i Cabarrocas, J, Non Crystalline Solids, **164&165**, 383 (1993).

Chapter 3

Bulk States

Sub-gap absorption [1-4] is a fundamental process that can measure the density and the energy position of all the states in the mobility gap, provided the matrix elements of the optical transitions are known. These are usually assumed to be constant and independent of photon energy (hν). In a-Si:H, disorder gives rise to the Urbach edge [5], whereas, other defects like the dangling bonds give deep states, responsible for the absorption at smaller hν. The α associated with the absorption in the deep gap states is too small to be measured by conventional transmission method. For this, two techniques namely, constant photocurrent measurement (CPM) [1,2] and photothermal deflection spectroscopy (PDS) [3,4] are employed. Details of CPM and PDS set ups along with the procedure to obtain $\alpha(h\nu)$ from CPM and PDS spectra are given in Chapter 2.

Sub-gap absorption coefficient $\alpha(h\nu)$ measurements have been used by earlier workers to obtain the density of bulk states in a part of the mobility gap of a-Si:H, using CPM [1,2] and PDS [3,4]. However, states in the entire mobility gap using sub-gap absorption have not been obtained. In particular, the slope of conduction band Urbach edge has not been measured. Further, there is a large variation in the value of correlation energy (U)(0<U<0.5eV) [6-8] measured using various techniques, although, it is generally agreed that U is not negative [6].

Estimation of DOS using $\alpha(h\nu)$ requires the knowledge of the shape of DOS a priori. But different authors [9,10] prefer different shapes for the mid-gap states. In particular,

Gaussian [9] and exponential [10] shapes for the mid-gap states have been proposed. It is noted that using the sub-gap absorption measurements one can not obtain the shape of the mid-gap states uniquely [11,12].

We have used α_{cpm} and α_{pds} data to obtain the density and distribution of the bulk states in the entire mobility gap for lithium doped a-Si:H [a-Si:H(Li)] and phosphorous doped a-Si:H [a-Si:H(P)]. Lithium (Li) is an interstitial n type dopant in a-Si:H [13], unlike phosphorus (P) which is a substitutional. Thus, it is interesting to see whether dopings by P and by Li change the DOS in a similar manner. Also, it is worthwhile to see if the uncertainties that plague the DOS in a-Si:H(P) remain for a-Si:H(Li) as well. One such uncertainty is the position of D^- in a-Si:H(P). Street et al [9], based on luminescence and transport measurements, conclude from their "Basic Model of DOS" that the positions of the D^- peak below the conduction band edge, in a-Si:H and a-Si:H(P) are the same. On the other hand, Kocka et al [14], based on sub-gap absorption measurements, and are of the view that on doping, D^- moves towards the center of the mobility gap, because of intimate bond pair formation between dangling bonds and dopants. This is known as "Intimate Pair Bond Model" [14]. However, Li may or may not form an intimate pair with the dangling bond, as P does. Therefore the position of D^- peak in a-Si:H(Li) may be different from that in a-Si:H(P). A comparison of the two different dopings shows that these are similar as far as the density of bulk states are concerned. Further, we find that even after a careful deconvolution of sub-gap absorption data and detailed error analysis in the case of a-Si:H(Li), we can not distinguish between the models by Street et al [9] and Kocka [14], regarding the position of D^-. We try to remove this uncertainty by combining the sub-gap absorption data with the conductivity activation energy data.

In Section 3.1, we describe the principle and analysis of sub-gap absorption data to obtain DOS in a-Si:H. First we describe various shapes of the DOS distribution proposed in the literature and sub-gap transitions. Determination of slopes of Urbach edges and deep gap states are discussed then. In the next subsection, we give the analysis of DBCPM results for the determination of U and the shape of deep gap states. In Section 3.2, we study the effect of doping on the density and distribution of bulk states. Results on P and Li doped a-Si:H with various concentrations of dopants are

given. Section 3.3 gives the summary and conclusions of this Chapter.

3.1 Undoped a-Si:H

3.1.1 Principle and Analysis

3.1.1.1 DOS distribution model and sub-gap transitions

Although, it is generally agreed that the states near the band edges are exponential, various authors prefer different shapes for the deep gap states [9,10]. Two shapes namely, Gaussian [9] and exponential [10], have been proposed. The schematics of these DOS distributions are shown in Figs. 3.1 and 3.2. We discuss them one by one.

Fig. 3.1 shows a model of DOS distribution [9] for undoped a-Si:H proposed to explain many measurements including the sub-gap absorption in the literature. Also shown are the various possible optical transitions (marked T_1 to T_5). The model DOS has an exponential shallow region (Urbach energy region) and deep defect region (dangling bond states). The neutral dangling bonds (D^o) are separated from the doubly occupied dangling bond states (D^-) by correlation energy ΔE. D^o and D^- are both assumed to have the same shape and number. The Fermi level is at the minimum of the DOS, as shown in Fig. 3.1. Fig. 3.2 shows another model of DOS, with the difference from the first that the deep gap states in this case, are exponential with a slope different from those in the Urbach edge region. Similar optical transitions (T_1 to T_5) are shown in this case also.

In undoped a-Si:H, the photocurrent at room temperature is dominated by electrons. Therefore, CPM will primarily see only those optical transitions which end in the conduction band extended states, namely, transitions T_1, T_2 and T_5. The transitions T_3 and T_4, on the other hand, take the electrons to localised final states and hence are not seen by CPM. All these transitions, however, generate heat and will clearly contribute to α measured by PDS. Here, transitions from one localised state to another localised state are neglected because the matrix elements for these transitions are likely to be small. Further, CPM is insensitive to the surface states because the electron hole pairs generated at the surface quickly recombine without contributing to the photoconduct-

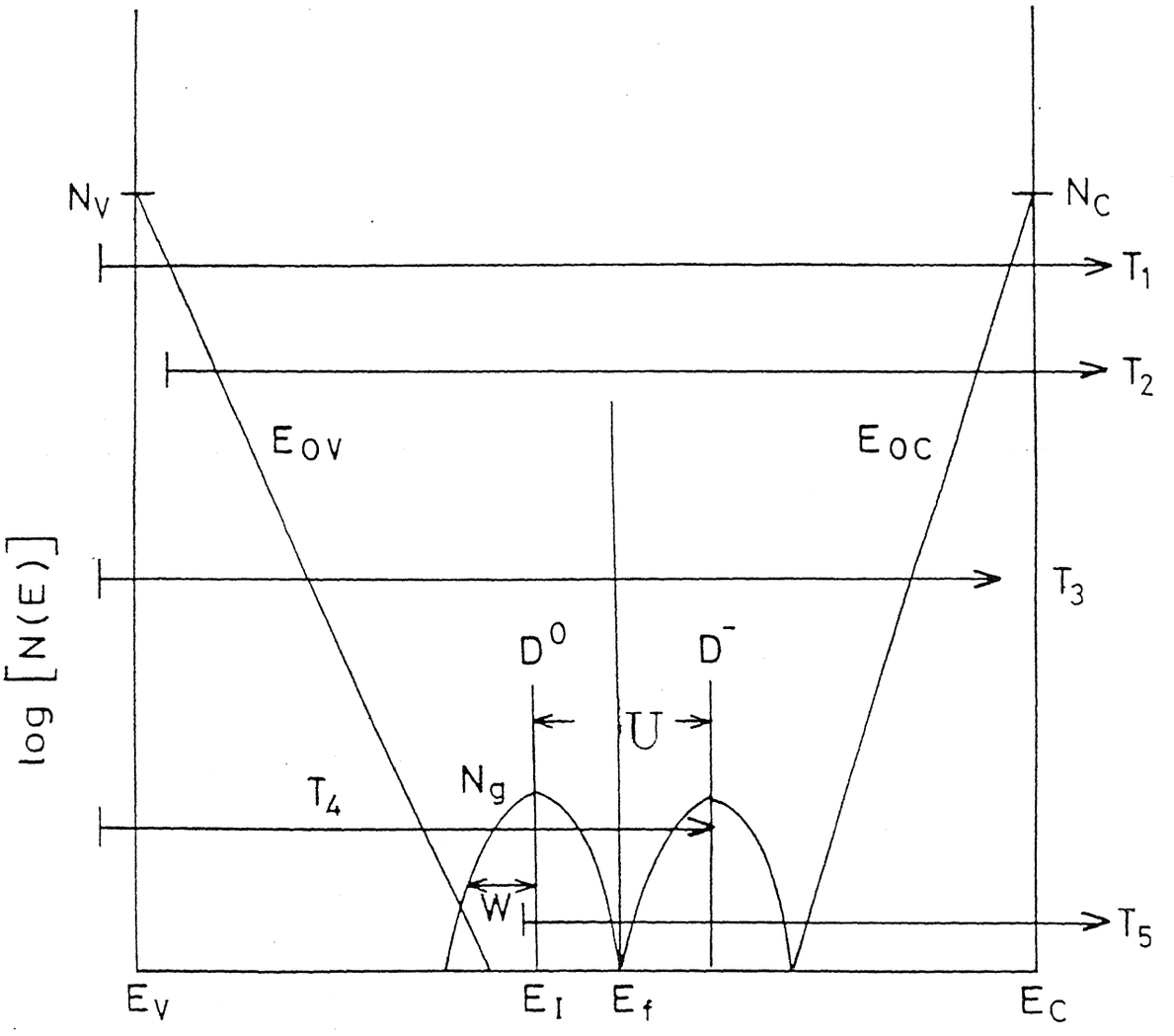

Figure 3.1: Distribution of density of bulk states[after reference 9] used in the model calculations along with the optical transitions in a-Si:H. It consists of exponential Urbach edges and Gaussian dangling bond states. PDS measurements see all the transitions T_1 to T_5 whereas CPM ignores the transitions T_3 and T_4. E_f and E_I have been measured from E_c.

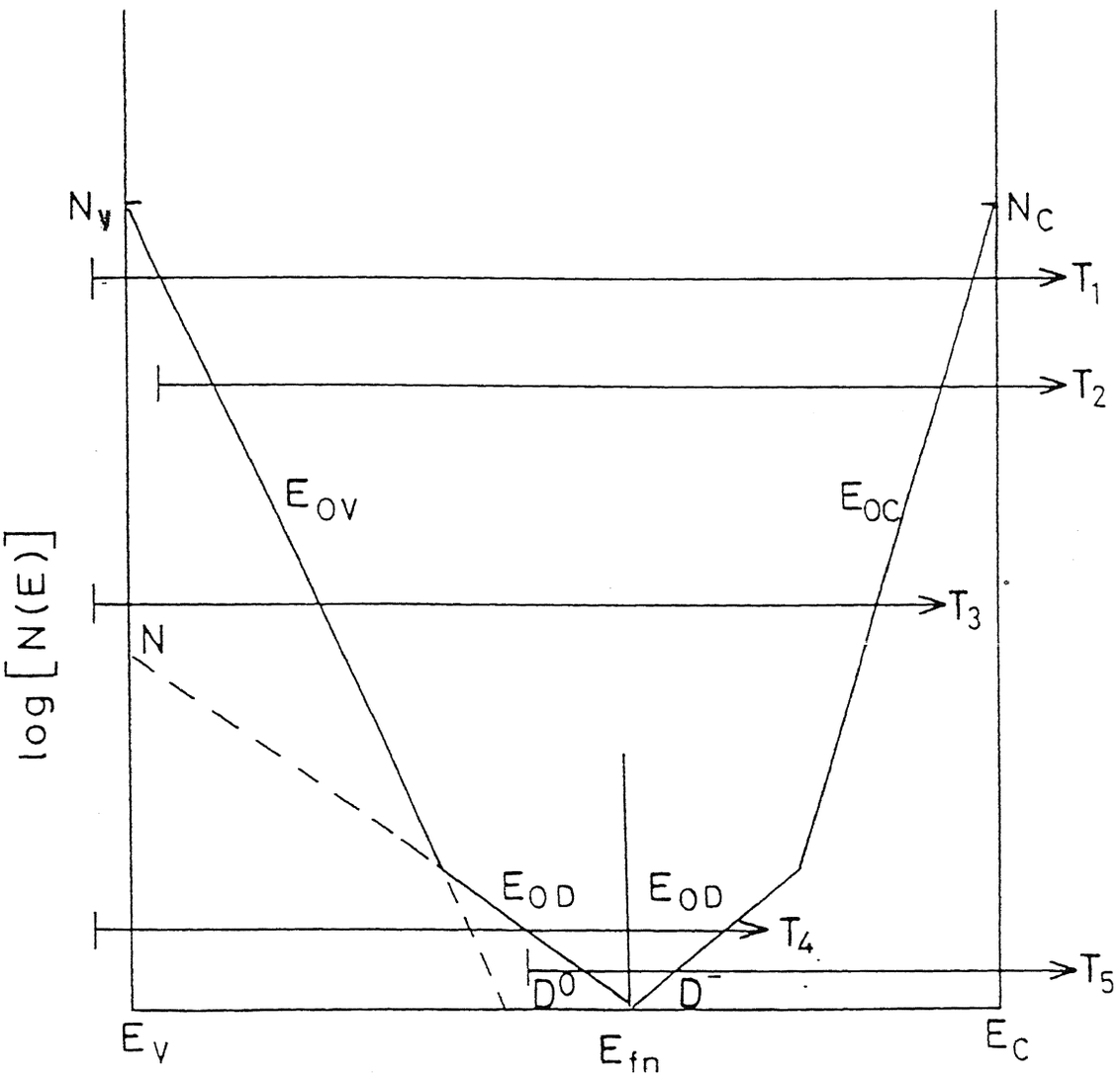

Figure 3.2: A different distribution of density of bulk states in which the density of bulk states are assumed to be exponential[after reference 10]. This DOS is also found to fit the CPM data well. E_{fn} has been measured from E_c.

ivity [15,16]. Hence, for the transitions in Figs. 3.1 and 3.2, we can write in an obvious notation

$$\alpha_{pds} = \alpha(T_1) + \alpha(T_2) + \alpha(T_3) + \alpha(T_4) + \alpha(T_5) + \alpha(T_s) \tag{3.1}$$

and,

$$\alpha_{cpm} = \alpha(T_1) + \alpha(T_2) + \alpha(T_5), \tag{3.2}$$

here, T_s refers to the transitions involving surface states (not shown in Fig. 3.1 and 3.2). Absorption attributed to the transitions T_s will be used in Chapter 4 for the determination of density of surface states in a-Si:H. Thus, various regions of absorption in CPM and PDS spectra shown in Fig. 3.3 may be represented by the following transitions:

Region I:

$$\alpha_{pds} = \alpha_{cpm} = \alpha(T_1). \tag{3.3}$$

Region II:

$$\alpha_{pds} = \alpha(T_2) + \alpha(T_3), \tag{3.4}$$

and,

$$\alpha_{cpm} = \alpha(T_2). \tag{3.5}$$

Region III

$$\alpha_{pds} = \alpha(T_4) + \alpha(T_5) + \alpha(T_s), \tag{3.6}$$

and,

$$\alpha_{cpm} = \alpha(T_5). \tag{3.7}$$

3.1.1.2 Determination of Slopes of Urbach edges

In region II (Fig. 3.3), known as the Urbach edge region, α_{cpm} is attributed to the transitions (Transitions T_2) from the localised valance band Urbach edge states to the conduction band extended states (T_2 in Figs. 3.1 and 3.2). The absorption curve can be fitted to an exponential curve [5]

$$\alpha_{urbach} = \alpha_o \, exp(h\nu/E_{ov}), \tag{3.8}$$

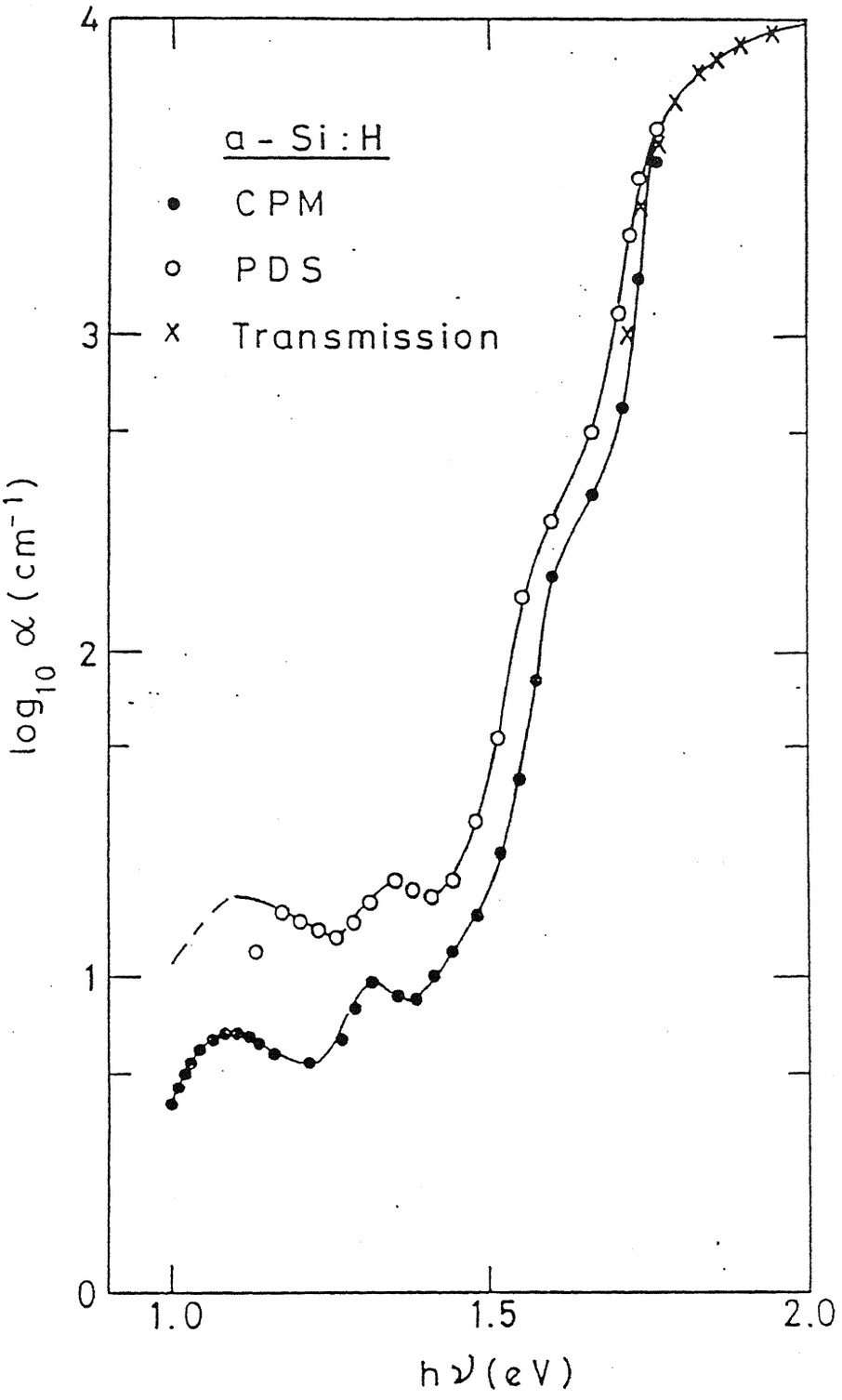

Figure 3.3: log α as a function of hν as measured by CPM (filled circles), PDS (open circles) and Transmission (crosses) for an undoped a-Si:H sample. Peaks in the curves arise from interference effects.

where, E_{ov} is the slope of valance band Urbach edge. In this region, α_{pds} is more than α_{cpm}. This is because of the additional transitions from VB extended states to the conduction band Urbach edge localised states (T_3, Figs. 3.1 and 3.2). It is clear from Eqs. (3.4) and (3.5) that, if the plot of $\log(\alpha_{pds} - \alpha_{cpm})$ as a function of $h\nu$ is a straight line (corresponding to the transition T_3), its slope gives E_{oc}.

3.1.1.3 Determination of Deep Gap States

a. Gaussian shape of mid-gap states (Fig. 3.1)

In the one electron approximation, the absorption coefficient $\alpha(h\nu)$ for transitions from initial states g_i to the final states g_f is given by the relation [17]:

$$\alpha(h\nu) = \frac{C}{h\nu} \int g_i(\epsilon) f(\epsilon)\ g_f(\epsilon + h\nu)[1 - f(\epsilon + h\nu)] d\epsilon. \tag{3.9}$$

The integration is carried over all the initial states $g_i(\epsilon)$ and final states $g_f(\epsilon + h\nu)$ separated by the energy $h\nu$. f is the Fermi Dirac function. We take zero temperature statistics and hence, the states above the Fermi level are taken to be empty ($f(\epsilon) = 0$) and the states below the Fermi level are filled ($f(\epsilon) = 1$). The factor C contains the spectral dependence of dipole matrix element which have been shown [18] to be a weak (within a factor of 2) function of $h\nu$ for transitions from localised states as well as extended states. C is taken to be a constant for transitions between the localised states to the extended states and also for the transitions between the extended states to the extended states. The constant C can be estimated by considering the transitions from the extended valance band states to extended conduction band states and assuming these states to be parabolic. It is further assumed that g(ϵ) at the band edges is given by free electron density of states ($6.7 \times 10^{21} cm^{-3} eV^{-1}$) [2]. Hence.

$$g_i(\epsilon) = 6.7 \times 10^{21}\ (\epsilon)^{(1/2)} = g_f(\epsilon), \tag{3.10}$$

where, ϵ is the difference between the energy of the states from the band edge. So, for the band to band transitions Eq. (3.9) gives [12]

$$\alpha(h\nu) = \frac{C}{h\nu}(6.7 \times 10^{21})^2 \int_o^{h\nu - E_{opt}} \epsilon^{1/2}\ (h\nu - E_{opt} - \epsilon)^{1/2}\ d\epsilon. \tag{3.11}$$

Thus measurement of α for $h\nu > E_{opt}$ gives an estimate of C using Eq. (3.11). It is evident from the Eq. (3.11) that α is a convolution of all the initial states and the final states, which obey the conservation of energy. So, to get information about DOS in the mobility gap we have to assume the shape of DOS a priori. The plateau region in $\alpha(h\nu)$ curve (region III in Fig. 3.3) is because of the transitions from Gaussian D^o level to the CB extended states (transition T_5) in Fig. 3.1. Under this assumption, g_i is given by the relation:

$$g_i(\epsilon) = N_g \; exp[-(E_I - h\nu)^2/2W^2], \tag{3.12}$$

where N_g is the height of the Gaussian peak, E_I is the position of the peak below the conduction band edge and W is the half width of the distribution. Using this distribution of DOS, Eq. (3.9) reduces to:

$$\alpha_{diff}(h\nu) = \frac{C}{h\nu}\; 6.7 \times 10^{21} N_g \int_a^b exp[-\frac{(\epsilon + E_I - h\nu)^2}{2W^2}]\epsilon^{1/2} d\epsilon, \tag{3.13}$$

where integration limits (a,b) is taken from 0 to a reasonable value 2eV [1] and $\alpha_{diff}(h\nu)$ = $\alpha(h\nu)$ - extrapolated value of α from region II (Fig. 3.3). α_{diff} is calculated using Eq. (3.13) in the region III (Fig. 3.3), taking $g(E_I)$, W and E_I as parameters. The best fit between the experimental and calculated values gives the fit parameters.

b. Exponential shape of mid-gap states (Fig. 3.2)

For the exponential distribution of the mid-gap states (Fig. 3.2), $g_i(\epsilon)$ is given as

$$g_i(\epsilon) = N exp(-\frac{E_{opt} - \epsilon}{E_{OD}}), \tag{3.14}$$

where, N is the extrapolated value of the mid-gap states at the valance band mobility edge and E_{oD} is the slope of deep states. For this distribution of the deep states Eq. (3.11) becomes

$$\alpha_{diff}(h\nu) = \frac{C}{h\nu}(6.7 \times 10^{21}) N \int_0^{E_{fn}} exp[-\frac{(\epsilon - E_{opt} + h\nu)}{E_{oD}}]\epsilon^{1/2} d\epsilon. \tag{3.15}$$

The parameters N, E_{oD} and E_{fn} are obtained from the best fit between the experimental α_{diff} and the calculated α_{diff}.

3.1.1.4 Dual Beam CPM Measurements

a. Principle and theory

Dual beam CPM [6] is ac CPM (using chopped light) in the presence of a strong dc (unchopped) light. The weak light from a monochromator, chopped at a frequency between 5Hz and 333Hz, is the probe beam. The strong dc light is the pump beam. The details of the experimental set up are given in Section 2.5. Fig. 3.4 shows normalised spectra measured by dc CPM (curve 1), and DBCPM with the weak light chopped at 333Hz (curve 2), 33Hz (curve 3), 9Hz (curve 4) and 5Hz (curve 5) respectively for photon energies 0.8eV to 1.8eV. All these spectra are normalised to the same value of α in the region of photon energy $1.8 < h\nu < 1.6eV$, obtained from the transmission measurements [19].

DBCPM spectra (Fig. 3.4) has two interesting features. First, the spectra at 5Hz chopping frequency has a prominent hump at low photon energy ($h\nu \leq 1.0eV$), which decreases with increasing chopping frequency. Second, there is a strong dependence of the entire DBCPM spectrum on the chopping frequency.

We first explain the hump in DBCPM spectra at low chopping frequency. Upon measuring the dual beam spectrum using PDS, on the same sample, at the same frequency, we find that the hump is absent (DBPDS data not shown) [6]. This indicates that the hump may not be true absorption and may arise because of a change in ac photoconductivity in the presence of dc light [6]. Therefore, we first discuss the dual beam photoconductivity in a-Si:H. It is assumed that the pump beam is so intense that the defect states lie within the quasi Fermi levels, E_{fn} and E_{fp} as shown in Fig. 3.5.

In DBCPM, the excess electrons in the conduction band generated by the chopped light, in the presence of the pump beam, are given by [6]

$$n = G\tau = \alpha F\tau, \tag{3.16}$$

where, τ is the recombination life time for the strong d.c. pump beam alone and G is the generation rate from the pump light and F is the intensity of the weak chopped light. Differentiating Eq. (3.16), we get:

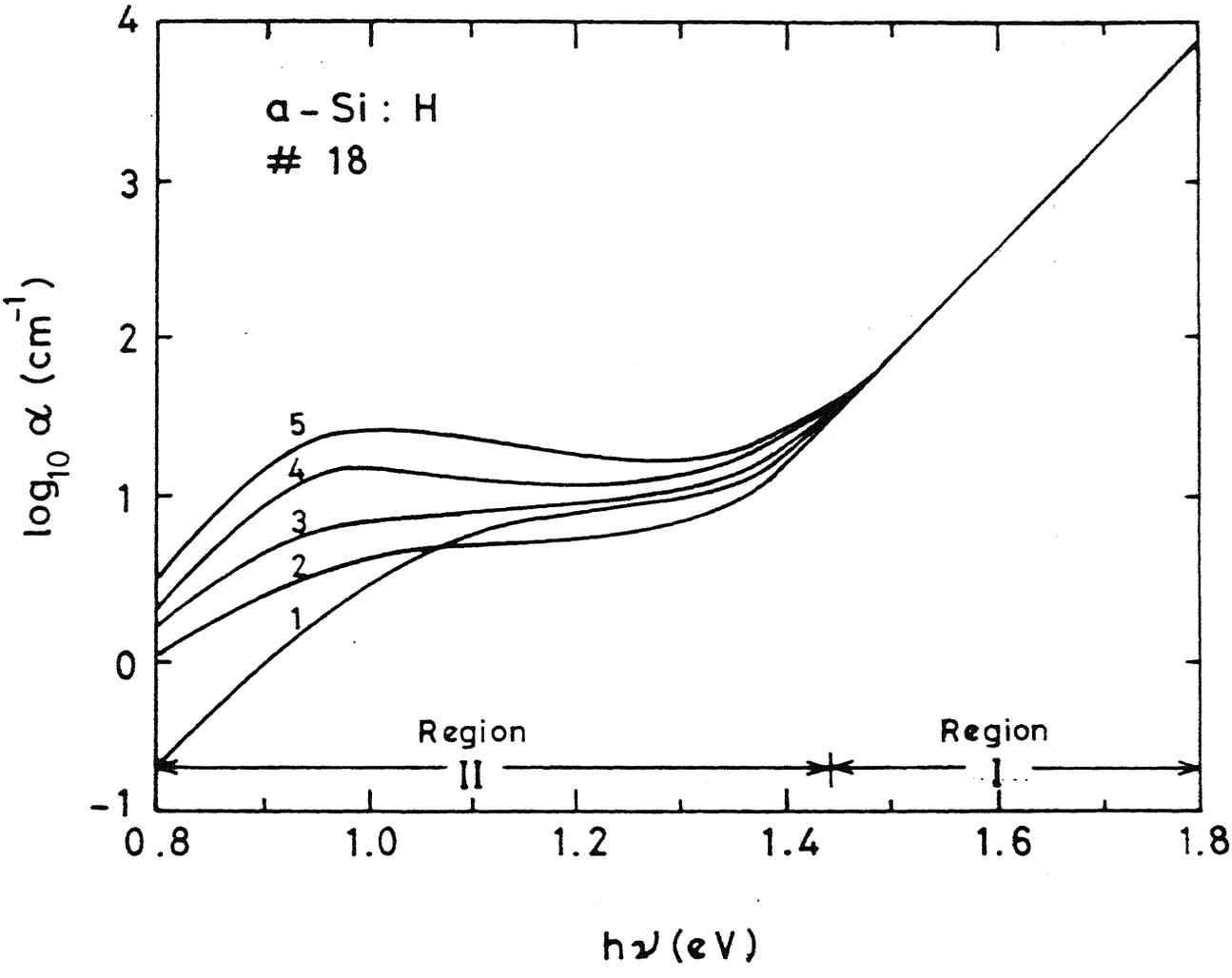

Figure 3.4: Absorption coefficient α as a function of hν obtained by dc CPM (curve 1), DBCPM with the weak (probe) light chopped at 333Hz (curve 2), 33Hz (curve 3), 9Hz (curve 4) and 5Hz (curve 5), for an undoped a-Si:H (Sample No. 18).

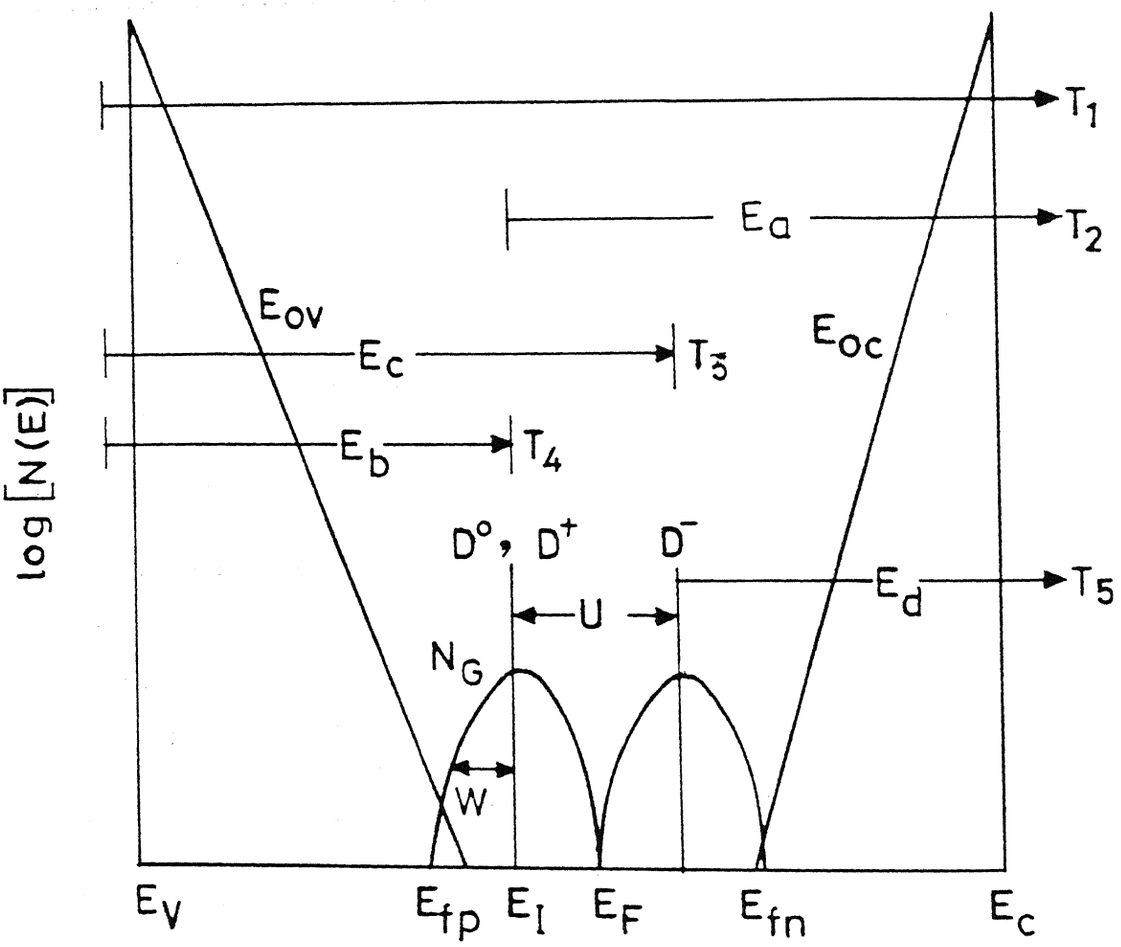

Figure 3.5: A schematic of density of localised states in undoped a-Si:H along with the optical transitions in the dual beam configuration. E_{fn} and E_{fp} are electron and hole quasi Fermi levels respectively (after reference 6).

$$\Delta n = G\Delta\tau + \alpha\Delta F\tau, \tag{3.17}$$

where, $\Delta\tau$ is the change in the recombination life time due to the weak chopped light, ΔF is the intensity of the weak chopped light. The hump in DBCPM spectra at low frequencies of chopping can be understood if $\Delta\tau$ has two components. We write

$$\Delta\tau = \Delta\tau_1 + \Delta\tau_2. \tag{3.18}$$

We discuss $\Delta\tau_1$ first. $\Delta\tau_1$ is identified with the known power law of photocurrent ($I_{ph} \propto F^{\gamma}$), with $\gamma \leq 1$, for a-Si:H [20]. Therefore for $\Delta\tau_1$ part,

$$\Delta\tau_1 \propto \frac{(\gamma - 1)}{\alpha} F^{\gamma-2}\Delta F, \tag{3.19}$$

or,

$$G\Delta\tau_1 = (\gamma - 1)\alpha\tau\Delta F, \tag{3.20}$$

Hence, from Eqs. (3.17), (3.18) and (3.20), we get :

$$\Delta n = G\Delta\tau_2 + \gamma\alpha\tau\Delta F. \tag{3.21}$$

If $\Delta\tau_2 = 0$, Eq. (3.21) correctly yields α, as in CPM. But the observation of hump suggests that $\Delta\tau_2 \neq 0$. We postulate that $\Delta\tau_2$ results from a change in the occupation of recombination centers through excitations by the probe light between the defect states and the conduction and valance band. The hump, therefore, requires two additional transitions in DBCPM, which are insignificant in single beam CPM. These transitions are identified as follows:

Fig. 3.5 shows schematic density of states along with the optical transitions (T_1 to T_5), in the dual beam configuration. For this discussion we have chosen the Gaussian distribution of deep states. Transitions T_4 (Fig. 3.5), with a lower onset energy convert some of the D^+ states to D°. This increases the photocurrent because, for electrons. D^+ is about 10 times more efficient recombination centers [18] than D°. Transitions T_2 with a higher onset energy, on the other hand, change some of the D° to D^+ and decrease the photocurrent. This explains the hump in the DBCPM spectrum.

b. Determination of correlation energy (U)

The correlation energy (U) can be obtained by analysing the DBCPM spectra at high chopping frequency (333 Hz). At this frequency of chopping, the second term in Eq. (3.17) dominates and the first term is insignificant, because the hump in the DBCPM spectrum disappears. DBCPM spectrum at 333Hz arises from the transitions from the filled D^- states to the conduction band extended states (T_5, Fig. 3.5). A fit between the experimental and calculated $\alpha(h\nu)$ gives the characteristic energy (E_d) of the transitions T_5. This gives $U = E_a - E_d$, where E_a is the characteristic energy for the transitions T_2 (Fig. 3.5) and has been obtained from the analysis of dc CPM spectrum.

c. Shape of mid-gap States

In the above calculations we have used Gaussian distribution of DOS [9] (Fig. 3.5). However, another shape of the DOS (exponential) (Fig.3.2) has also been suggested [10]. We use the two DOS to fit dc CPM and DBCPM data to see which shape fits our data. The parameters N_G, W and E_a (Fig. 3.5) are varied to get best fit between the experimental $\alpha_{diff}(h\nu)$[= α in region II - $\alpha_o exp(-h\nu/E_o)$ extrapolated in region II (Fig. 3.4)] and the calculated α_{diff}, for dc CPM curve. We get a good fit between the two. Also, good fit is obtained for exponential shape of DOS. We are, therefore, unable to determine the distribution of DOS uniquely from the CPM measurements. A similar conclusion was reached by Payson and Guha [11], for their PDS results. Although, a Gaussian distribution for the mid-gap states explains the luminescence, time of flight and junction measurements [9], it remains to be seen whether some other distribution of DOS also fits the observed results.

We now fit DBCPM data at 5 Hz chopping frequency using the Gaussian and exponential shapes of DOS. The hump at low photon energy (Fig. 3.4) is attributed to the transitions T_2 and T_4 (Fig. 3.5), as discussed in the Section 3.1.1.4a. The first term in Eq. (3.21) is the dominant term for DBCPM spectra obtained for low frequency of chopping (5 Hz). An expression for the $\Delta\alpha$ (= α_{dbcpm} at 5Hz - α_{cpm}), in region II (Fig. 3.4) can be written as :

$$\Delta\alpha = A[\int_{E_b-2W}^{h\nu-E_b} exp(-\epsilon^2/2W^2)d\epsilon - \int_{E_a-h\nu}^{E_a-2W} exp(-\epsilon^2/2W^2)d\epsilon], \qquad (3.22)$$

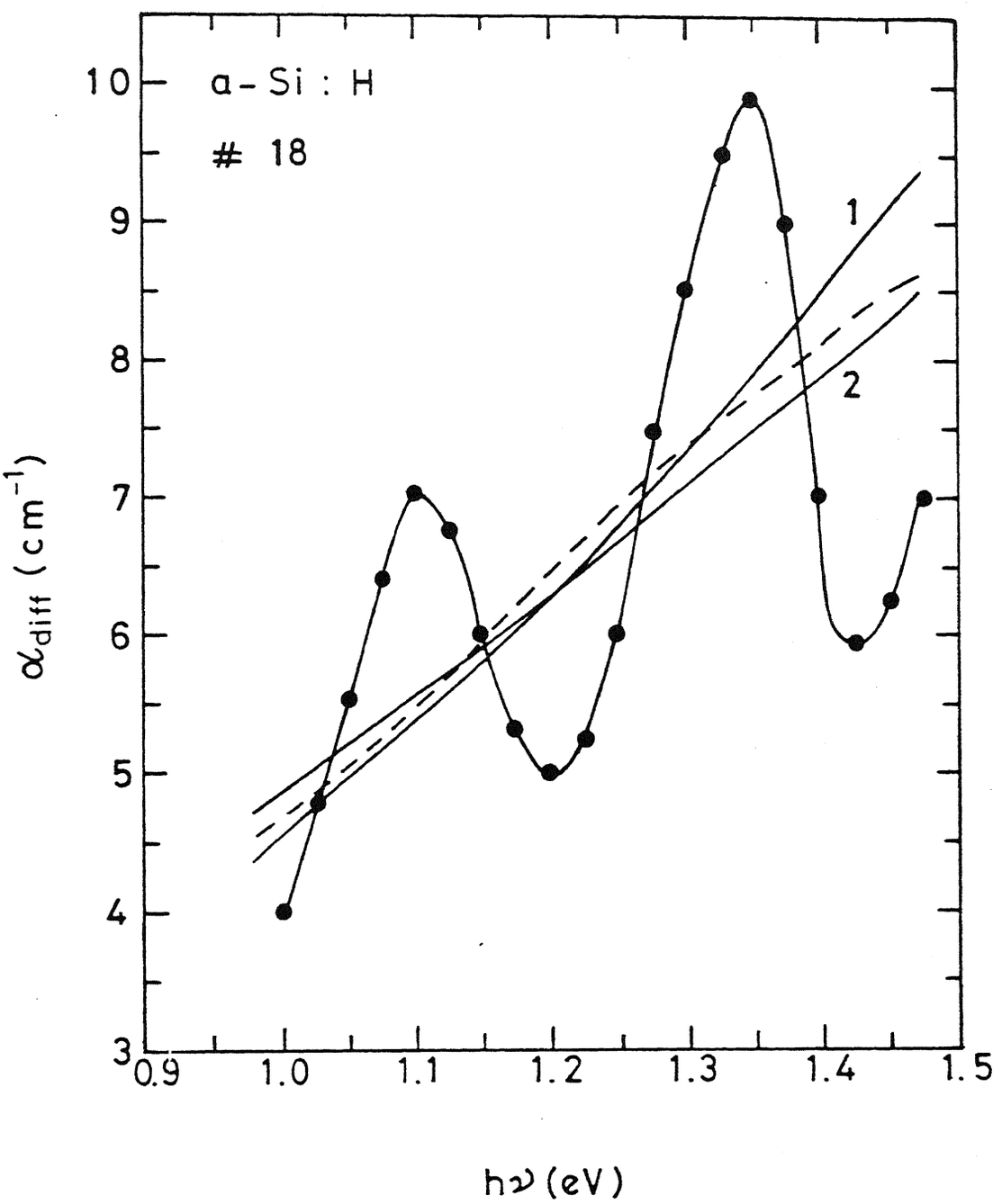

Figure 3.6: The peaks in the experimental data (o o o) are from interference effects. These are averaged to obtain the mean experimental curve (- - -). Curve marked 1 and 2 are theoretically calculated using Gaussian and exponential deep states, respectively.

where, E_a and E_b are the characteristic energies for the transitions T_2 and T_4 respectively (Fig. 3.5). A is the constant of proportionality. The first term in Eq. (3.22) is proportional to the net number of D^+ changing to D^o and therefore, represents the increase in photocurrent because of the presence of pump light. Similarly, the second term is proportional to D^o changing to D^+, and represents the decrease in photocurrent. We already know E_a, N_G and W from the deconvolution of DC CPM spectrum. Hence, from the best fit between the theoretical and experimental $\Delta\alpha$, we get E_b which is the characteristic energy of the transitions T_4. It may be mentioned that $E_a + E_b = E_g$, the band gap of the material. E_g has been obtained from transmission measurements (Section 2.4) [19], also. This gives a check to the analysis.

$\Delta\alpha$ can be calculated for the exponential shape of the deep gap states (Fig. 3.2), using the following relation :

$$\Delta\alpha = C\{\int_{E_v-E_{fp}}^{h\nu} exp(-\epsilon/E_{oD})d\epsilon - \int_{E_v-h\nu}^{E_v-E_F} exp(-\epsilon/E_{oD})d\epsilon\}, \qquad (3.23)$$

where, C is the constant of proportionality. The Fermi level split is taken to be the same as in the case of Gaussian shape of deep gap states. This gives $E_F - E_{fp} \approx 0.25eV$. Hence, in this case there is no other fit parameter.

3.1.2 Results and Discussion

Slopes of Urbach edges

Fig. 3.7 shows $\alpha(h\nu)$ measured by transmission ($h\nu > 1.6eV$), CPM and PDS (in the region II and III). This figure is the same as Fig. 3.2, but the interference fringes have been averaged out. For all the CPM and PDS spectra from now onwards, we will show the fringes averaged out. For $1.8eV > h\nu > 1.45eV$ (region II) the CPM curve can be fitted to an Urbach tail with E_{ou} = 52±5meV [Eq. (3.10)]. Fig. 3.8 shows $\log(\alpha_{pds}(h\nu)$ - $\alpha_{cpm}(h\nu))$ plotted as a function of $h\nu$ in region II. E_{oc} is found to be 28 ±5meV.

Mid-gap states

$\alpha_{diff}(h\nu) = \alpha_{cpm}(h\nu) - \alpha_o exp(-h\nu/E_{ou})$ in the region III of Fig. 3.7, is calculated using the method discussed in Section 3.1.1.3 for various choices of the Gaussian deep

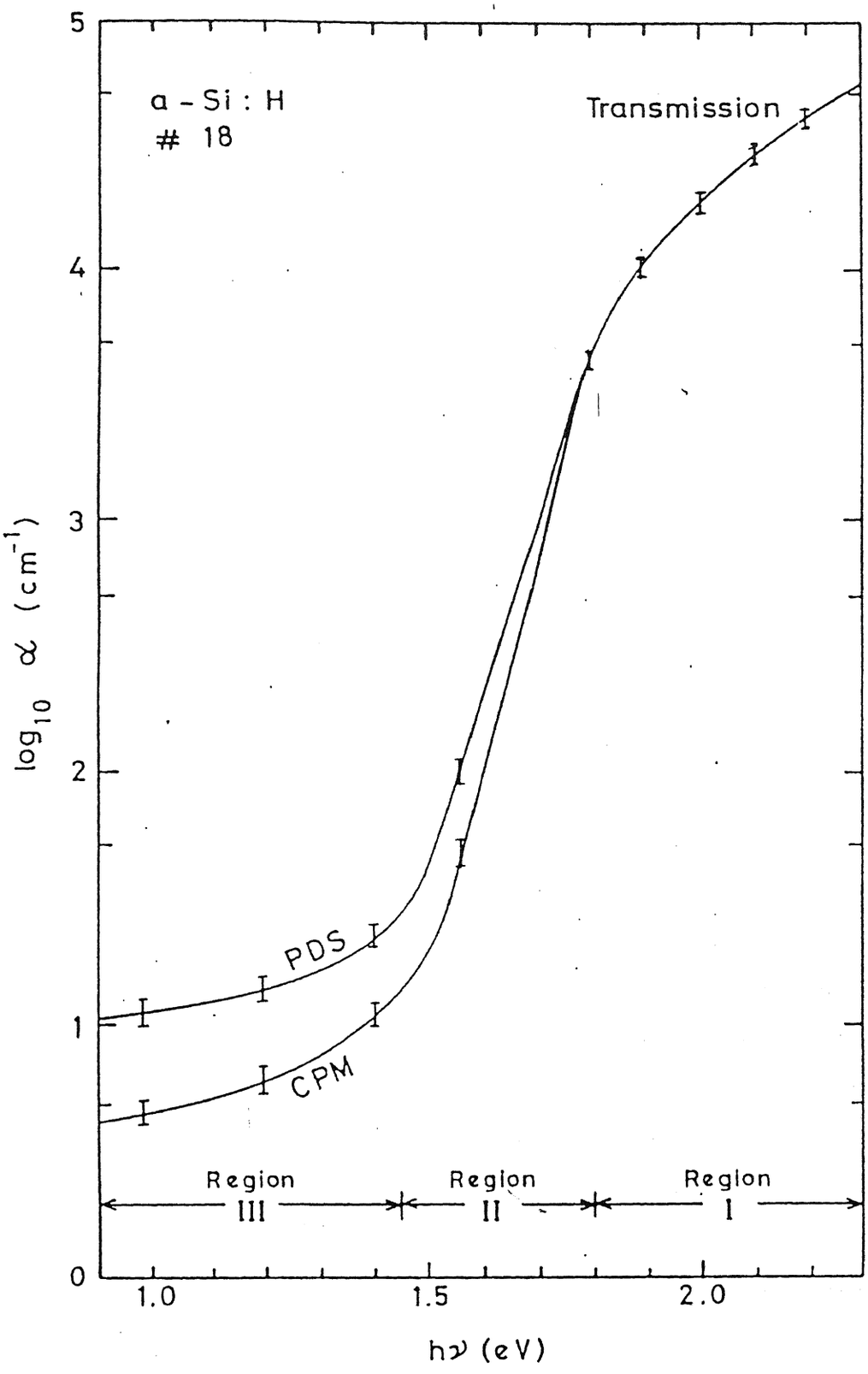

Figure 3.7: $\alpha(h\nu)$ measured using CPM and PDS, for the same sample shown in Fig. 3.3. The interference fringes in the curves have been averaged out.

gap states parameters N_G, W and E_I. The best fit between the experimental and calculated α_{diff} gives values of N_G, W and E_I. C, calculated using Eq. (3.11), is found to be 2×10^{-38}. This compares favorably with the reported value [1,2]. Here E_{opt} is taken to be 1.8eV as calculated by the Tauc's plot [21] (Section 2.3.3). The following parameters are obtained for Gaussian deep gap states (Fig. 3.1),

$$N_G = (1.8 \pm 0.5) \times 10^{18} cm^{-3} eV^{-1}$$

$$E_I = (1.0 \pm 0.05) eV$$

$$W = (0.14 \pm 0.01) eV$$

For the exponential shape of deep gap states (Fig.3.2), a satisfactory fit between calculated and experimental α_{diff} is found for the following DOS parameters:

$$N = 4.0 \times 10^{18} cm^{-3} eV^{-1},$$

$$E_{oD} = 0.3 eV,$$

and,

$$E_{Fn} = 0.6 eV.$$

α_{diff} calculated using the two shapes of mid-gap states along with the experimental points are plotted in Fig. 3.8.

Correlation Energy (U)

Section 3.1.1.4 gives how analysis of DC CPM and DBCPM with ac light chopped at 333Hz can be used to get characteristic energies E_a and E_d for transitions T_2 and T_5 respectively (see Fig. 3.5). We find E_a and E_d to be 0.10 ± 0.03eV and 0.85 ± 0.03eV respectively. This gives correlation energy U = 1.0 - 0.85 = 0.15 ± 0.06eV.

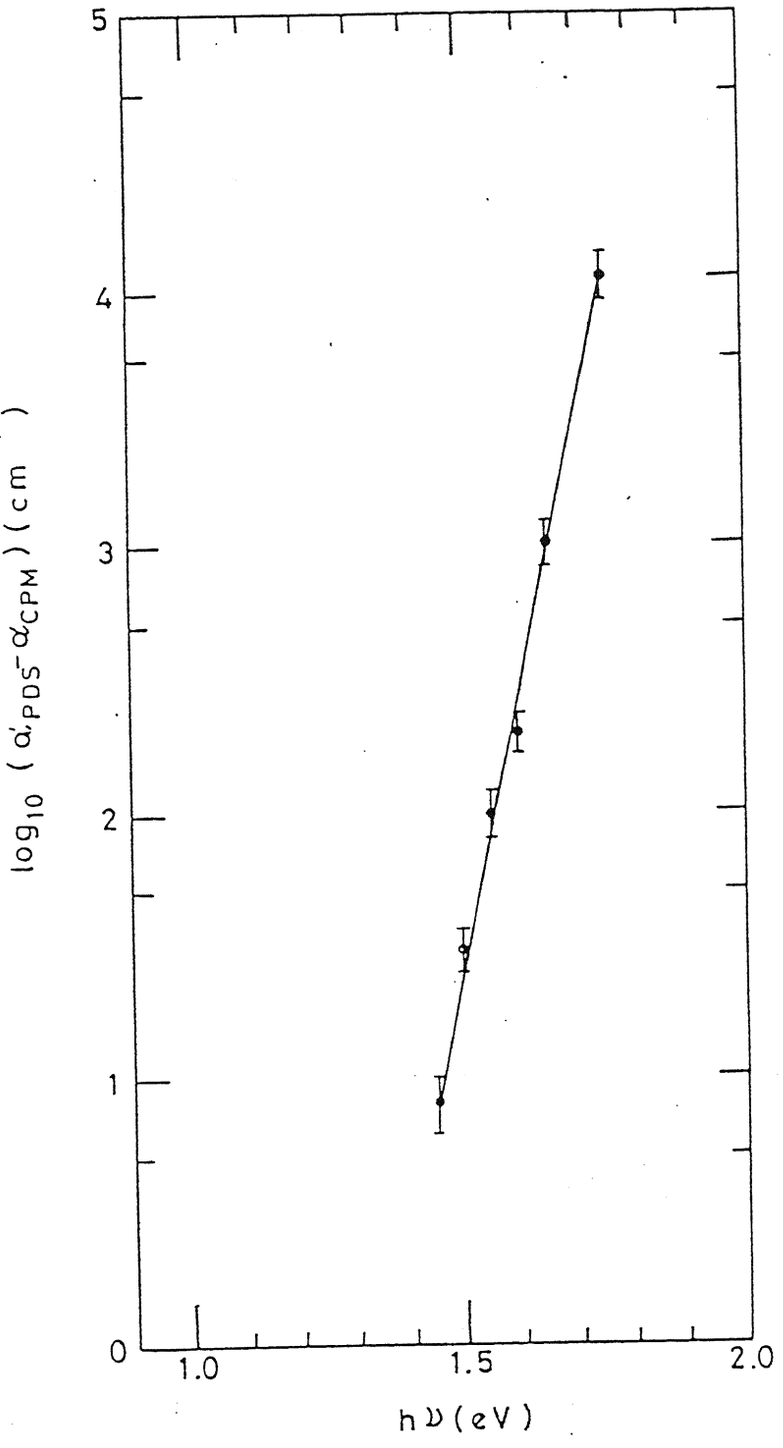

Figure 3.8: $\log(\alpha_{PDS} - \alpha_{CPM})$ plotted as a function of photon energy in the Urbach edge region. The slope gives E_{oc}.

Shape of deep gap states

As discussed above both Gaussian and exponential mid-gap states fit $\alpha(h\nu)$ data satisfactorily. We are, therefore, unable to determine the distribution of DOS from CPM measurements alone. As discussed in Section 3.1.1.4, $\Delta\alpha$ is calculated for Gaussian as well as exponential deep gap states using Eqs. (3.18) and (3.19) respectively. Fig. 3.9 shows $\Delta\alpha$ as a function of hν obtained experimentally as well as calculated using Gaussian and exponential shapes of the deep defect states. For the Gaussian shape the fit parameters are $E_a = (1.0\pm.03)$eV and $E_b = (0.80\pm.03)$. This gives the band gap, $E_g = E_a + E_b = 1.8 \pm 0.06$eV. which compares well with the values calculated for the sample using transmission measurement [19]. This gives confidence in our analysis. The absence of a good fit, between the experimental and the theoretical values of $\Delta\alpha$ for the exponential shape of deep defect states leads us to believe that the hump in the DBCPM spectra can not be explained using the exponential shape of the deep defect states. Therefore, using a combination of DC CPM and the DBCPM spectra, we have been able to distinguish between the two shapes of the deep defect states and our data prefer the Gaussian shape.

3.2 Effect of Doping on Bulk States

3.2.1 Principle and Analysis

3.2.1.1 DOS distribution and sub-gap Transitions

Fig. 3.10 shows a schematic of the distribution of DOS for a-Si:H doped n type doped [9] along with the optical transitions (T_1 to T_4). Not shown in the figure are the transitions to and from the surface states (T_s). Therefore, we can write as before, in the case of undoped a-Si:H (Section 3.1.1.1):

$$\alpha_{PDS} = \alpha(T_1) + \alpha(T_2) + \alpha(T_3) + \alpha(T_4) + \alpha(T_s) \tag{3.24}$$

$$\alpha_{CPM} = \alpha(T_1) + \alpha(T_2) + \alpha(T_4). \tag{3.25}$$

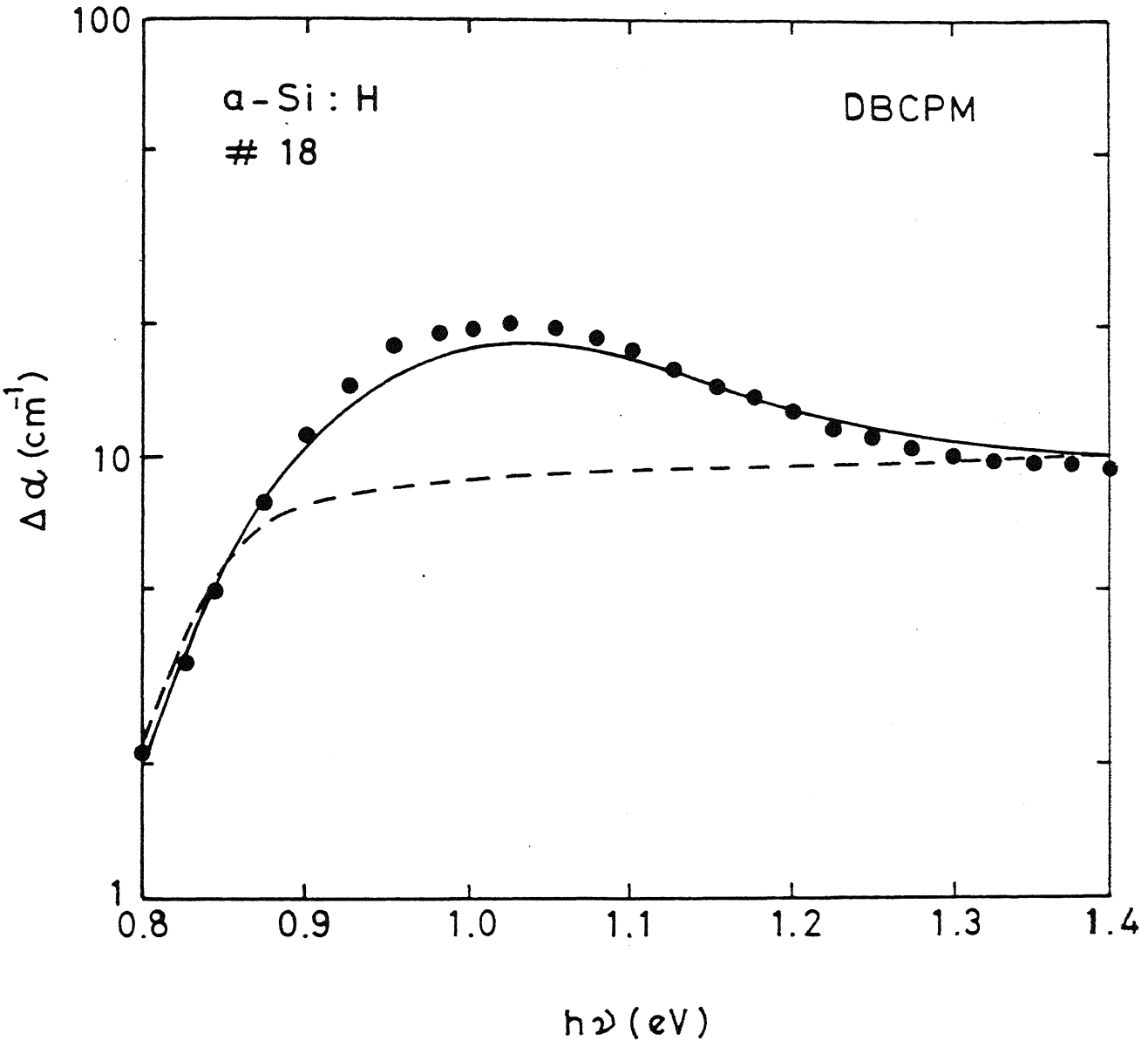

Figure 3.9: $\Delta\alpha$ (= α_{DBCPM} at 5 Hz - α_{CPM}), plotted as a function of photon energy. Solid circles are the experimental points, solid line is the theoretical fit using the Gaussian and dotted line is the theoretical fit using exponential shape of the deep gap states.

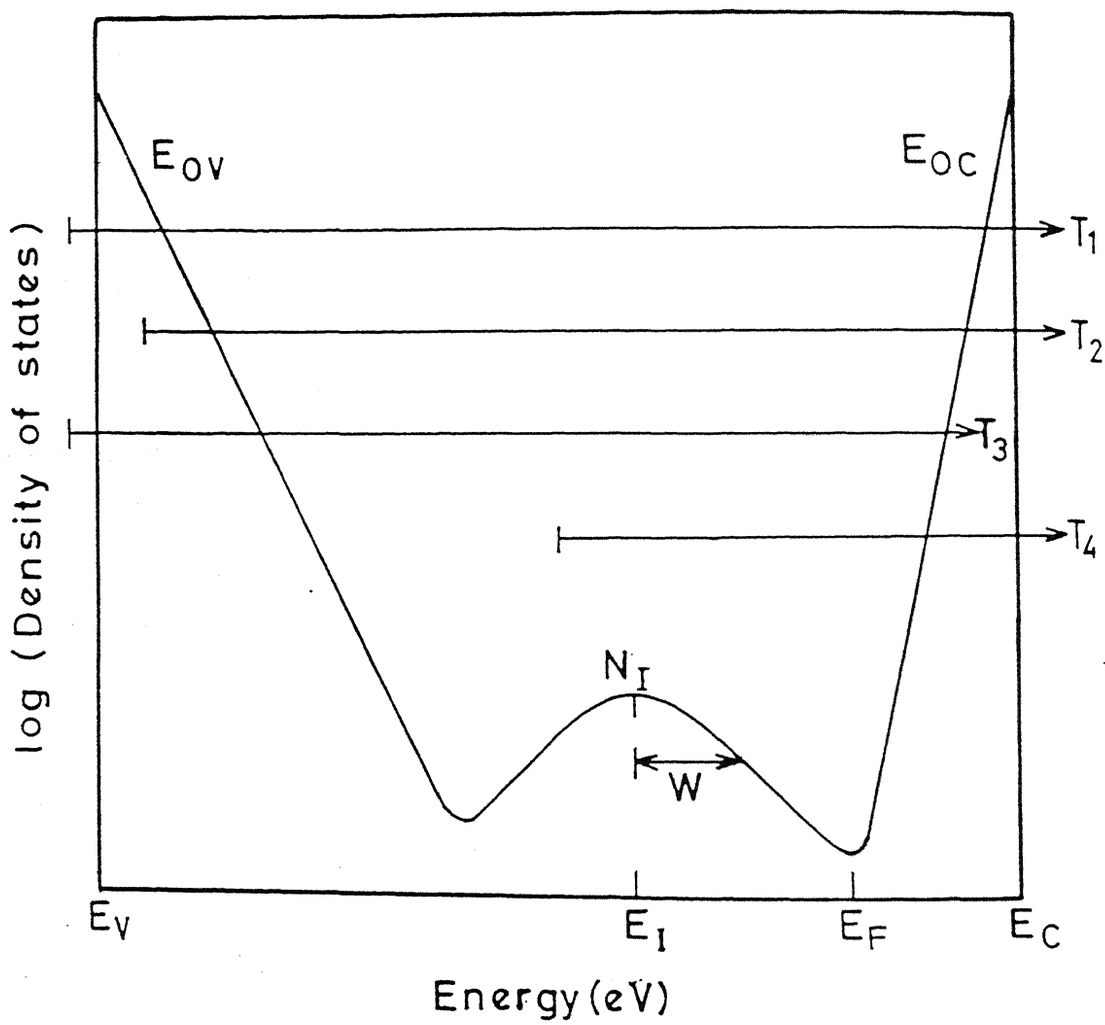

Figure 3.10: Distribution of density of bulk states used in the model calculations along with the optical transitions in n type doped a-Si:H. It consists of exponential valence band and conduction band Urbach edges with slopes E_{ov} and E_{oc} respectively. PDS measurements see all the transitions T_1 to T_4 whereas CPM ignores the transitions T_3 [after reference 9].

3.2.1.2 Determination of Slopes of Urbach edges

Slopes of valance band and conduction band Urbach edges in doped a-Si:H are determined using the procedure given in Section 3.1.1.2.

3.2.1.3 Determination of Deep Gap States

Deep gap states are determined by the deconvolution of $\alpha_{cpm}(h\nu)$ for photon energies $<$ 1.5eV. The procedure is the same as discussed in Section 3.1.1.3 for undoped a-Si:H.

3.2.1.4 Position of D^- in a-Si:H(Li)

In the "Basic Model" of Street et al [9], D^- in a-Si:H(P) is separated from D^o in undoped a-Si:H by a correlation energy (U) of $\approx$ 0.15eV. On the other hand, in the "Intimate Pair Bond Model" by Kocka et al [14] D^o in undoped a-Si:H and D^- in a-Si:H(P) are located at the same position, because doping creates predominantly intimate pairs of Si-dangling bonds with dopants. The energy of these pairs lie deeper (measured from CB) than the energy of isolated Si dangling bonds.

As discussed in Section 3.1.1, we can obtain the position of D^- states (E_I), W and $N(E_I)$ by deconvolution of $\alpha_{cpm}(h\nu)$. An error analysis is done for determining of E_I accurately, as described below. Error (e) = $\sum$ (calculated value of α_{diff} - measured value of α_{diff} at several points)^2 is plotted as a function of E_I for various values of W. $N(E_I)$ is kept constant. An absolute minimum in these curves gives the value of E_I. In spite of careful analysis, we are not able to distinguish between the models of Street et al, and Kocka et al, because both models are within error bars. In order to resolve this issue, we measure the position of the Fermi level in these samples by measuring E_σ, the activation energy of dark conductivity. E_σ can be taken to be approximately E_c - E_F, within 10meV or so [22]. The equality is not strictly valid because there may be a statistical shift of Fermi level as well as other effects. It is clear from Fig. 3.10 that the DOS at the Fermi level $g(E_F)$ for a-Si:H(Li) can be written as

$$g(E_F) = 2N_I exp[-(E_I - E_\sigma)^2/(2W^2)]. \qquad (3.26)$$

It is seen from Eq. (3.22) that the value of $g(E_F)$ strongly depends upon E_I. We

Table 3.1: DOS parameters (E_{ov}, N_I, E_I, W and E_{oc}) for a-Si:H(Li) with two Li concentrations and a-Si:H(P) with two P concentrations.

Sample details	E_σ (eV)	E_{ov} (meV)	N_I $\times 10^{-18}$ $(cm^{-3}eV^{-1})$	E_I (eV)	W (eV)	E_{oc} (meV)
a-Si:H(Li)(#1)	0.45	70±5	1.5±.1	0.92±.06	0.17±.005	32±5
a-Si:H(Li)(#2)	0.38	90±5	3.1±.1	0.95±.06	0.18±.005	34±5
a-Si:H(P)(#5)	0.30	85±5	3.0±.1	0.88±.06	0.185±.005	32±5
a-Si:H(P)(#15)	0.28	90±5	3.2±.1	0.85±.06	0.185±.005	30±5

calculate the value of $g(E_F)$ taking the value of E_I assuming the Street's model and Kocka's model to be correct. The value of $g(E_F)$ under preferred model will be in agreement with that obtained from other methods of determining $g(E_F)$ [23].

3.2.2 Results and Discussion

3.2.2.1 Lithium doped a-Si:H(Li)

Figs. 3.11 and 3.12 show $\alpha(h\nu)$ for a-Si:H(Li) measured by CPM and PDS for samples #1 and #2 respectively. The interference fringes have been averaged out [22]. The sample #2 (E_σ = 0.38eV) has a higher Li concentration than the sample #1 (E_σ = 0.45eV), as is clear from the E_σ value.

Slopes of Urbach edges

The slope of the valance band Urbach edge (E_{ov}) is determined by Eq. (3.10) in region I (Figs. 3.11 and 3.12). E_{ov} is found to be (70 ± 5)meV and (90 ± 5)meV for samples #1 and #2 respectively.

Fig. 3.13 shows the log α_{diff} as a function of hν in the region I for both the samples. E_{oc} is obtained from the slope of this curve (see Section 3.2.1.2). and found to be (32 ± 5)meV and (34 ± 5)meV for the samples #1 and #2 respectively. The values of slopes of the Urbach edges are given in Table 3.1.

Deep gap states

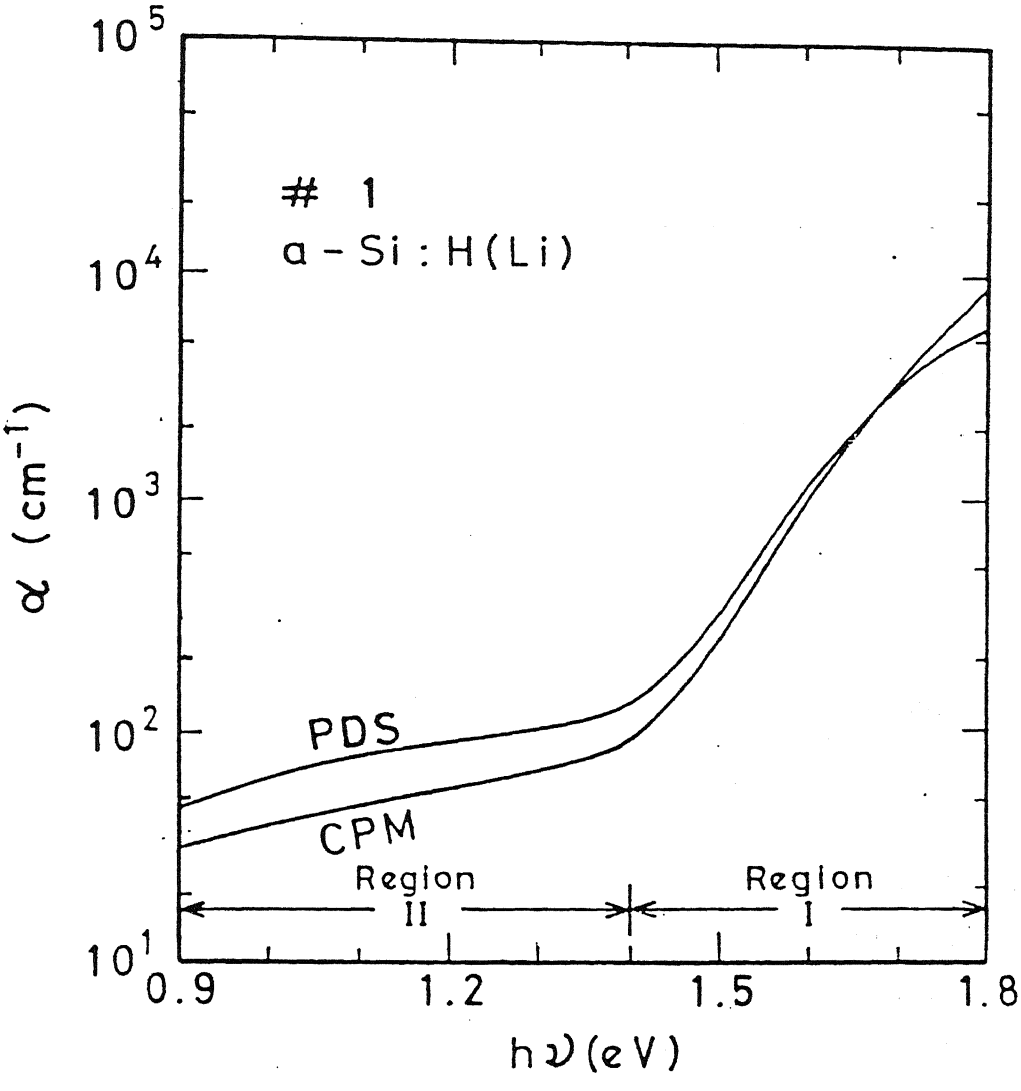

Figure 3.11: Absorption coefficient α as a function of hν as measured by CPM and PDS for a-Si:H(Li) (sample #1). CPM curve have been normalised by suitably matching CPM data with $\alpha(h\nu)$ obtained from the transmission measurements in the region 1.8 to 1.6 eV. The error bars shown in this figure are the same for Figs. 3.12 also.

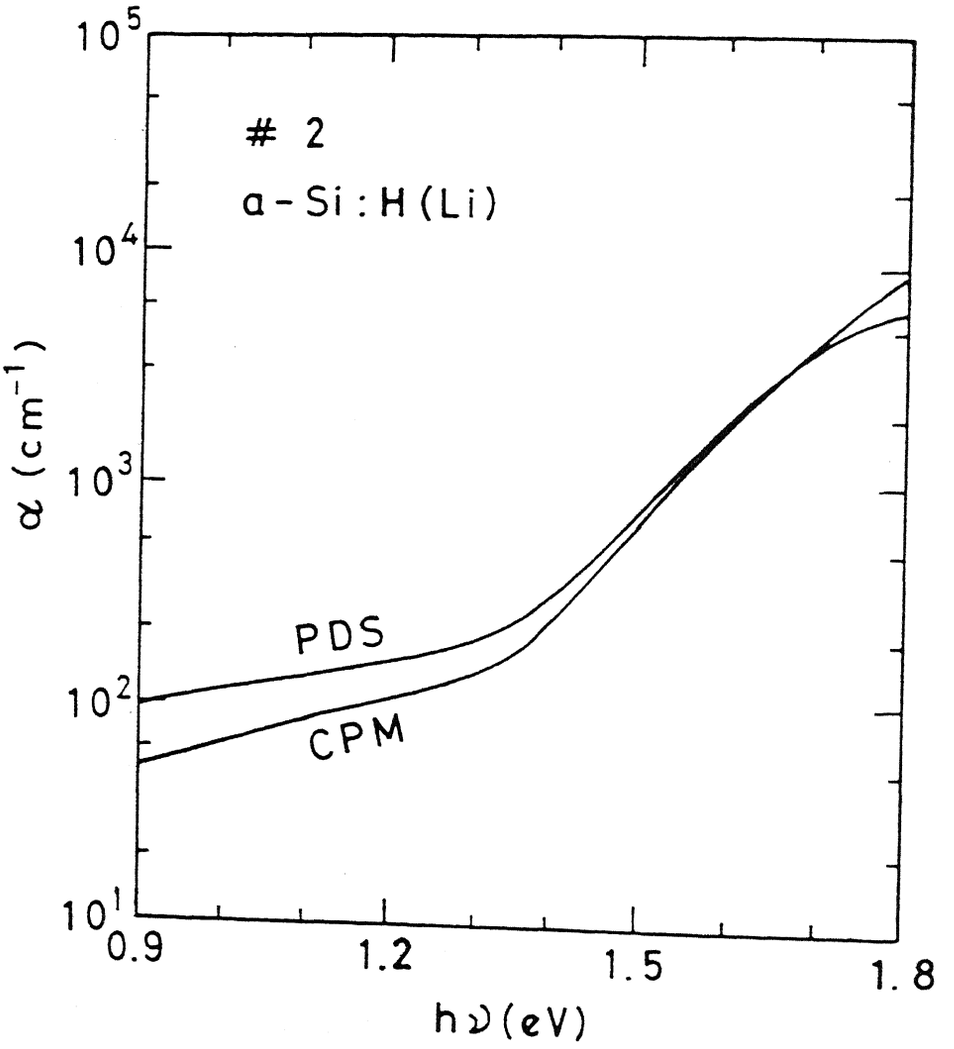

Figure 3.12: Absorption coefficient α as a function of hν as measured by CPM and PDS for a-Si:H(Li) (sample #2).

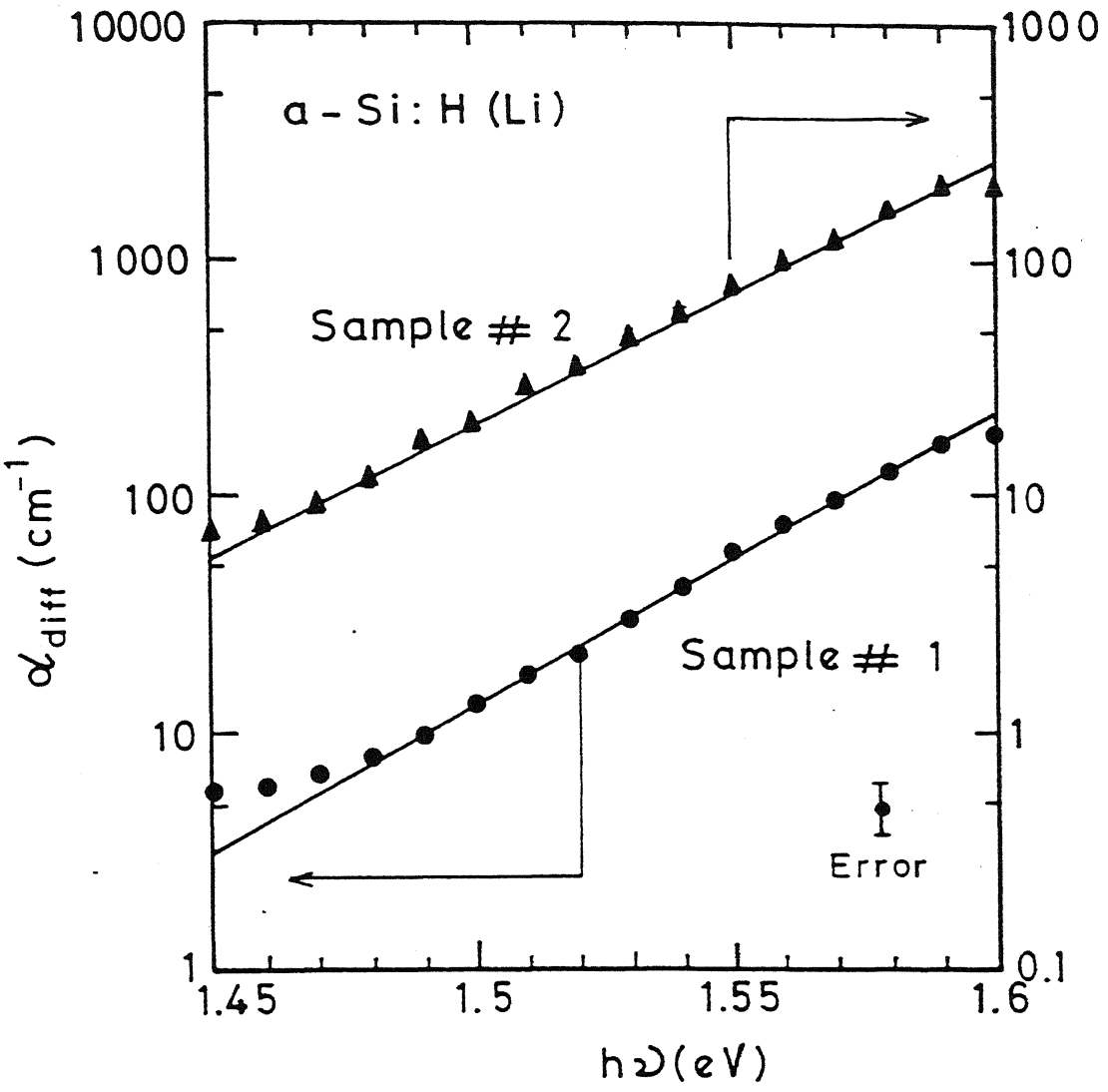

Figure 3.13: α_{diff} plotted as a function of hν for samples #1 (circles) and #2 (triangles). Theoretical fit (—) is based on the analysis discussed in section 3.2.1.2. Please note the different scales for the two samples.

As discussed in section 3.2.1.3, α_{cpm} in the region II is analysed under the assumption of the Gaussian distribution of deep gap states. The Gaussian parameters $g(E_I)$, W and E_I are obtained from the best fit between the measured $\alpha(h\nu)$ and the theoretical $\alpha(h\nu)$. The values of these parameters for both the samples are given in Table 3.1.

As discussed in Section 2.1.2, we have made the Li doping by vacuum evaporation of Li on undoped a-Si:H. Although, extended annealing have been done to ensure uniform diffusion of Li throughout the bulk, secondary ion mass spectroscopy (SIMS) have not been done. So, the non uniform distribution of Li in the bulk can not be ruled out. It is known that the the density of bulk states strongly depends upon the concentration of the dopant. Hence, the density of the bulk states obtained, shows an average value using the present analysis.

3.2.2.2 Phosphorous doped a-Si:H

Figs. 3.14 and 3.15 show $\alpha(h\nu)$ for a-Si:H(P), sample #5 and #15 respectively measured by CPM and PDS. Following the analysis discussed in section 3.2.1.2 slopes of Urbach edges E_{ov} and E_{oc} are obtained for the samples from region I (Fig. 3.13 & 3.14). Figs. 3.16 shows α_{diff} (= α_{pds} - α_{cpm} in region I (Fig. 3.5)) plotted as a function of hν for samples #5 and #15. The slopes give E_{oc} for the two samples. We find E_{ov} = (85± 5)meV and E_{oc} = (32± 5)meV for sample #5. The values for the sample #15 are E_{ov} = (90± 5)meV and E_{oc} = (30± 5)meV.

Using α_{cpm} in region II (Fig. 3.13), we obtain parameters for the deep gap states, under the assumpton of the Gaussian shape of the deep gap states. These values for both the samples (#5 and #15) along with the slopes of the Urbach edges are given in Table 3.1.

3.2.3 Position of D^- in a-Si:H(Li)

Fig. 3.17 shows α as a function of hν between 0.9eV and 1.8eV for a-Si:H and a-Si:H(Li) with various concentrations of Li, using CPM. Using α (hν) curves, dangling bond parameters are obtained under the assumption of Gaussian deep gap states. The DOS parameters are shown in Table 3.2. The position of D^o in a-Si:H and D^- in

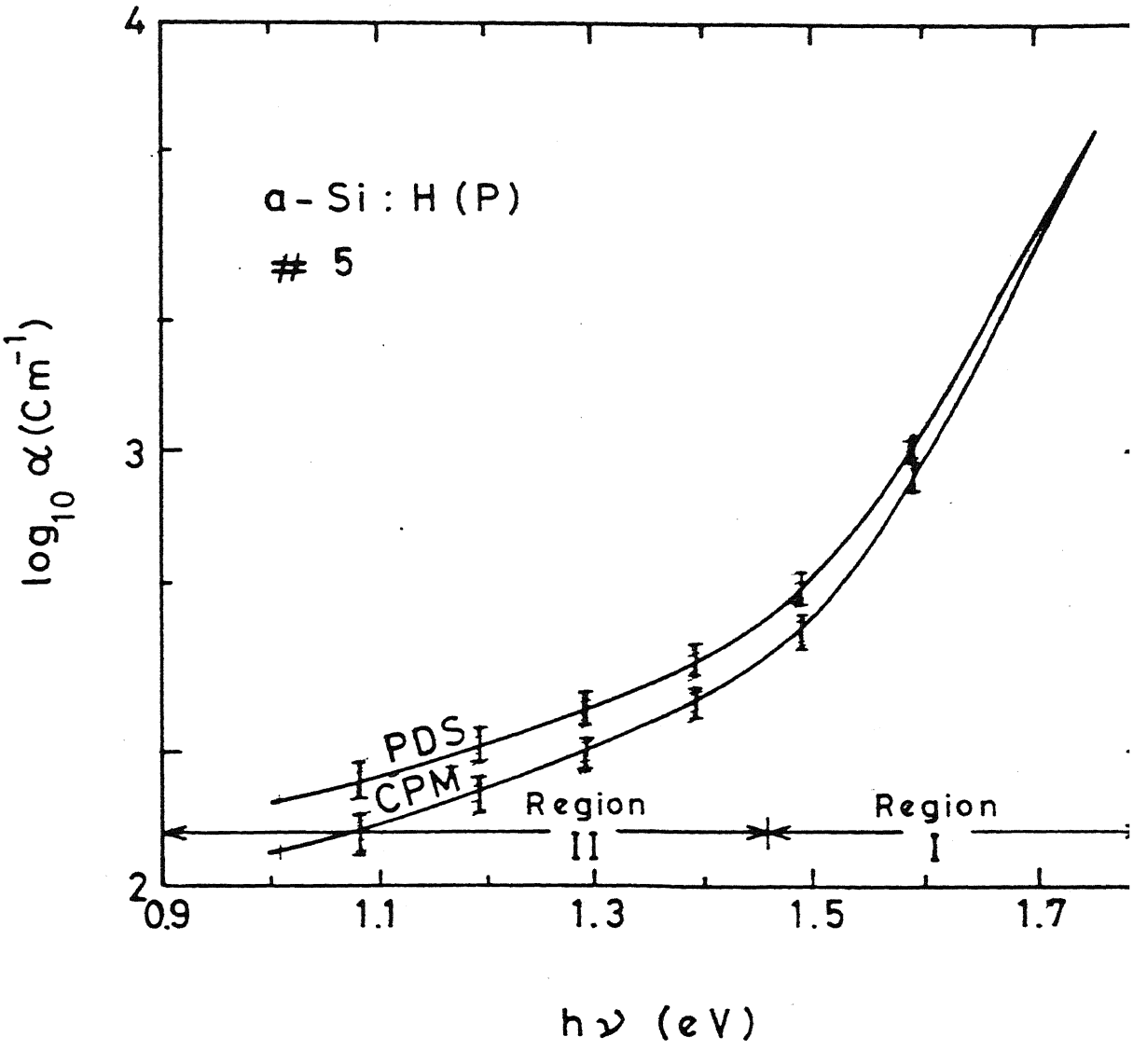

Figure 3.14: Absorption coefficient α as a function of $h\nu$ as measured by CPM PDS for a-Si:H(P) (sample #5).

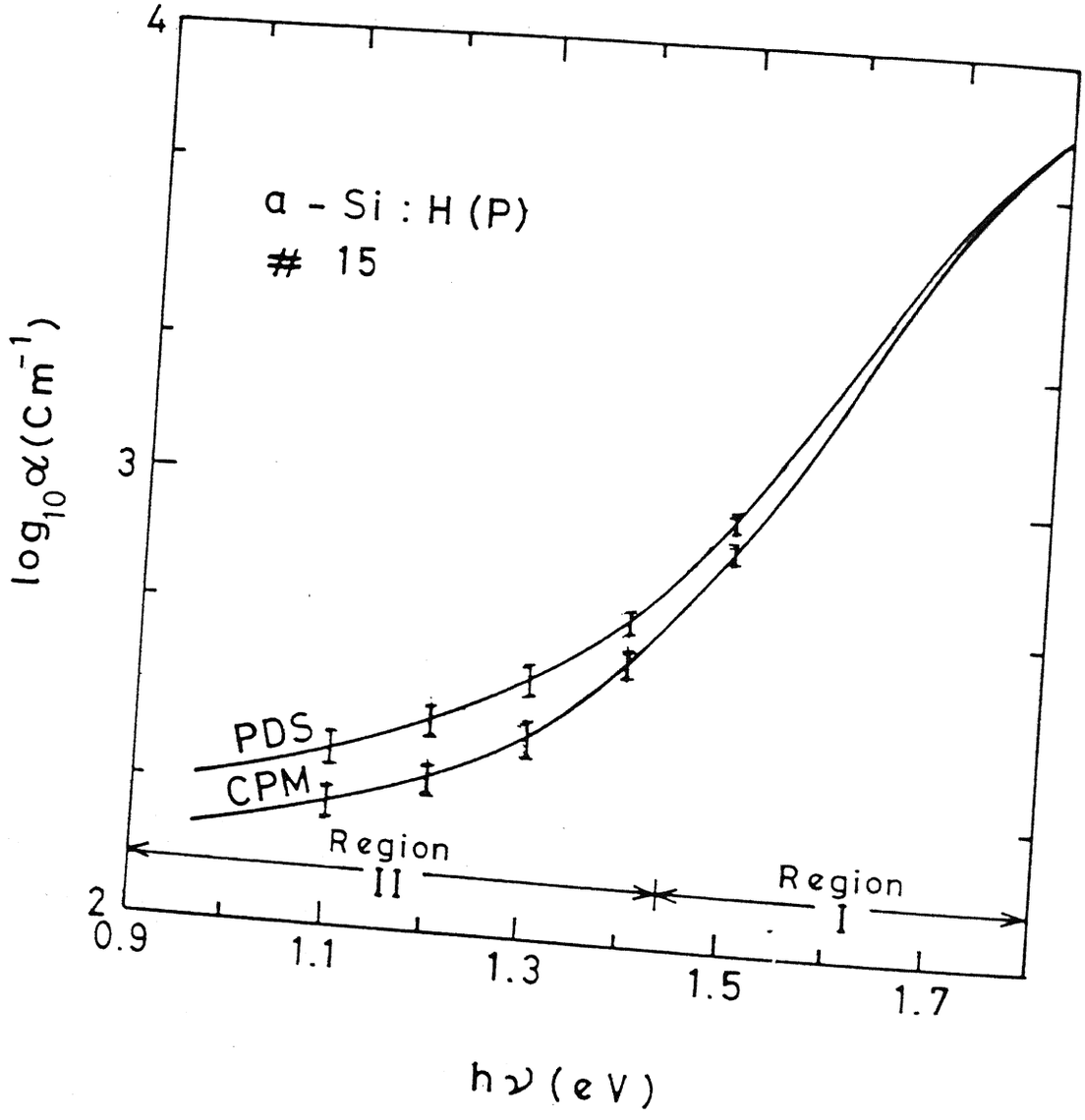

Figure 3.15: Absorption coefficient α as a function of $h\nu$ as measured by CPM and PDS for a-Si:H(P) (sample #15).

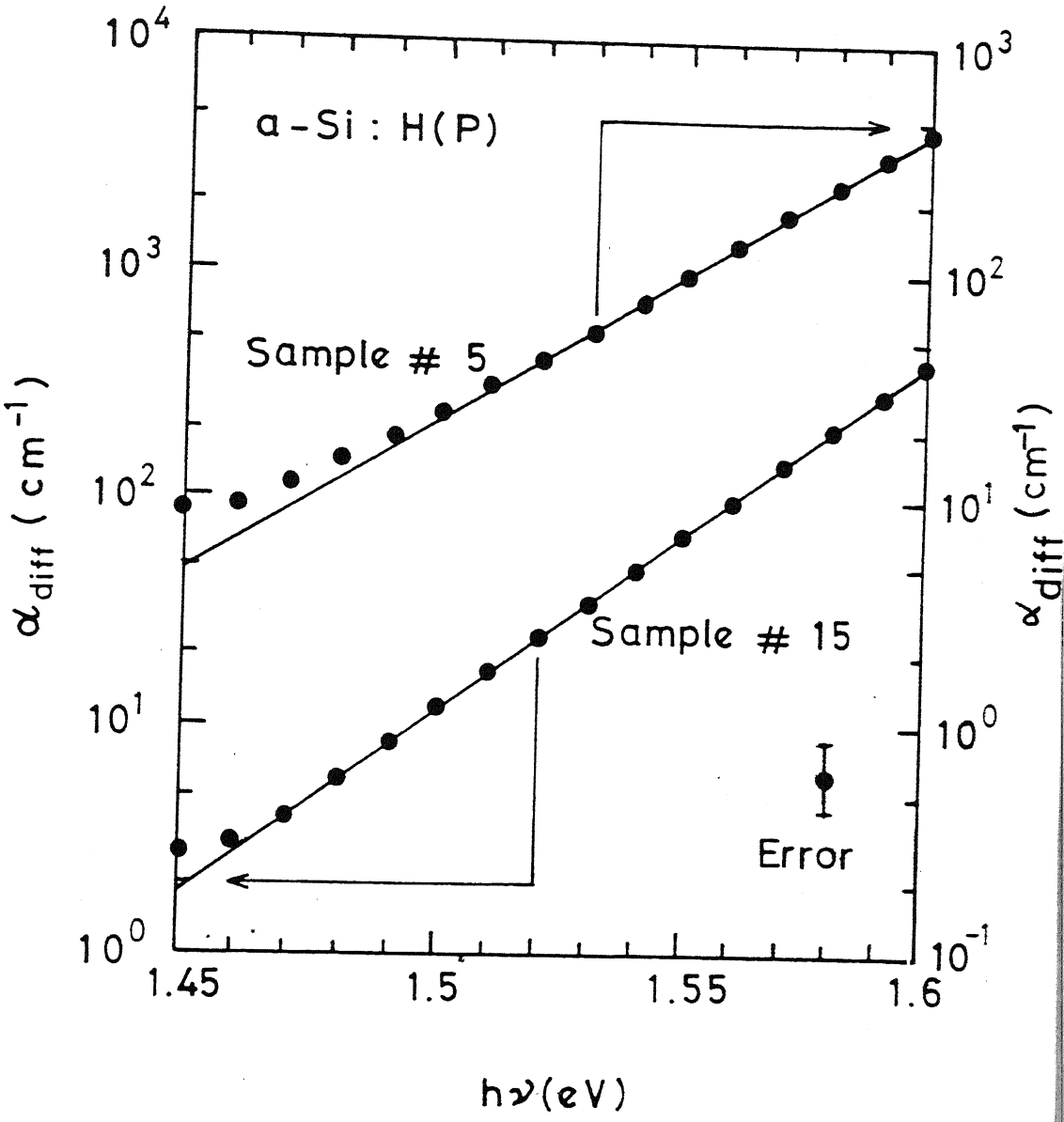

Figure 3.16: α_{diff} plotted as a function of hν for samples #5 (circles) and #15 (triangles). Theoretical fit (—) is based on Eq. 3. . Please note the different scales for the two samples.

a-Si:H(Li) are obtained by a detailed error analysis. We find that prediction of the position of D^- in Li doped a-Si:H using the basic model of Street et al and intimate pair bond model of Kocka et al are within the error bars. However, g(E_F) for a-Si:H(Li) calculated using Eq. (3.22), is 2.5 $\times 10^{17}\ cm^{-3}eV^{-1}$ for the model by Street et al [9] and 9.1 $\times 10^{15}\ cm^{-3}eV^{-1}$ for the model by Kocka et al [14]. We find that g(E_F) in the case of Kocka's model is unrealistically low, when compared with the values obtained by other methods for a similar (decided by E_σ value) a-Si:H(P) sample. Thus we conclude that the "Basic model" of Street et al [9] is probably tangible and is favoured by our data, for lithium doped a-Si:H. This looks reasonable because Li is an interstitial dopant in a-Si:H and hence may not form an intimate pair with the dangling bond states.

3.3 Summary and Conclusions

1. Sub band gap α has been measured using CPM and PDS on undoped and P and Li doped a-Si:H thin films between photon energies (hν) 0.9eV and 2.5eV. α_{pds} is found to be larger than α_{cpm} in the sub-gap region (h$\nu < 1.8eV$). This has been reported by others, as well [24]. The difference is explained by arguing that α_{cpm} is not sensitive to a part of the bulk states transitions and also the transitions to and from the surface states. Using CPM and PDS for determining α as complementary techniques, we obtain density of bulk states in the entire band gap. The slope of conduction band Urbach edge has been obtained, which is not possible using CPM or PDS alone. We have calculated the bulk states using a Gaussian as well as an exponential mid-gap states. Both give good fits to $\alpha(h\nu)$ data. The parameters obtained are in agreement with the literature. This shows that the shape can not be determined uniquely using CPM and PDS measurements.

2. Shape of the mid-gap states, however, have been uniquely obtained using DBCPM measurements at low chopping frequency (5 Hz). A prominent hump appearing in the spectrum can be fitted using the Gaussian shape of the mid-gap states alone. So, we conclude that our data favour the Gaussian shape of the mid-gap states. Further, DBCPM spectrum at 333Hz is used to obtain the correlation energy (U) between the two electrons occupying the same defect site. We find U = 0.15 $\pm$ 0.06eV, in agreement

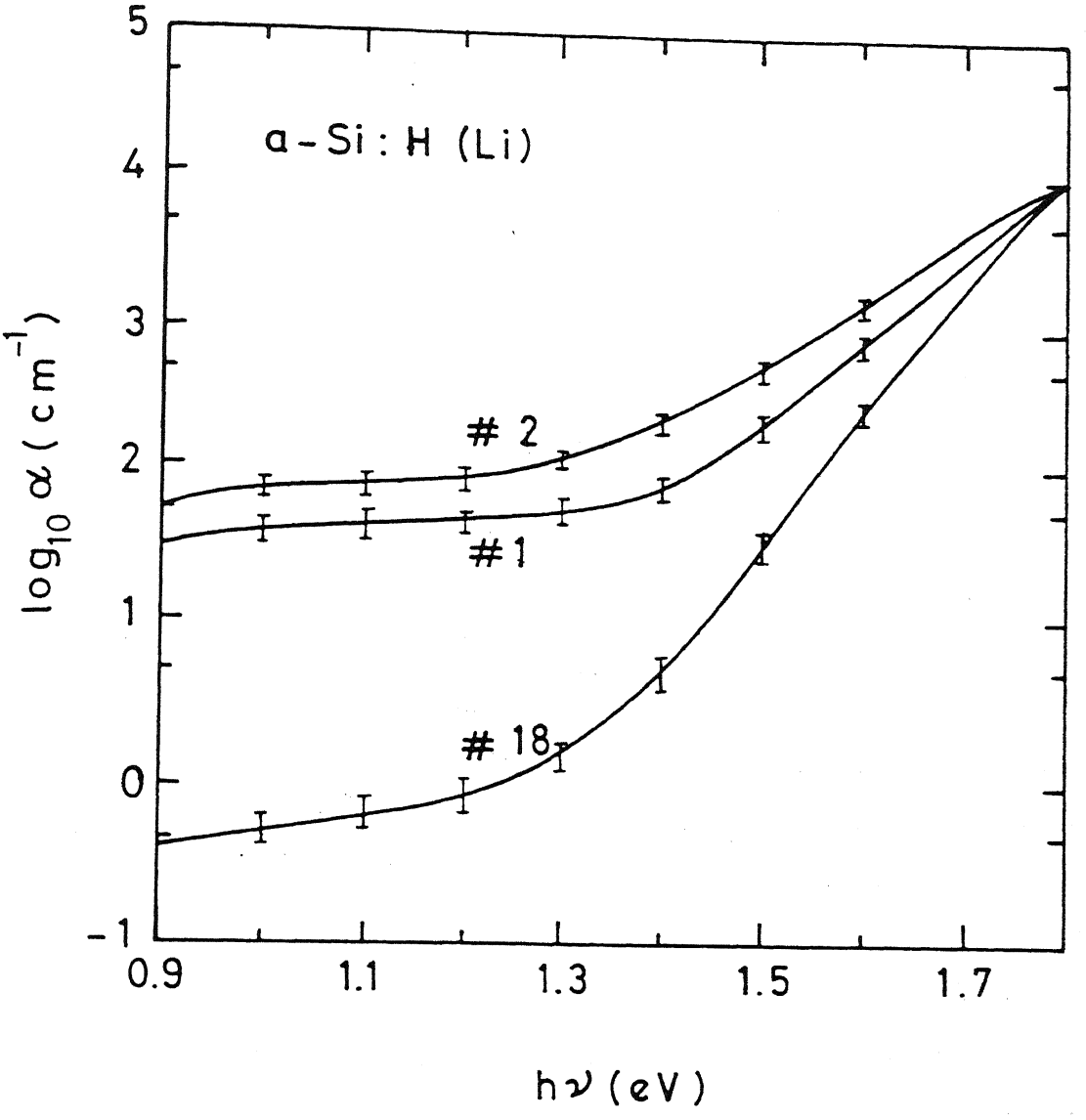

Figure 3.17: Absorption coefficient α as a function of hν measured using by CPM for undoped a-Si:H (sample #18) and a-Si:H doped with Li (samples #1 and #2).

Table 3.2: DOS parameters (E_{ov}, N_I, E_I, and W), activation energy (E_σ) and DOS at the Fermi level calculated using Eq. (4.5) assuming Street's model [$g_S(E_F)$] and Kocka's model [$g_K(E_F)$] of DOS for a-Si:H (#18) and a-Si:H(Li) with two Li concentrations.

Sample details	E_{ov} (meV)	$N_I \times 10^{-16}$ ($cm^{-3}eV^{-1}$)	E_I (eV)	W (eV)	E_σ (eV)	$g_S(E_F) \times 10^{-16}$ ($cm^{-3}eV^{-1}$)	$g_K(E_F) \times 10^{-16}$ ($cm^{-3}eV^{-1}$)
a-Si:H(#18)	45	5.85	1.03	0.119	0.81	-	-
a-Si:H(Li)(#1)	70	150	0.92	0.170	0.45	24	0.90
a-Si:H(Li)(#2)	90	310	0.90	0.180	0.38	28	0.92

with the Literature [6].

3. Bulk states in the entire mobility gap have been calculated using α_{CPM} and α_{PDS} measurements for P doped a-Si:H with two P concentrations. We find an increase in E_{ov} with the increasing P concentration. This is also found by others [25]. Also, the density of deep gap states increases with increasing P concentrations. However, E_{oc} does not change. This is in agreement with the published results [26], in which E_{oc} has been measured using time of flight measurements.

4. For a-Si:H(Li), we find that E_{ov} increases with the concentration of Li. However, E_{oc} does not change, being 30±5meV for undoped as well as doped samples. This is in qualitative agreement with our P doped samples and also with the literature [1,3]. The density of mid-gap states is found to increase with Li concentration, again in qualitative agreement with our P doped samples (see Table 3.1). This leads us to conclude that Li and P are qualitatively similar dopants as far as the bulk states are concerned.

5. We have obtained the position of D^- in a-Si:H(Li) by combining sub-gap absorption and activation energy data. We find that our data favour Street's model of DOS [9] for a-Si:H(Li), in which the position of D^- in n type a-Si:H is same as that of D^o in undoped a-Si:H. This is explained as below. In the other model (by Kocka et al), D^- moves deeper in the band gap because of intimate pair formation between dopants and dangling bond states. However, Li is interstitial dopant and may not form the intimate pair. Hence, position of D^- in a-Si:H(Li) is the same as that in undoped a-Si:H.

Bibliography

1. M. Vanecek, J. Kocka, J. Stuchlik and A. Triska, Sol. State Comm. **39**, 1199. (1981).

2. M. Vanecek, J. Kocka, J. Stuchlik, Z. Koicek, O. Stika, and A. Triska, Solar Energy Materials, **8**, 411 (1983).

3. W. B. Jackson and N. M. Amer, Phys. Rev. **B25**, 5559 (1982).

4. W. B. Jackson, N. M. Amer, A. C. Boccara, and D. Fournier, Appl. Optics, **20**. 1333 (1981).

5. F. Urbach, Phys. Rev. **92**, 1324 (1953).

6. J. Z. Liu, G. Lewen, J. P. Conde and P. Roca i Cabarrocas, J. Non-Cryst. Solids **164 & 165**, 383 (1993).

7. Z. Vardeny and J. Tauc, Phys. Rev. Lett. **54**, 1844 (1985).

8. J. M. Essick and J. D. Cohen, Phys. Rev. Lett. **64**, 3062 (1990).

9. R. A. Street, J. Zesch and M. J. Thompson, Appl. Phys. Lett. **43**, 672 (1983).

10. M. Hack and M. Shur, J. Appl. Phys. **54**, 5858 (1983); S. Guha, J. Non. Cryst. Solids, **77&78**, 1451 (1985).

11. J. S. Payson and S. Guha, Phys. Rev. **B32**, 1326 (1987).

12. A. K. Sinha, M. Malhotra, S. Kumar, E. Bhattacharya and S. C. Agarwal, Ind. J. Pure & Appl. Phys. **31**, 548 (1993).

13. W. Beyer and R. Fischer, Appl. Phys. Lett. **31**, 850 (1977).

14. J. Kocka, M. Vanecek and A. Triska, in Amorphous Silicon and Related Materials. ed. H. Fritzsche (World Scientific, 1988), pp. 329-363.

15. H. Curtnis, N. Wyrsch and A. V. Shah, Electronics Letters, **23**, 228 (1987).

16. M. Favre, H. Curtnis and A. V. Shah, J. Non-Cryst. Solids, **97 & 98**, 731 (1987).

17. N. Mott and E. A. Davis, Electronic Processes in Non-Crystalline Materials (Cambridge University, 1979) Chapter 6.

18. R. A. Street, Hydrogenated Amorphous Silicon (Cambridge University, 1991) Chapter 8.

19. R. Swanepoel, J. Phys. **E16**, 1214 (1983).

20. A. Rose, "Concepts in Photoconductivity and Allied Problems" , R. Krieger (Huntington Publishing, 1978), Chapter 3.10.

21. J. Tauc in Amorphous and Liquid Semiconductors, ed. J. Tauc, (Plenum Press N.Y. 1974), Chap. 4, p. 172.

22. H. Fritzsche, Solar Energy Materials, **3**, 447 (1980).

23. A. K. Sinha, S. K. Tripathi, G. S. Narayana and S. C. Agarwal, Solid State Phenomena, (Scitec Publications, Switzerland) **55**, 137 (1997).

24. Z. E. Smith, V. Chu, K. Shepard, S. Aljishi, D. Slobodin, J. Kolodzey, S. Wagner, and T. L. Chu, Appl.Phys.Lett. **50**, 1521 (1987).

25. K. Pierz, B. Hilgenberg, H. Mell and G. Weiser, J. Non-Cryst. Solids, **97-98**, 63(1987).

26. T. Tiedje, in Semiconductors and Semimetal, Vol 21(C), ed. J. I. Pankov (Academic Press, Orlando, 1984) Chapter 6.

Chapter 4

Surface States

In Chapter 3, we described the determination of the bulk states in undoped and doped a-Si:H from sub-gap absorption measurements. This Chapter presents the determination of the surface states using these measurements. In the literature [1-3], $\alpha(h\nu)$ measurements have been used to determine the density of surface states by measuring $\alpha_{pds}(h\nu)$ for a number of samples with identical bulk states but varying thicknesses. This is difficult to achieve and gives large uncertainty in the measured value of density of surface states. This difficulty can be overcome by using both CPM and PDS techniques on the same sample, since the two techniques have complementary informations about the bulk and surface states. Smith et al [4] have calculated surface states using the relation: Integrated α attributed to the surface states = (Integrated $\alpha)_{pds}$ - 2 $\times$ (Integrated $\alpha)_{cpm}$. The factor 2 comes from the assumption that CPM is sensitive to about the half the bulk state transitions compared to those seen by PDS. However, this assumption is found to hold good only for good quality a-Si:H [5]. Also, this method can not be applied to the doped samples. Amato et al [6] use the difference in the height of the interference fringes in $\alpha(\mathrm{h}\nu)$ measured by CPM and PDS to determine the density of surface states. However, this method needs perfect uniformity of the film and requires identical areas of the film to be probed by PDS and CPM. This is difficult to achieve.

Equivalent occupied surface state density for undoped and doped a-Si:H have been measured by Winer et al [7], using total-yield photoelectron spectroscopy. They find

that the density of surface states depends on the doping level as well as dopant. For B doping, the density of surface states decreases with the increasing doping concentration. On the other hand, on P doping the density of surface states increases as the 1/4 power of the doping concentration. Recently Fejfar et al [8] have suggested absolute constant photocurrent measurement for estimating the difference in capture cross sections between the bulk and the surface states, but do not measure their densities. In this Chapter, we suggest an alternative method of measuring surface states, which requires only one sample.

We have used sub-gap α measured by CPM and PDS to determine the density of surface states. α measured by PDS is larger than that measured by CPM in the sub-gap region. This difference arises because CPM is not sensitive to the transitions involving some of the bulk states and all of the surface and the interface states [4], whereas, PDS is sensitive to all the transitions. By measuring PDS for front and rear illumination, at high modulation frequency; so that the thermal diffusion length is of the order of the film thickness, Chahed et al [10] concluded that the additional sub gap absorption in PDS below 1eV comes essentially from the surface region.

In this Chapter, results on the density of surface states for undoped a-Si:H and a-Si:H doped with various concentrations of phosphorous and lithium are presented. The motivation for studying Li doped a-Si:H is two fold. First Li is interesting because it is an interstitial dopant in a-Si:H [11], unlike P which is substitutional. Also, Li has been doped by in diffusion of Li in undoped a-Si:H, at low temperatures (100-150K). Thus we expect that the hydrogen concentration is unchanged upon Li doping. This allows us to study the effect of dopant alone. Further, although the bulk states in a-Si:H(Li) have been studied [12], there is no report on the measurement of surface states in a-Si:H(Li), so far.

The present method of calculating the density of surface states has the following advantages over the existing methods [4,5]. This method requires only one sample and there is no specific requirement of the uniformity of the films. Since the technique is based on detailed calculations, the assumption that CPM sees about half the bulk states compared to PDS is not required. Finally, the technique has been applied to undoped as well as n type doped a-Si:H. For CPM, the only requirement is that the sample

should be photoconducting.

4.1 Methodology for Obtaining Surface States

4.1.1 Undoped a-Si:H

Chapter 3 gives the methodology to obtain distribution of bulk DOS in the entire mobility gap of a-Si:H. Now, in the mid gap absorption region (region III, Fig. 3.3). transitions T_4 (Fig. 3.1) are seen by PDS but ignored by CPM. Since, we have already obtained the bulk DOS parameters, $\alpha(T_4)$ can be calculated using equation similar to Eq. (3.15), from Gaussian distribution of mid gap states. From Eqs. (3.6) and (3.7). we get:

$$\alpha(T_s) = \alpha_{pds} - \alpha_{cpm} - \alpha(T_4). \tag{4.1}$$

As the distribution of surface states is not known, we have chosen several trial distributions of surface states. These include a delta function, a rectangular distribution and a Gaussian distribution. All these are assumed to be located near the center of the band gap. This assumption is justified because $\alpha(T_s)$ is non zero only in the region III (Fig. 3.3). Further, we have assumed that the surface states are located below the Fermi level. This is done for the simplicity in calculation. Our calculations show that even if the surface states are situated differently with respect to the Fermi level, only a small difference (<10%) in the value of N_s is observed, provided they are located around the middle of the gap.

From $\alpha(T_s)$ the density of surface states $[N_s(cm^{-2})]$ is calculated as follows:

$$\alpha(T_s, h\nu) = (C/h\nu) \int g_i(h\nu - \epsilon) g_f(\epsilon) d\epsilon, \tag{4.2}$$

where g_i and g_f are the densities of initial and final states respectively. The constant C includes the transition matrix elements, these are assumed to be the same for all the transitions considered here.

We take

$$g_f(\epsilon) = 6.7 \times 10^{21}\ \epsilon^{1/2}, \tag{4.3}$$

where, ϵ is the energy of the final states measured from the conduction band edges. The following distributions of surface states, g_i, are used:

i) δ function: $g_i(h\nu - \epsilon) = \delta(\epsilon - (h\nu - E_f))(N_s)/(d)$

ii) Gaussian distribution: $g_i(h\nu - \epsilon) = (N_G/d)exp(-(\epsilon + E' - h\nu)^2/2w^2)$

iii) rectangular distribution: $g_i(h\nu - \epsilon) = (N_r/d)$

where, $N_G(cm^{-2}eV^{-1})$ is the height, w the half width at half maximum and E' the energy position of the peak of the Gaussian distribution. $N_r(cm^{-2}eV^{-1})$ is the height of the rectangular distribution and d is the film thickness in cm.

For the delta function shape of the density of surface states, using Eqs. (4.2) and (4.3), we get

$$N_s(cm^{-2}) = \alpha(T_s)\ h\nu\ d/(K\ (h\nu - E_f)^{1/2}), \tag{4.4}$$

and for the rectangular shape, we get

$$N_r(cm^{-2}eV^{-1}) = 2\alpha(T_s)\ h\nu\ d/[3K\ (h\nu - E_f)^{3/2}] \tag{4.5}$$

The constant K depends upon the matrix element of transition and is assumed to be equal to that obtained for VB extended states to CB extended states transitions [13,14].

For the Gaussian shape of surface states, Eq. (4.2) is numerically integrated and a good fit between the calculated $\alpha(T_s)$ and experimentally obtained $\alpha(T_s)$ [Eq. (4.1)] is obtained by varying N_G, E' and w. This gives N_s.

4.1.2 n-type doped a-Si:H

Section 3.2.1 describes the determination of bulk DOS in the entire gap for n type doped a-Si:H. In the region II (Fig. 3.), we define α'_{pds} and α'_{cpm} by the relations: $\alpha'_{pds} = \alpha_{pds}$ - (extrapolated value of α_{pds} from region I) and $\alpha'_{cpm} = \alpha_{cpm}$ - (extrapolated value of α_{cpm} from region I). Hence, we write in an obvious notation:

$$\alpha'_{pds} = \alpha(T_4) + \alpha(T_s) \ ,$$

$$\text{and, } \alpha'_{cpm} = \alpha(T_4).$$

Therefore, $\alpha(T_s) = \alpha'_{pds}$ - α'_{cpm} is attributed to the absorption involving the surface states. Density of surface states can be obtained from $\alpha(T_s)$ using an analysis similar to that for undoped a-Si:H described in Section 4.1.1.

4.2 Results and Discussion

4.2.1 Undoped a-Si:H

Fig. 4.1 shows $\alpha(T_s)$ plotted as a function of hν obtained experimentally along with those obtained theoretically using a delta function, rectangular and Gaussian distributions of the surface states. The analysis is given in section 4.1.1. We find:
i) For delta function distribution of the surface states: $N_s = (4.0 \pm 1.0) \times 10^{12} cm^{-2}$.
ii) For rectangular distribution of the surface states: N_r is found to be $\approx 6.0 \times 10^{12}$ $(cm^{-2}eV^{-1})$ and b $\approx$ 0.6eV; this gives $N_s = (3.6 \pm 1.0) \times 10^{12} cm^{-2}$.
iii) For Gaussian distribution of the surface states: N_G is found to be $\approx 1.0 \times 10^{13}$ $(cm^{-2}eV^{-1})$, w = 0.16eV and E' = 1.0eV. This gives $N_s = (4.0 \pm 1.0) \times 10^{12} cm^{-2}$.

These N_s values, for the three distributions of the surface states, are quite close and are also in agreement with the values reported in the literature $(1-5 \times 10^{12}\ cm^{-2})$ [2,3].

4.2.2 Li doped a-Si:H

Using $\alpha(h\nu)$ data shown in Figs. 3.11 and 3.12, the density of surface states (N_s) is calculated following the analysis of undoped a-Si:H (Section 4.1.2). Calculated $\alpha(T_s)$ using the three shapes of the surface states along with experimental $\alpha(T_s)$ are shown in Fig. 4.2 for the two Li doped samples studied. We find that the fit is reasonable in all the cases. The fit parameters are given in Table 4.1. N_s is found to be $(5.0 \pm 1.0) \times 10^{12} cm^{-2}$ for sample #1 and $(5.5 \pm 1.0) \times 10^{12} cm^{-2}$ for sample #2 for all the shapes considered. Therefore, the density of surface states obtained does not appear to be very sensitive

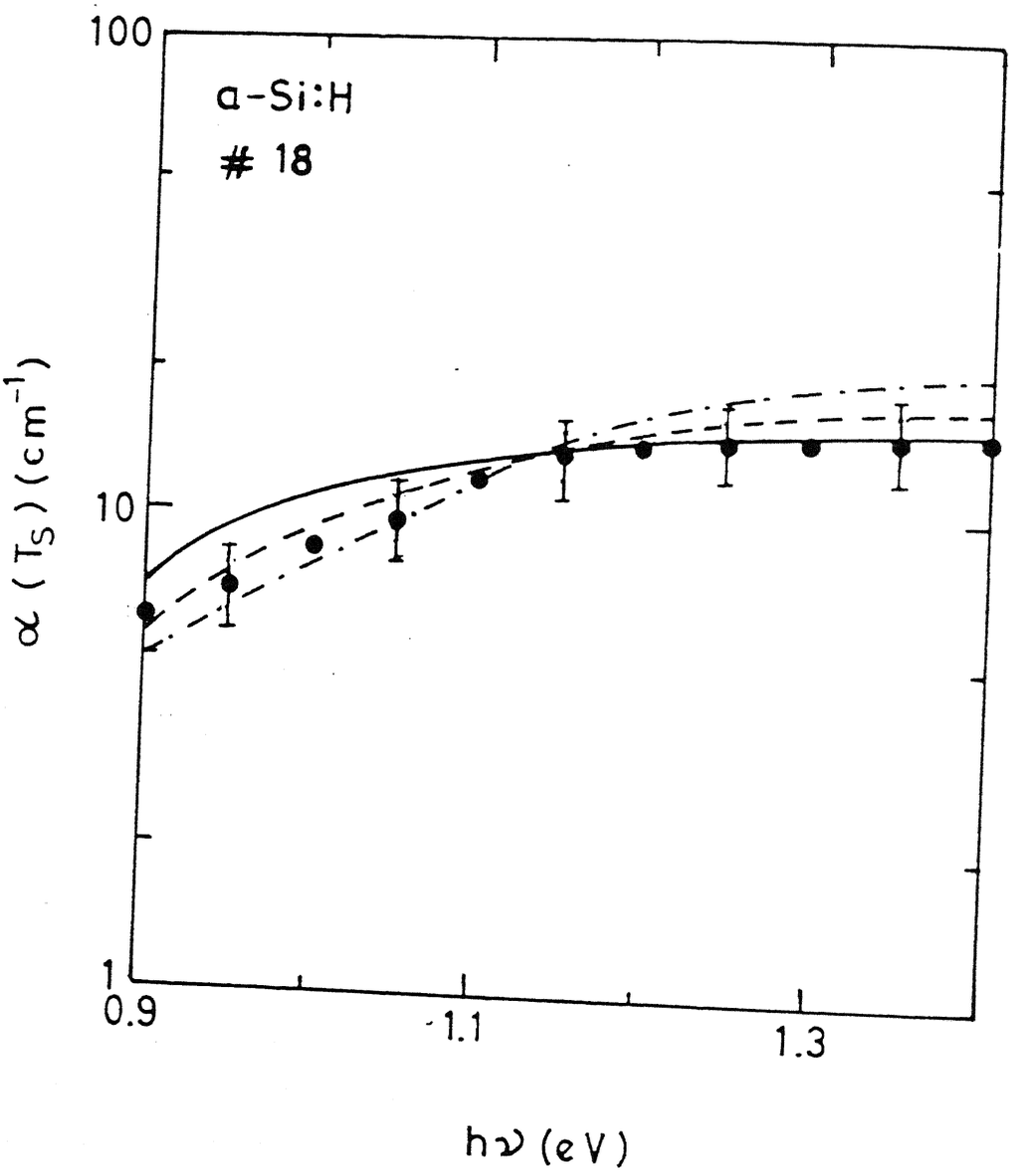

Figure 4.1: $\alpha(T_s)$ plotted as a function of hν for undoped a-Si:H(#18) are shown along with the theoretical fit for Gaussian (full line, —), rectangular (dot dashed line, - . -) and delta function (dashed line, - - -) distributions of the surface states. The error bars shown in this figure are the same for Figs. 4.2 and 4.3.

to the shape of their distribution. These numbers also compare favourably with the reported N_s values for a-Si:H(P) [2].

So far, we have considered the "Standard Defect Model" [15] for bulk states, which assumes a narrow Gaussian peak near the mid gap. These are charged defects which are all below the Fermi level, in n type material. We now consider the "Defect Pool Model" [16], in which there may be unoccupied defect states above the Fermi level. The optical transitions from the valance band extended states to these states are detected by PDS but ignored by CPM. However, the number of these states are about two orders of magnitude smaller than the charged D^- defect states [16]. An analysis, similar to that done by us in the case of undoped a-Si:H [17] (Section 4.1.1), shows that the density of surface states calculated using the defect pool model is lower by about 2%, which is well within the error bars.

Although we have tried to make the Li distribution uniform by extended annealing, a non uniform distribution of Li can not be ruled out, because SIMS profiling was not done. Street and Winer [18], based on their SIMS measurements, find that surface concentration is more than bulk concentration. Since, our analysis assumes a uniform distribution of Li it is worthwhile discussing the effect that the non uniformity of Li may have on our results. A non uniform Li distribution may change the density of surface states. Also, the DOS in the bulk may vary as a function of depth. Since, our analysis assumes the interior states to be uniform, the interior DOS obtained from analysis represents an average. However, the calculated surface states density will still be, the actual value for that sample, because of the way we have treated the two absorptions.

4.2.3 P doped a-Si:H(P)

Fig. 4.3 shows the calculated $\alpha(T_s)$ for the three distributions (delta function, Gaussian and rectangular distributions) of the surface states along with the experimental $\alpha(T_s)$. The fits are reasonable in all the cases. The fit parameters and the calculated values of N_s are given in Table 4.1. We find that the density of surface states under the assumption of delta function distribution of the surface states has a value $(4.8\pm 1.0)\times 10^{12} cm^{-2}$ for sample #5 ($E_\sigma = 0.30$eV) and $(4.2\pm 1.0)\times 10^{12} cm^{-2}$ for the sample #15

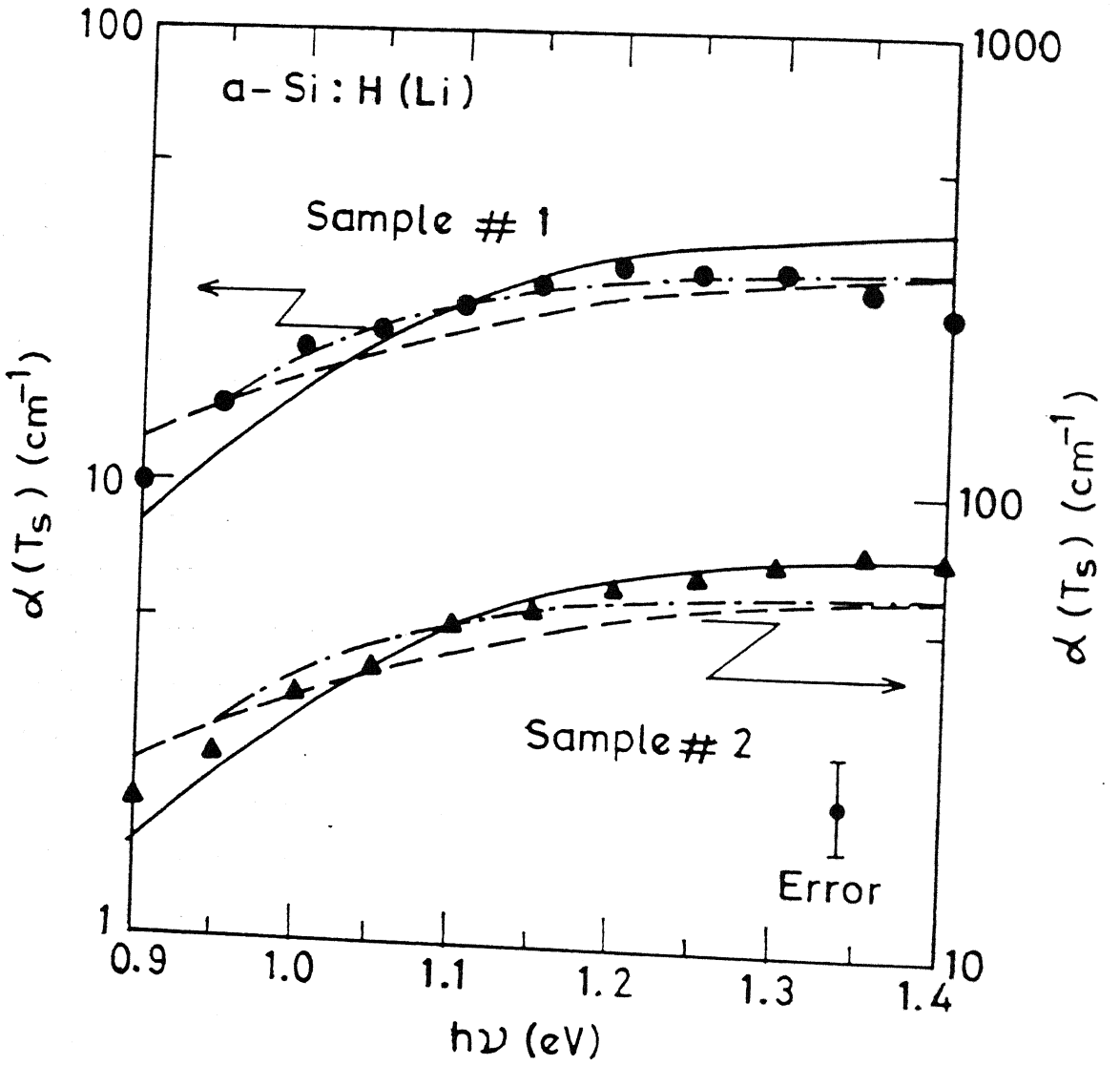

Figure 4.2: $\alpha(T_s)$ plotted as a function of hν for Li doped a-Si:H samples, #1 (circles) and #2 (triangles) are shown along with the theoretical fit for Gaussian (full line, —), delta function (dot dashed line, - . -) and rectangular (dashed line, - - -) distributions of the surface states. Please note the different scales for the two samples.

Table 4.1: Surface state parameters and density of surface states calculated assuming delta function, Gaussian and rectangular distributions of the surface states for a-Si:H(Li) with two Li concentrations and a-Si:H(P) with two P concentrations.

Sample Details	Delta function	Gaussian				Rectangular		
	N_s $\times 10^{-12}$ (cm^{-2})	w (eV)	N_G $\times 10^{-13}$ $(cm^{-2}eV^{-1})$	E' eV	N_s $\times 10^{-12}$ (cm^{-2})	b (eV)	N_r $\times 10^{-12}$ $(cm^{-2}eV^{-1})$	N_s $\times 10^{-12}$ (cm^{-2})
a-Si:H(Li)(#1)	5±1	0.14	4.4	1.0	5±1	0.6	8.0	4.8±1
a-Si:H(Li)(#2)	5.5±1	0.14	4.9	1.0	5.5±1	0.6	9.0	5.4±1
a-Si:H(P)(#5)	4.8±1	0.14	4.4	1.0	5.0±1	0.6	8.0	4.8±1
a-Si:H(P)(#15)	4.2±1	0.14	4.0	1.0	4.4±1	0.6	7.0	4.2±1

($E_\sigma = 0.28$eV), independent of the shape of the surface states.

As found for the undoped and Li doped a-Si:H, we see that for a-Si:H(P) also, the technique is not sensitive enough to distinguish between the various shapes of the surface states. The values of N_s for a-Si:H(P) is found to compare favourably with that given in literature [2] (1-5 $\times 10^{12} cm^{-2}$). These values are also similar to those obtained for our a-Si:H(Li). This leads us to believe that a-Si:H(Li) and a-Si:H(P) behave similarly as far as the bulk and the surface density of states are concerned. We also conclude that the density of surfaces states for doped samples may be slightly (within error bars) larger than that in undoped a-Si:H and it does not depend much on the doping concentrations.

4.3 Summary and Conclusions

Using α_{cpm} and α_{pds} measurements, we have obtained the density of surface states for a-Si:H, a-Si:H(P) and a-Si:H(Li) with various concentrations of P and Li. This method of calculating N_s has several advantages over the method proposed in the literature, such as, this method needs only one sample, can be applied to both undoped and doped

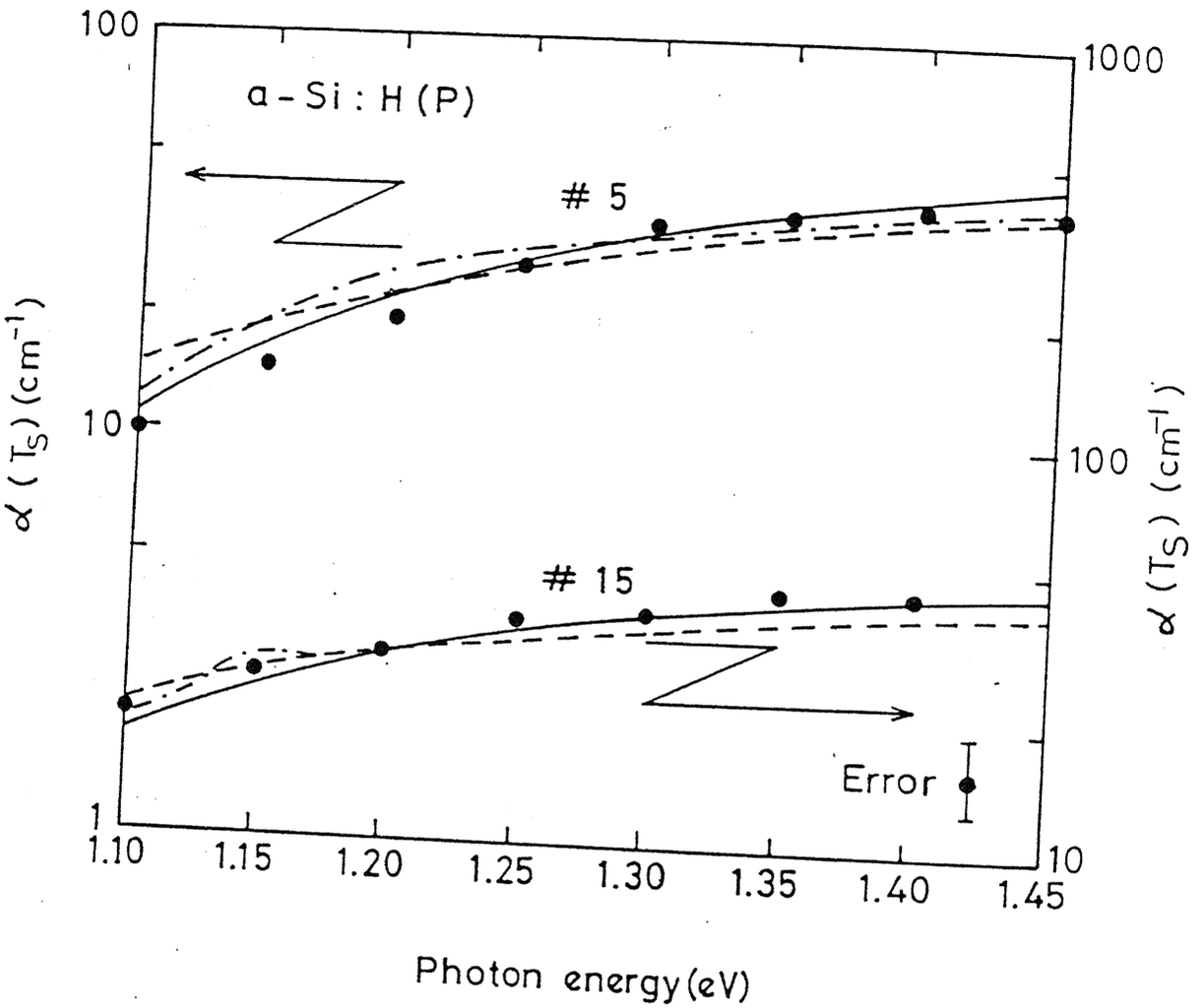

Figure 4.3: $\alpha(T_s)$ plotted as a function of hν for P doped a-Si:H samples, #5 (circles) and #15 (triangles) are shown along with the theoretical fit for Gaussian (full line, —), delta function (dot dashed line, - . -) and rectangular (dashed line, - - -) distributions of the surface states. Please note the different scales for the two samples.

samples and has no specific requirement like perfect uniformity of the film. It, however, requires that the sample should be photoconducting, so that CPM can be done.

N_s is found to be about $(4.0 \pm 1.0) \times 10^{12} cm^{-2}$ for undoped a-Si:H. This value of N_s is in agreement with the literature [2,3]. Further, we have studied the effect of shape of the distribution of the surface states on N_s. We have taken three distributions of surface states namely, a delta function, a Gaussian and a rectangular distributions. We find that values of N_s are within error bars of one another, for all the three distributions. This shows that the density of surface states is not very sensitive to their distribution.

The proposed technique for determining density of surface states has been applied to Li doped a-Si:H. We find that N_s in a-Si:H(Li) is about $(5.0 \pm 1.0) 10^{12} cm^{-2}$ and does not seem to vary much for the two Li concentrations studied. Also, N_s is found not to depend very much on the distribution of the surface states. However, N_s is found to increase slightly from the value for the undoped a-Si:H. N_s values for a-Si:H(Li) are in agreement with the value reported in literature for a-Si:H(P) [2,3].

The density of surface states for a-Si:H(P) is found to be $(4.5 \pm 1)\ 10^{12} cm^{-2}$ independent of the doping concentrations for the two concentrations studied. The values are in agreement with our N_s values for Li doped samples and also in agreement with the literature for P doped samples. Therefore, we conclude that Li and P give the same surface states in spite of Li being an interstitial dopant unlike P which is a substitutional dopant.

Finally, we conclude that for all the samples, N_s is not very sensitive to the shape of the distribution of the surface states. N_s increases slightly on Li doping but does not depend on the Li concentration. Also Li and P dopings seem to affect the density of surface states in a similar manner.

Bibliography

1. W. B. Jackson, D. K. Biegelsen, R. J. Nemanich, and J. C. Knights, Appl. Phys. Lett. **42**, 105 (1983).

2. H. Curtnis, N. Wyrsch and A. V. Shah, Electronics Lett. **23**, 228 (1987).

3. M. Favre, H. Curtnis and A. V. Shah, J. Non-Cryst. Solids, **97 & 98**, 731 (1987).

4. Z. E. Smith, V. Chu, K. Shepard, S. Aljishi, D. Slobodin, J. Kolodzey, S. Wagner and T. L. Chu, Appl. Phys. Lett. **50**, 1521 (1987).

5. E. Bustarret, D. Jousse, C. Chaussal and F. Boulitrop, J.Non.Cryst. Solids, **77&78**, 295 (1985).

6. G. Amato, G. Bendetto, L. Boarino, and R. Spagnolo, Sol. State Comm.

7. K. Winer, I. Hirabayashi and L. Ley, Phys. Rev. **B38**, 7680 (1988).

8. A. Fejfar, A. Poruba, M. Vanecek and J. Kocka, J. Non-Cryst. Solids, **198-200**, 304 (1996).

9. A. C. Boccara, D. Fournier, W. B. Jackson and N. M. Amer, Optics Letters, **5**, 377 (1980)

10. L. Chahed and M. L. Theye, Phys. Rev. **B43**, 14488(1991).

11. W. Beyer and R. Fischer, Appl. Phys. Lett. **31**, 850 (1977).

12. M. Stutzmann, Phil. Mag. **B60**, 531(1989).

13. A. K. Sinha, M. Malhotra, S. Kumar, E. Bhattacharya and S. C. Agarwal, Ind. J. Pure & Appl. Phys. **31**, 548 (1993).

14. M. Vanecek, J. Kocka, J. Stuchlik, Z. Koicek, O. Stika, and A. Triska, Solar Energy Materials, **8**, 411 (1983).

15. R. A. Street, J. Zesch and M. J. Thompson, Appl. Phys. Lett. **43**, 672 (1983).

16. M. J. Powell and S. C. Deane, Phys. Rev. **B48**, 10815 (1993); H. Steigbig and F. Siebig, J. Non-Cryst. Solids, **198-200**, 351 (1996). -

17. A. K. Sinha and S. C. Agarwal, Phil Mag. (1998) (Accepted).

18. K. Winer and R. A. Street, J. Appl. Phys. **65**, 2272 (1989).

Chapter 5

Effect of Surface Treatment

The characterisation of the surface in a-Si:H is important for both understanding of the properties of this material and for device fabrication. In particular, it is desirable to find a surface treatment steps which reduce the density of surface states. In crystalline silicon, this is achieved by cleaving the Si surface in ultra high vacuum, or by heating or sputtering followed by annealing [1]. None of these methods can be used for a-Si:H. This is because heating at high temperatures (more than 300°C) leads to hydrogen evolution from the material and increases the bulk density of states in a-Si:H, quite significantly [2]. This renders the material useless, for device purposes. Also, sputtering increases the electronic states significantly [3]. Therefore, it is desirable to devise an optimised surface treatment step to produce a clean surface having lower density of surface states. Attempts have been made to characterise the surfaces for contamination in order to produce atomically clean surface in crystalline silicon [1] as well as amorphous silicon [4]. However, no systematic studies of estimation of density of surface states have been reported after such treatments, in the case of a-Si:H.

In this Chapter, we use the technique, described in Chapter 4, for the measurement of density of surface states in undoped a-Si:H to see how the density of surface states changes when it is subjected to various surface treatments. This also checks the sensitivity of the technique proposed in Chapter 4. We have also calculated the density of bulk states (N_b), after various surface treatments using the following relation [5]:

$$N_b = 1.6 \times 10^{16} \int_{regionII} \alpha_{diff} dE, \tag{5.1}$$

where, α_{diff} is the difference between measured α using CPM, in the region II and extrapolated value of α from region I (Fig. 5.1).

5.1 Surface Treatments

We have used various surface treatment steps. which are defined below. State A is the rested state of the as deposited sample. States B and C are the light soaked ($20mW/cm^2$ for 15 hours) and the annealed ($150°C$ for 2 hours) states respectively.

State D is obtained by etching (HF etched. 15 % in DI water) the native oxide from a-Si:H surface. The surface is again oxidised by treating with concentrated H_2SO_4 and subsequent annealing (State E). States F and H are the room temperature plasma treated states. State F is obtained by treating the sample in state E with room temperature nitrogen plasma (300K, 40mW/cm^2 for 2 hours). State G is obtained by annealing the sample in state F (Annealed at $150°C$ for 2 hours). State H is hydrogen plasma (300K, 40mW/cm^2 for 2 hours) treated state. More details of the various treatment steps are given in Section 2.1.4.

5.2 Results and Discussion

In Figs. 5.1 - 5.4, we present our results on sub gap absorption measured as a function of hν by CPM and PDS for an undoped a-Si:H (Sample No. #18) in state A (rested state) and state B (light soaked state) [Fig. 5.1]; States D (oxide etched state) and E (oxidised state) [Fig. 5.2]; States F (nitrogen plasma treated state) and G (subsequently annealed state) [Fig. 5.3]; and state H (hydrogen plasma treated state) [Fig. 5.4]. Sub gap absorption data is analysed and the density of surface states (N_s) are obtained using the analysis described in Chapter 4 [6,7]. Also, the density of the bulk states (N_b) are calculated using Eq. (5.1). The values of N_s and N_b are plotted in Fig. 5.5 after various surface treatments; from states A to H.

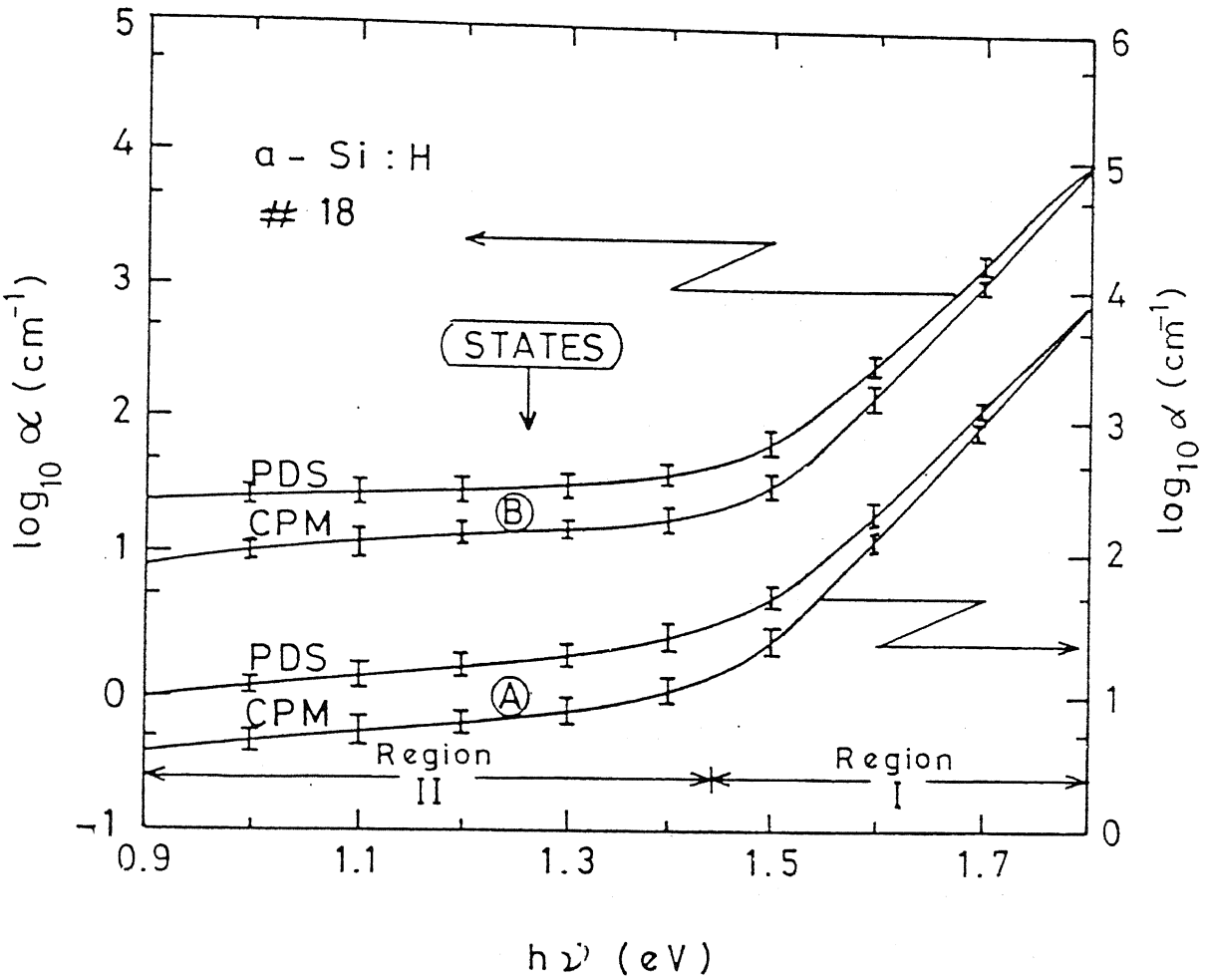

Figure 5.1: log α as a function of hν as measured by CPM, PDS and Transmission for a-Si:H sample. Fringes in the curves arising from the thin film interference have been averaged out. States A and B represent the rested and the light soaked states respectively. Note different α axes for the two states in Figs. 5.1 to 5.3. The error bars in this figure is the same for the Figs. 5.2 and 5.3.

Fig. 5.1 shows $\alpha(h\nu)$ measured by CPM and PDS in the rested state (state A) and after light soaking (state B) in undoped a-Si:H. N_b and N_s calculated using CPM and PDS data in Fig. 5.1, are shown in Fig. 5.5. From Fig. 5.5, we find that after light soaking (State B) the density of dangling bond states (N_b) increases from $\approx 5\times10^{16}cm^{-3}$ to $\approx 1\times10^{17}cm^{-3}$ without much change in the surface states. This is in agreement with the literature [8,9]. Annealing the sample (150°C for 2 hours; state C) brings N_b back to its rested value ($\approx 5\times10^{16}cm^{-3}$).

Fig. 5.2 shows $\alpha(h\nu)$ measured using CPM and PDS on etching a-Si:H in state C (annealed state) with 15% HF in deionised water (state D). Fig. 5.2 also gives $\alpha(h\nu)$ measured using CPM and PDS after re growth of oxide layer (state E) by treating the sample with concentrated H_2SO_4 followed by annealing. We find (Fig. 5.5) that the density of surface states increases from $\approx 4\times10^{12}cm^{-2}$ in the annealed state (state C) to $\approx 6.5\times10^{12}cm^{-2}$ after etching with HF (state D). The bulk states, however, remain unchanged within the errors. This shows that freshly etched surface, which is devoid of the native oxide, has a higher density of surface states. This may be explained as follows. One type of structural disorder that might lead to the surface states in the gap is the presence of near surface dangling bonds [10]. Removal of oxide from the surface might increase the near surface dangling bond and hence an increase in the density of surface states on oxide etching. We confirm this by growing oxide again and measuring the surface states. The oxide passivates the surface and brings back the density of surface states to its starting (lower) value in the annealed state (state E).

Finally, we have treated the a-Si:H sample first with nitrogen plasma (state F) and then with hydrogen plasma. Fig. 5.3 shows $\alpha(h\nu)$ measured using CPM and PDS in state F along with that in state G. State G is obtained by annealing the state F. Nitrogen plasma (300K, $40mW/cm^2$,dc plasma for 2 hours) treatment is found to increase the density of surface states from $\approx 4\times10^{12}cm^{-2}$ to $\approx 5\times10^{12}cm^{-2}$. This small change is within the errors of measurement. Also there is a small increase in the density of bulk states, which is within the errors of measurement. This shows that treatment with nitrogen plasma does not have much effect on either the bulk states or the surface states. No change in bulk states as well as the surface states was observed on annealing the sample after nitrogen plasma treatment.

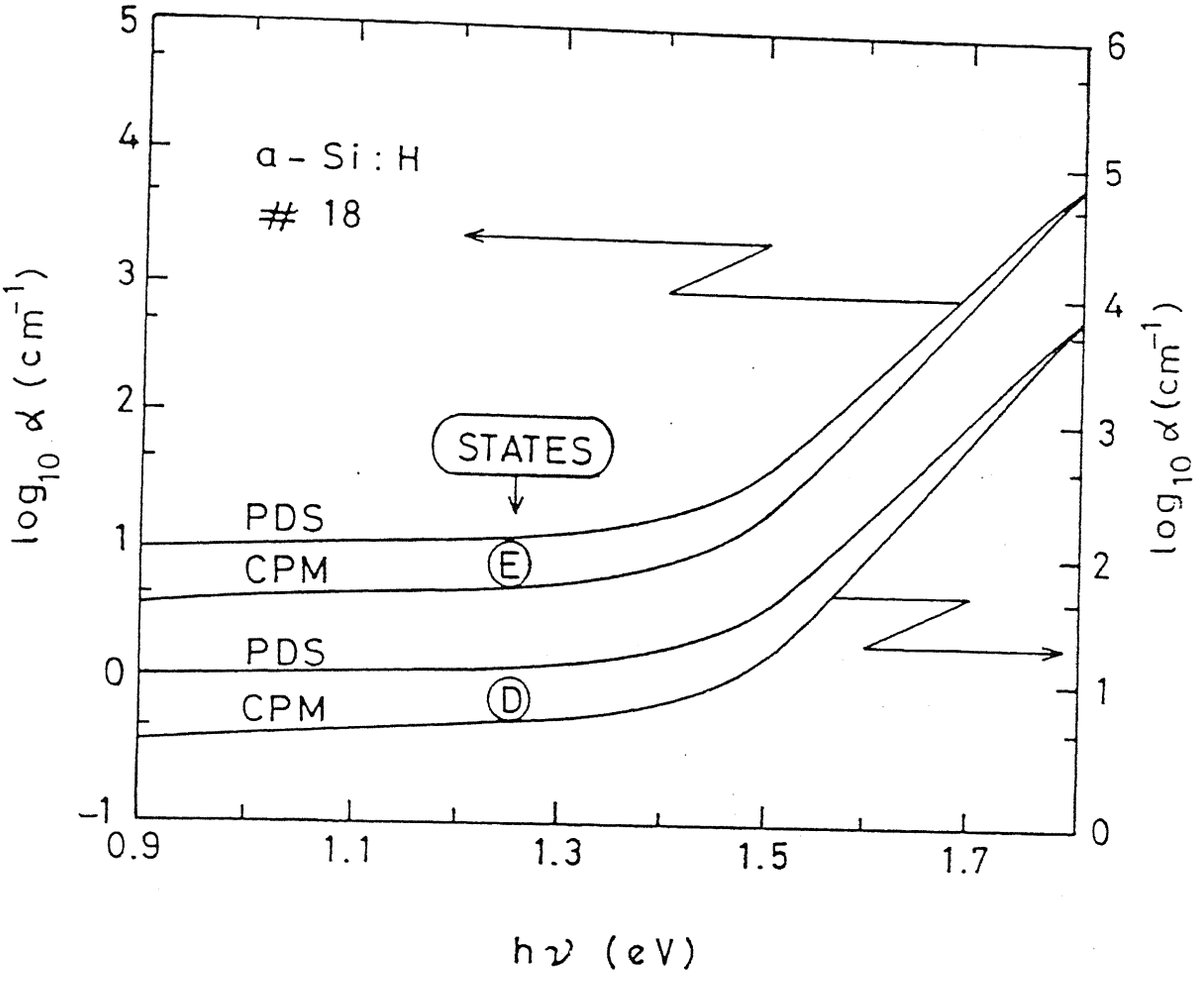

Figure 5.2: log α as a function of hν as measured by CPM, PDS for a-Si:H sample. Fringes in the curves arising from the thin film interference have been averaged out. States D and E represent the HF etched and the oxidised states respectively.

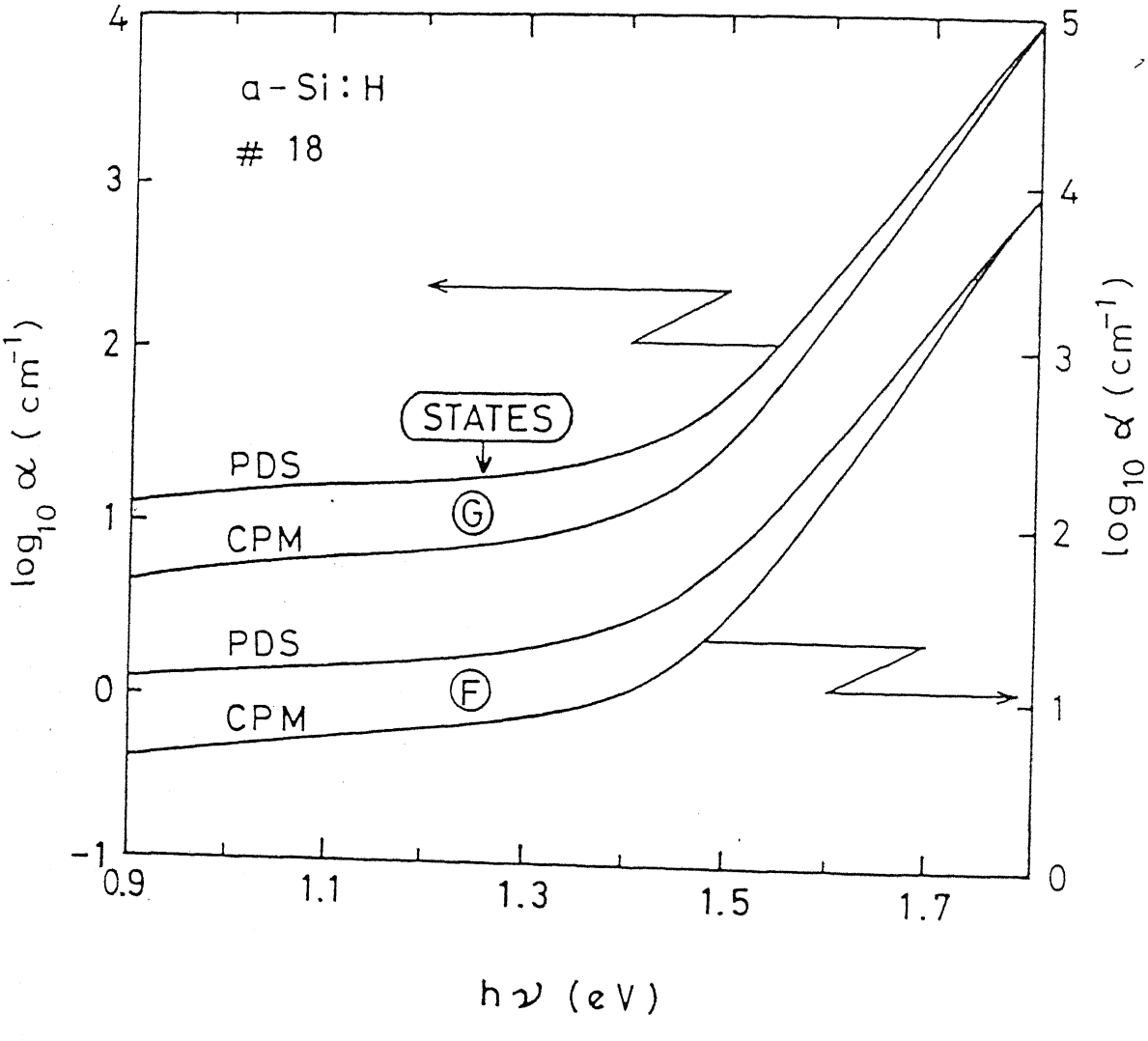

Figure 5.3: log α as a function of hν as measured by CPM, PDS for a-Si:H sample. Fringes in the curves arising from the thin film interference have been averaged out. States F and G represent the nitrogen plasma treated and the subsequent annealed states respectively.

Fig. 5.4 shows $\alpha(h\nu)$ measured using CPM and PDS after hydrogen plasma treatment (300K, $40mW/cm^2$,dc plasma for 2 hours). Hydrogen plasma is found to do the surface passivation by decreasing the surface states to $\approx 2.5 \times 10^{12}cm^{-2}$. This may be because of surface dangling bond termination by H atoms in the plasma. We thus conclude that Hydrogen plasma gives a surface with a low density of surface states ($\approx 2.5 \times 10^{12}cm^{-2}$). Etching of native oxide, however, increases the density of surface states by about 50%.

5.3 Summary and Conclusions

We have measured sub gap absorption coefficient as a function of photon energy using CPM and PDS for a-Si:H after various surface treatments. These include light soaking (B), annealing (C), etching of the native oxide using HF (D) and subsequent oxide growth by concentrated sulfuric acid (E) and treatment with nitrogen (F) and hydrogen plasma (H). Density of surface states and the bulk states are calculated after each surface treatment. We find that light soaking increases the density of bulk states by a factor of 2, without changing the surface states. This is in agreement with the literature that light soaking is mainly a bulk effect. Another notable results regarding the surface states are that the surface states increase from $\approx 4\times10^{12}cm^{-2}$ in the annealed state (state C) to $\approx 6.5\times10^{12}cm^{-2}$ after etching with HF (state D). Hydrogen plasma treatment, however, is found to decrease the density of surface states from $\approx 5\times10^{12}cm^{-2}$ in state G) to $\approx 2.5\times10^{12}cm^{-2}$ after etching (state H). This explains why exposing with hydrogen plasma produce better results whenever a-Si:H based devices involving several interfaces (e.g. solar cells) are made.

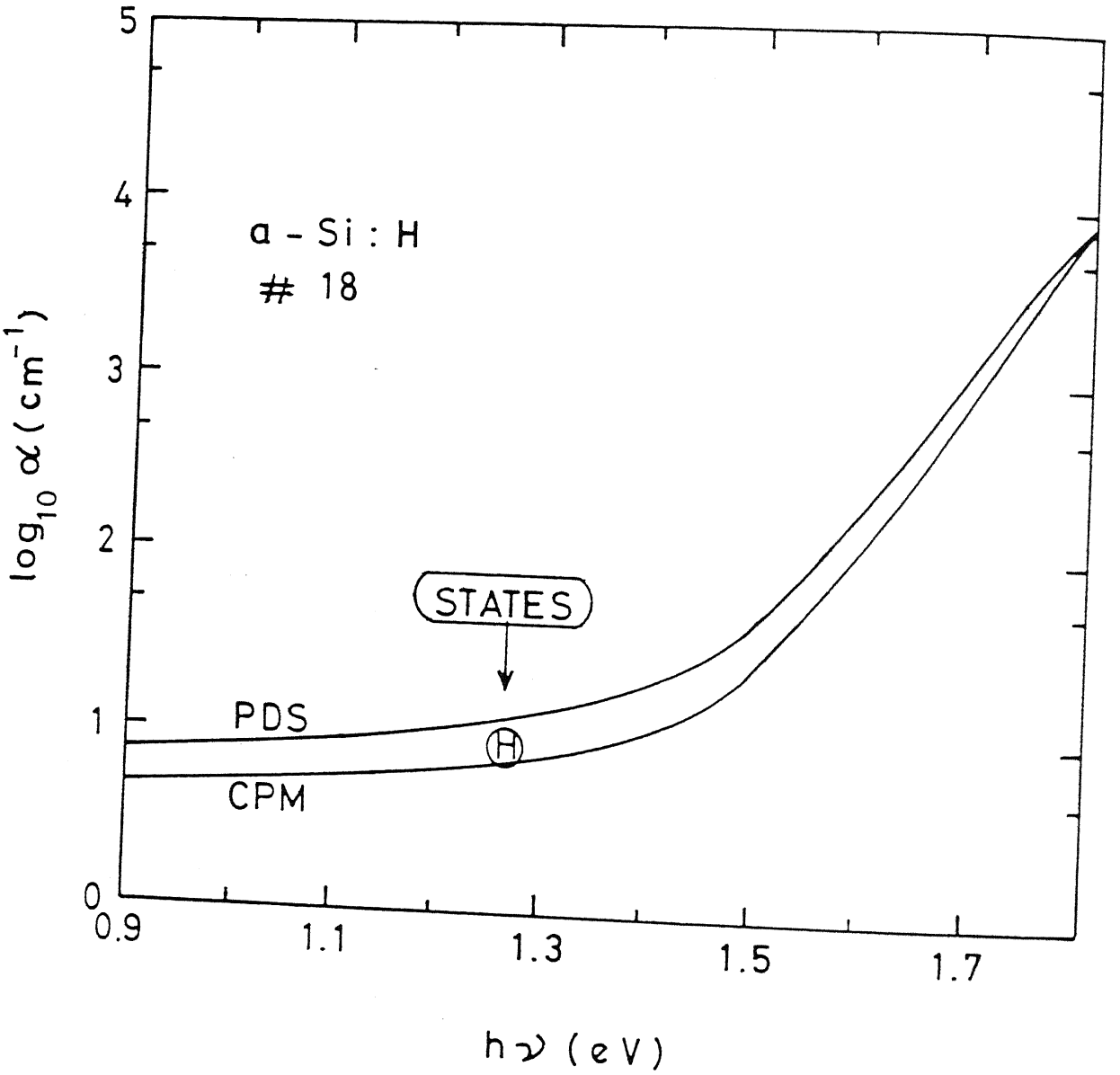

Figure 5.4: log α as a function of hν as measured by CPM, PDS for a-Si:H sample. Fringes in the curves arising from the thin film interference have been averaged out. States H represents the hydrogen plasma treated state.

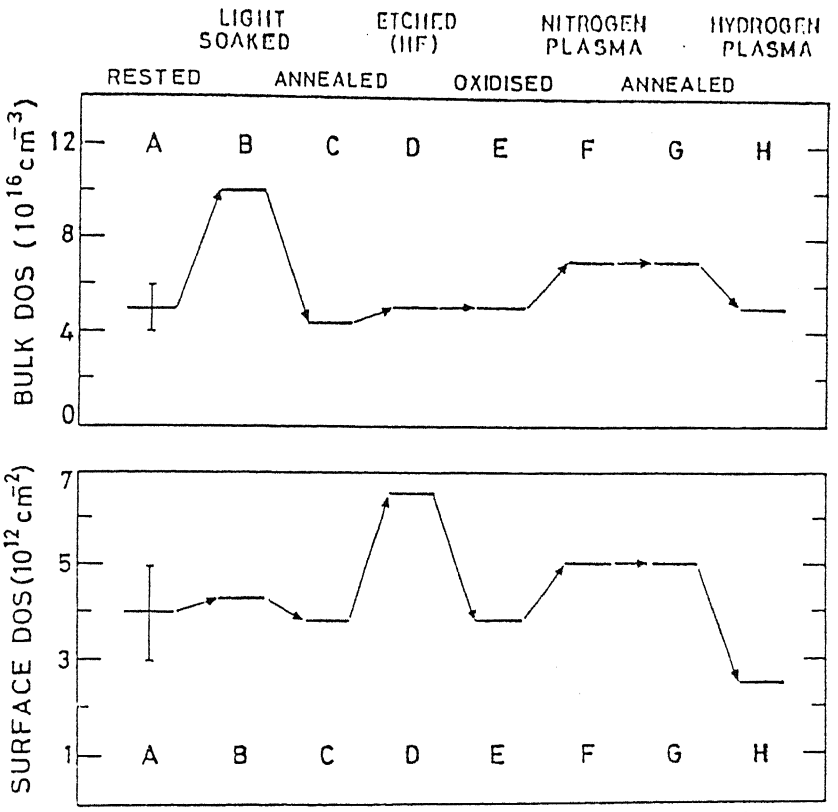

Figure 5.5: Bulk and surface density of states after various surface treatments. State A (Rested), State B (Light Soaked, $20mW/cm^2$ for 15 hours), State C (Annealed at $150°C$ for 2 hours), State D (HF etched, 15 % in DI water), State E (concentrated. H_2SO_4 treated and annealed), State F (exposed to Nitrogen plasma, 300K, $40\text{mW}/cm^2$ for 2 hours), State G (Annealed at $150°C$ for 2 hours) State H (exposed to Hydrogen, 300K, $40\text{mW}/cm^2$ for 2 hours). The vertical lines in the state A gives the error bars of the measurements (after reference 6).

Bibliography

1. D. B. Fenner, D. K. Biegelsen, and R. D. Bringans, J. Appl. Phys. **66**, 419 (1989).

2. J. D. Joannopoulos and G. Lucovsky (ed) in The Physics of Hydrogenated Amorphous Silicon (Springer, Berlin) 1984.

3. L. Ley, H. Richter, R. Karcher, R. L. Johnson and J. Reitchardt, J. Physique Coll. **C4 42**, 753 (1981).

4. C. Anandan, and R. H. Williams, Semicond. Sci. Technol. **5**. 265 (1990).

5. Z. E. Smith, V. Chu, K. Shepard, S. Aljishi, D. Slobodin, J. Kolodzey, S. Wagner, and T. L. Chu, Appl. Phys. Lett. **50**, 1521 (1987).

6. A. K. Sinha and S. C. Agarwal, Phil. Mag. B , (1998)(in Press).

7. A. K. Sinha, G. S. Narayana, S. K. Tripathi and S. C. Agarwal, To appear in J. Non Cryst. Solids (1998).

8. S. Guha, J. Non-Cryst. Solids, **77 & 78**. 1451 (1985).

9. S. Kumar and S. C. Agarwal, Phil. Mag. **B 49**, L53 (1984).

10. K. Winer and L. Ley, Phys. Rev. **B36**, 6072 (1987).

Chapter 6

Potential Fluctuations

6.1 Potential fluctuations in a-Si:H

So far, we have explained sub-gap absorption results in terms of single particle density of states, assuming a-Si:H to be a homogeneous material. In reality, however, a-Si:H is heterogeneous. The heterogeneities give rise to potential fluctuations in a-Si:H. Several experiments like NMR [1] show that even the best quality (device grade) a-Si:H contains voids and clusters of hydrogen. giving rise to potential fluctuations. Additionally, potential fluctuations may also arise from the variations in bond length and bond angles. Further, neutral and charged dangling bonds as well as the dopants (if present) may also contribute to the potential fluctuations in a-Si:H [2,3]. It is not easy to deal with the potential fluctuations in a fundamental manner. Nevertheless, it is important to study them because they are expected to influence the electronic properties in a profound manner [4].

The range of these potential fluctuations has been estimated to be of the order of inter atomic distances ($\approx 3\mathring{A}$) [5]. However, in the transport measurements (conductivity and thermopower) the carriers move through these potential fluctuations. So the carriers are likely to overlook very sharp changes in the potential because of quantum mechanical tunneling. Therefore, these measurements are sensitive to the range of fluctuations, which is likely to be longer ($\approx 80\mathring{A}$) [6,7]. Overhof and Beyer [6,7], have explained the difference between the activation energies of conductivity and thermopower

by considering the long range potential fluctuations [6,7]. The details are described below:

The general expression for conductivity, assuming extended state conduction by electrons, is given as

$$\sigma = \int \sigma(E)dE = \sigma_o exp(-(E_c - E_f)/kT) = \sigma_o exp(-E_\sigma/kT), \tag{6.1}$$

where, σ_o contains the mobility factor. E_σ = E_c - E_f is the conductivity activation energy. Similarly, thermopower S can be written as

$$S = \frac{1}{eT\sigma}\int (E - E_f)\sigma(E)dE, \tag{6.2}$$

For the extended band conduction, Eq. (6.2) gives

$$S = -\frac{k}{e}[(E_c - E_f)/kT + A] = -\frac{k}{e}(E_s/kT + A), \tag{6.3}$$

where, A $\approx$ 1, is a constant. Again, E_s = E_c - E_f is the thermopower activation energy. In a-Si:H, in general we expect E_σ = E_s, contrary to the observations. The following reasons have been proposed for this difference [8]:

1. If both electrons and holes are conducting, S will have opposite signs for the two carriers, making E_s different from E_σ. But this effect can be neglected for doped (n-type) a-Si:H, where, only one type of the carriers (electrons) dominate.

2. Mobility edge may not be very sharp.

3. Conductivity may not be spatially homogeneous, because of the heterogeneities in the material. This appears most likely in a-Si:H.

In order to eliminate the effect of Fermi level position because of either the statistical shift or any other agency like doping, Overhof and Beyer [4,5], have defined a function Q given by

$$Q = ln\ \sigma + (e/k)S = Q_o + E_Q/kT, \tag{6.4}$$

where, Q_o =ln σ_o + A and E_Q = E_σ - E_s. In order to explain non zero value of E_Q, Overhof and Beyer [6,7] have done model calculations for σ and S, in which a-Si:H sample is divided into small cells. Each cell has a disorder potential attributed to it by

random number generation, which decides the local mobility edge. Their model shows that E_Q is a measure of the width of the long range potential fluctuations (Δ), and the two is related by [6,7]

$$E_Q = 1.25\Delta \tag{6.5}$$

As already explained, these measurements can give only the long range potential fluctuations, which may be some kind of average of the short range potential fluctuations. Optical measurements, on the other hand are the vertical transitions. Therefore, optical measurements are likely to sense the short range potential fluctuations, inherent in the material. Attempts [5,9] have been made to calculate $\alpha(h\nu)$ in the sub gap region using potential fluctuations, theoretically. These attempts are limited to obtaining the exponential absorption in the Urbach edge region, starting from the Gaussian potential fluctuations. It is found [10] that for the range of potential fluctuations, L >> λ (where λ is the de broglie wave length of the free electrons); a Gaussian Urbach edge is obtained from a Gaussian potential fluctuations. On the other hand, Halprin and Lax [11] find that for L << λ, the density of localised states in the Urbach edge, g(E) $\propto exp(E^{1/2})$. Quantum mechanical calculations of John et al [5], successfully predict the exponential shape of the Urbach edge, starting from the Gaussian potential fluctuations, provided the correlation length of the potential fluctuations is taken to be ≈ 3 Å. Thus, we expect that the range of the potential fluctuations seen by optical absorption measurements are short, of the order of the inter atomic distances (≈ 3 Å). The calculations by John et al [5] show that the width of the short range potential fluctuations (V_s) is related to the slope of the Urbach edge E_o by the relation [5]:

$$V_s^2 = 20 E_o \epsilon_L, \tag{6.6}$$

where, $\epsilon_L = h^2/(8\pi^2 L^2) \approx 0.5$eV.

6.2 Determination of potential fluctuations

In this section, we first determine the width of long range potential fluctuations using transport measurements in undoped a-Si:H and a-Si:H doped with various concentra-

tions of phosphorous (P). We then estimate the short range potential fluctuations using sub gap absorption data, measured by PDS on the same samples for which width of long range potential fluctuations were estimated. An empirical relation between the two widths is discussed. Also, we explain the difference in $\alpha(h\nu)$ measured by CPM and PDS qualitatively.

6.2.1 Determination of potential fluctuations using transport measurements

We estimate the long range potential fluctuations from the transport data following Overhof and Beyer [6,7]. We take E_c to be constant in a cube of linear dimensions L ($\approx$ 80 $\AA$). It is, therefore, possible to define a local conductance inside a cube of volume L^3 centered around a site X_i as:

$$g_i(X_i) = (\sigma_o/L)exp[-(E_c(X_i) - E_F)/kT] \tag{6.7}$$

where, $E_c(X_i) = < E_c > + V(X_i)$ is the position of the local conduction band. The probability that $V(X_i)$ has a value ϵ is given by [6,7]

$$p(\epsilon) = p_o^{'}exp(-\epsilon^2/\Delta^2) \tag{6.8}$$

Therefore, the sample is replaced by a resistance network, and gives a^3 interconnecting resistances. a^3 is the number of sites in which the sample is divided for the model calculations. We use Kirchoff's relations to solve the problem. a^3 simultaneous equations are solved by the inversion of $a^3 \times a^3$ matrix. The matrix inversion is done by Gauss elimination technique, because the matrix is sparse. We find, in agreement with the literature [6,7], that the slope E_Q of the function Q (= lnσ + e/k S) as a function of 1/T plot is related to the width Δ as

$$E_Q = 1.25\Delta \tag{6.9}$$

Using Eq. (6.9) we calculate the width of potential fluctuations (Δ). Fig. 6.1 shows Q function plotted as a function of 1000/T for three P doped samples. E_Q is estimated

Table 6.1: Conductivity activation energy (E_σ), slope of Q function as a function of 1/T (E_Q) and width of the long range potential fluctuations (Δ). Samples are listed in the order of increasing P concentration. *E_Q for undoped sample is taken from Ref 12 and is not for the sample #18

Sample details	E_σ (eV)	E_Q (eV)	Δ (eV)
a-Si:H(#18)	0.70±0.01	(.05 ±.01)*	.04 ± .005
a-Si:H(P)(#5)	0.30±0.01	.08 ±.01	.06 ± .005
a-Si:H(P)(#12)	0.28±0.01	.08 ±.01	.06 ± .005
a-Si:H(P)(#11)	0.24±0.01	.10 ±.01	.08 ± .005

from the slope of these curves. Δ for all the samples is calculated. Values of E_Q along with Δ are given in Table 6.1. It may be noted that Q for undoped sample could not be measured because the sample is highly resistive. E_Q in Table 6.1 has been taken from the literature [12] for a similar sample. We find that Δ increases from 0.040± 0.005eV for the undoped sample (sample No. 18, $E_\sigma \approx 0.7eV$) to 0.08± 0.01eV for the sample with highest doping (sample No. 11, $E_\sigma \approx 0.24$eV).

6.2.2 Determination of potential fluctuations from optical absorption data

Fig. 6.2 shows sub gap $\alpha(h\nu)$ measured between 0.9eV and 1.8eV using CPM [13,14] and PDS [15,16]. It is found that in the sub gap region, $\alpha_{pds} > \alpha_{cpm}$. This difference is qualitatively explained using potential fluctuations as follows:

Fig. 6.3 shows schematic of the potential fluctuations as might be present in a-Si:H [17], E_c and E_v represent the conduction band and the valance band percolation levels respectively. Representative optical transitions are also shown in the figure. Transitions of type 1 takes an electron to the final state above the conduction band percolation level; whereas, transitions of type 2 and 3 take the electrons to the levels below the critical percolation level. In CPM, only those transitions are seen, which are able to conduct

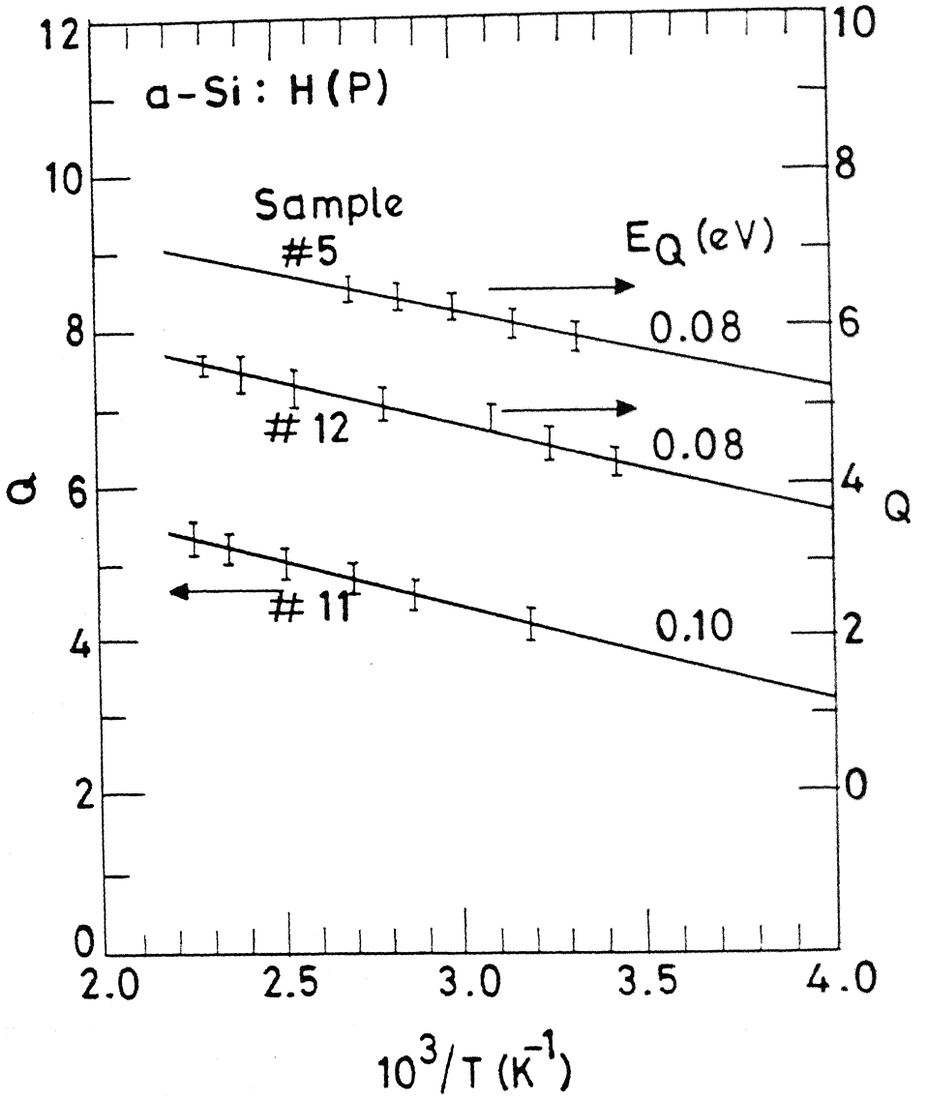

Figure 6.1: Function Q = lnσ +(e/k)S plotted as a function of 1000/T for three P doped samples; sample #5, sample #12(ref. 8) and sample #11(ref. 8). Note the different scales for different samples.

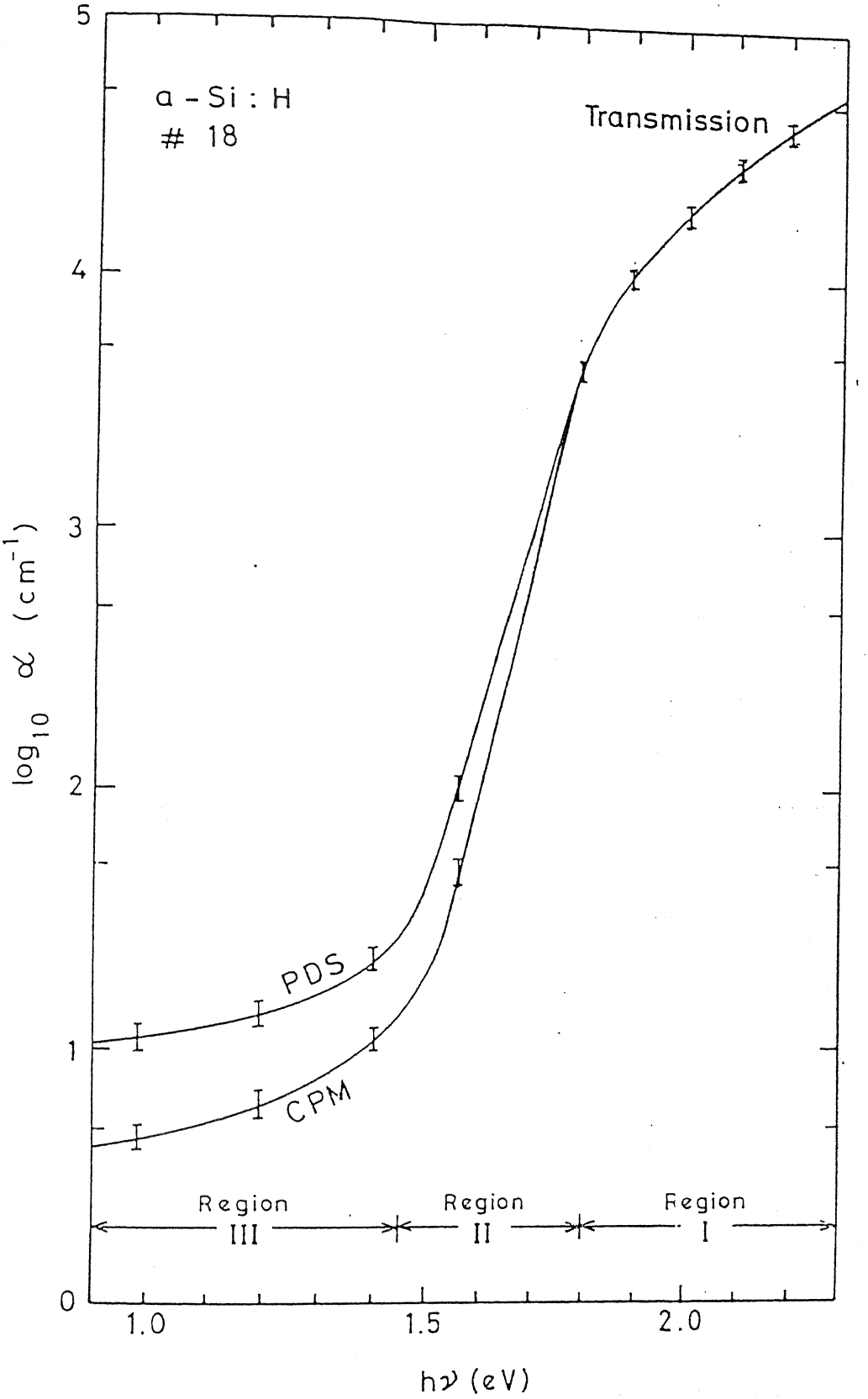

Figure 6.2: Sub gap absorption measured as a function of photon energy using CPM and PDS(regions II and III) and using transmission(region I) for undoped a-Si:H. The interference fringes in the data have been averaged out.

i.e. which are above E_c level. So, CPM is not sensitive to transitions of type 2 and 3. On the other hand, PDS is a thermal effect and is likely to be sensitive to all the transitions from 1 to 3. This qualitatively explains the difference between α_{pds} and α_{cpm} in a-Si:H. As estimation of α_{cpm} in the potential fluctuations model requires a knowledge of both the optical absorption as well as transport in a complicated manner, and is not discussed here. We used PDS data for quantitative estimation of the potential fluctuations.

In the literature, considerable amount of work [5,9] has been done to explain the exponential nature of the optical absorption edge in the Urbach region. So far, the only successful attempt in explaining the exponential edge starting from Gaussian potential fluctuations, seems to be by John et al [5]. The authors show that if $L \approx \lambda$, it is possible to get an exponential absorption edge although the potential fluctuations follow a Gaussian distribution. Indeed they argue that $L \approx \lambda$ is the experimentally observed range in the Urbach edge region. Here, $\lambda = h/2\pi(2mE)^{1/2}$ and is found to be ≈ 3 Å, for free electron mass. If the Gaussian distribution of the potential fluctuations in Urbach edge region is given by

$$p_u(\epsilon) = p_o^u[\frac{1}{\sqrt{(2\pi)}V_s} exp(-\epsilon^2/V_s^2)]. \tag{6.10}$$

The slope of Urbach edge E_o is related to V_s as [5],

$$V_s^2 = 20 E_o \epsilon_L \tag{6.11}$$

where, $\epsilon_L = h^2/8\pi^2 L^2 \approx 0.5$eV [5]. From the measured Urbach slope E_o, V_s is calculated using Eq. (6.11) for all the samples, and are given in Table 6.2.

Let us now consider region II (Fig. 6.4) of sub gap absorption curve. No attempt has been made in the literature to calculate potential fluctuations giving rise to absorption in this region. The potential fluctuations in this region may arise from the deep defects like dangling bonds. We propose that the dangling bonds also give rise to a Gaussian distribution of potential fluctuations. These potential fluctuations are superimposed on the potential fluctuations given by Eq (6.10). We assume that this second component of the potential fluctuations has a smaller height and a larger width than the first

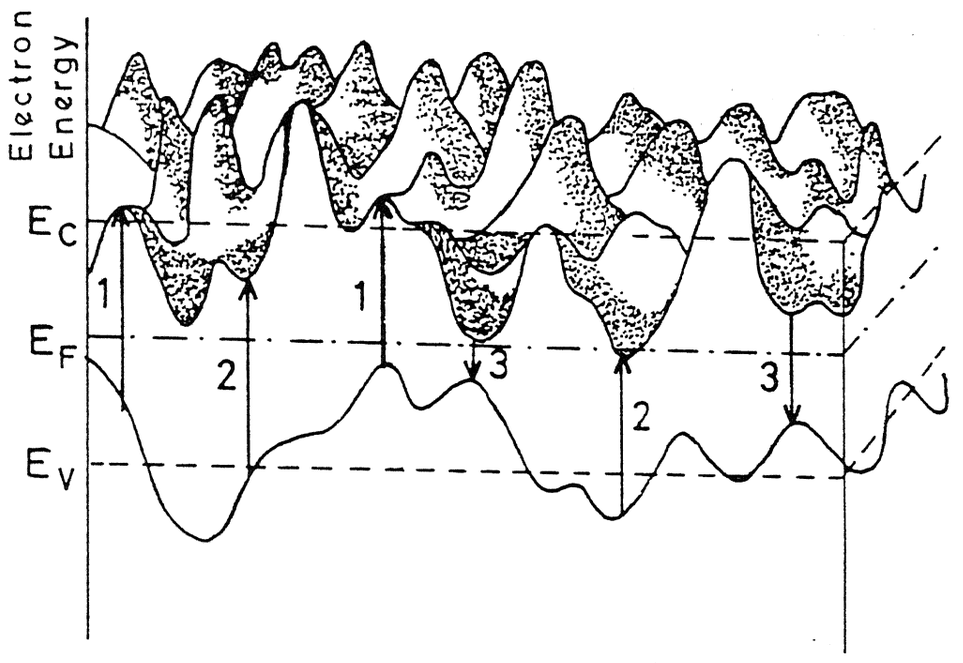

Figure 6.3: Long range potential fluctuations as might be present in a-Si:H(E_V and E_C represent the valance and conduction band mobility edges; E_F is the Fermi level). CPM sees the optical transitions marked 1, whereas, PDS sees all the transitions marked 1 and 2(after reference 17).

component ($V_s' >> V_s$). We further assume that the width of the second component of the potential fluctuations is also given by a relation similar to that given in Eq (6.11):

$$(V_s')^2 = 20E_o'\epsilon_L \tag{6.12}$$

where, E_o' is the slope of the region II of the optical absorption curve (Fig. 6.4). Therefore, the probability, $p(\epsilon)$, that the local conduction band is ϵ away from its mean value is given by the following sum of two Gaussians, one each because of the absorption from the Urbach edge region and from the plateau region:

$$p(\epsilon) = p_o[\frac{1}{\sqrt{(2\pi)}V_s}exp(-\epsilon^2/V_s^2) + \frac{B}{\sqrt{(2\pi)}V_s'}exp(-\epsilon^2/(V_s')^2] \tag{6.13}$$

where the zero of the energy is chosen at the mean of the fluctuating conduction band. p_o is the normalisation factor for $p(\epsilon)$ and is found to be $p_o = \sqrt{(2)}/(1+B)$. We define the total width (V_T) for all the potential fluctuations taken together by:

$$V_T = [\int_{-\infty}^{+\infty}(\epsilon^2 p(\epsilon)d\epsilon)]^{1/2} \tag{6.14}$$

Using $p(\epsilon)$ from Eq. (9), we get $V_T = [(V_L)^2 + B(V_L')^2)/(1+B)]^{1/2}$. The scaling factor B is calculated by taking the ratio of $\alpha(1.8eV)$ and the extrapolated value of α at 1.8eV from the plateau region.

We find that E_o increases with the doping level; being $\approx$ 55meV for the undoped a-Si:H ($E_\sigma \approx 0.7$eV) and $\approx$ 110meV for highest doping ($E_\sigma \approx 0.24$eV). The width of the potential fluctuations (V_T), estimated from the optical absorption data, is also found to increase with the level of doping, being $\approx$ 0.8eV for the undoped sample (No. 18) and 1.45eV for the sample (No 11), with the highest P doping. The values of E_o', V_s', A and V_T for all the samples are given in Table 6.2. Also, the width of the long range potential fluctuations (Δ) estimated from the transport measurements is found to increase with the doping level. $\Delta \approx 0.04$eV for the undoped sample (No. 18) and $\approx$ 0.08eV for sample with highest P doping (No. 11).

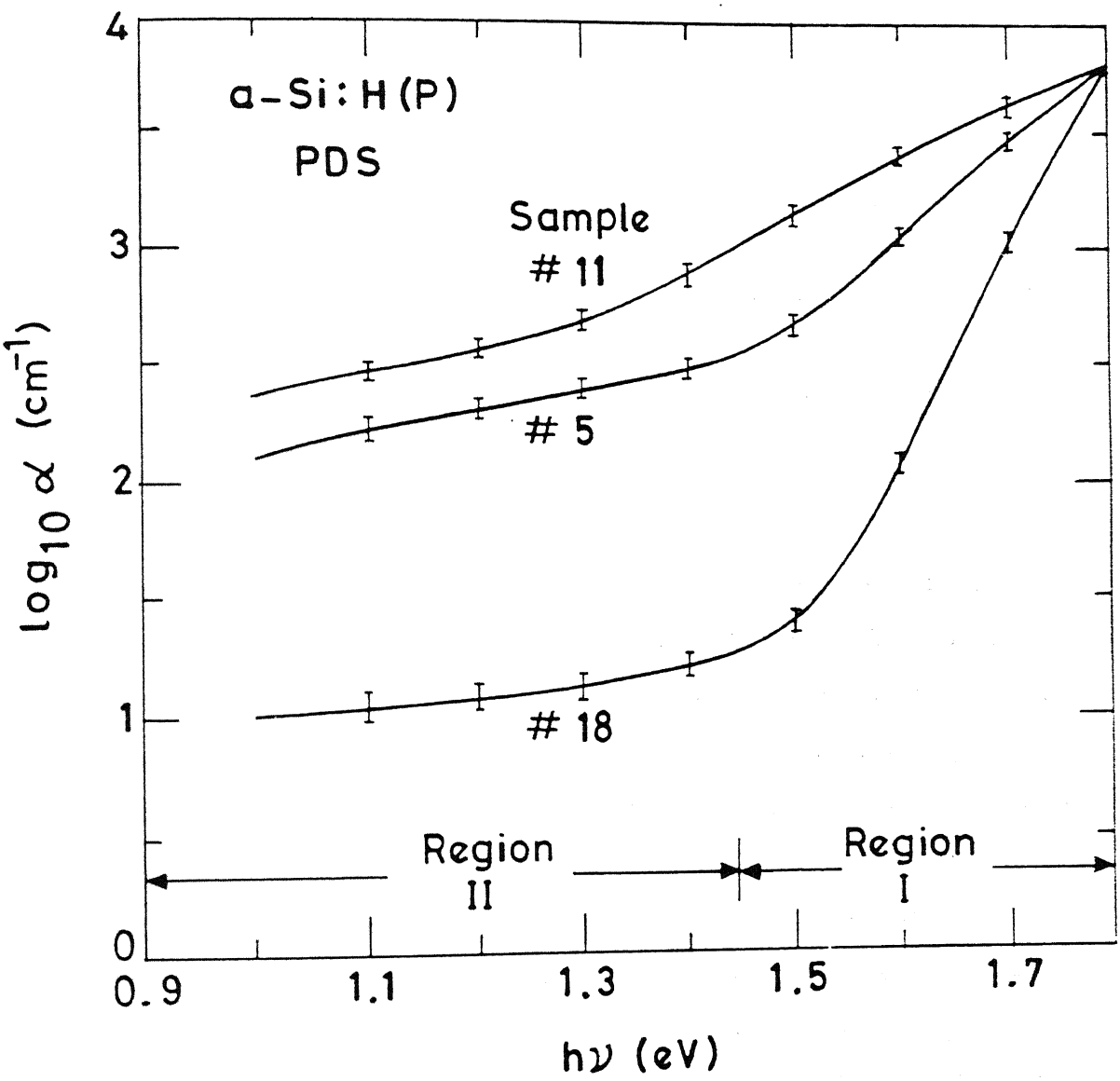

Figure 6.4: Sub gap absorption as a function of photon energy measured using PDS for undoped(#18) and P doped a-Si:H(#5 and #11). The interference fringes have been averaged out.

Table 6.2: Slope(E_o) of Urbach edge, width(V_s) of the first term of the short range potential fluctuations, Slope(E_o') of plateau part of $\alpha(h\nu)$, width(V_s') of the second term of the short range potential fluctuations, B and total width(V_T) of the short range potential fluctuations. The samples are listed in the order of increasing phosphorous concentration

Sample details	E_o (meV)	V_s (eV)	E_o' (eV)	V_s' (eV)	B	V_T (eV)
a-Si:H(#18)	55±5	0.74±.05	0.56±.02	2.37 ±.05	0.01 ±.001	0.75 ± .05
a-Si:H(P)(#5)	85±5	0.92±.05	0.51 ±.02	2.26 ± .05	.05 ±.001	1.05 ± .05
a-Si:H(P)(#12)	100±5	1.0±.05	0.48±.02	2.19 ± .05	.1 ±.001	1.20 ± .05
a-Si:H(P)(#11)	110±5	1.05±.05	0.45±.02	1.12 ± .05	.1 ±.001	1.30 ± .05

6.3 Discussion

We find that $V_T > \Delta$ for all the samples studied. This is not surprising because transport measurements may not see the sharp short range fluctuations, because the carriers can tunnel through them (quantum mechanical tunneling). Therefore, the transport measurements see only the long range potential fluctuations which are likely to be an average of the short range potential fluctuations, inherent in the material. On the other hand, optical measurements are vertical transitions in the real space and hence are sensitive to short range potential fluctuations, whose width may be larger than the width of the long range potential fluctuations.

A relation between V_T and Δ has not been attempted either experimentally or theoretically, so far. It is interesting to see how the width of the potential fluctuations scale with the range of the potential fluctuations. We plot V_T as a function of Δ in Fig. 6.5, and find that the data can fit a straight line of the form:

$$V_T = K\Delta \tag{6.15}$$

Here, K is found to be 20±5 for our samples. Qualitatively, it may be argued that in the long range potential fluctuations, we see a kind of averaging of the fluctuations.

The averaging decreases the width of the fluctuations by a factor of ≈ 20, in our case. Further, it is interesting to see that $K \approx L/L'$, where, L and L' are the ranges of the long and the short range potential fluctuations, which are 80 $\AA$ and 3 $\AA$ respectively. This shows that the transport measurements are sensitive to a potential fluctuations which get averaged by a factor of $\approx L/L'$. This is, however, only an empirical result and needs to be further justified theoretically. This has not been done, so far.

6.4 Summary and Conclusions

We have proposed explanation of sub gap absorption measurements using potential fluctuation model, in undoped as well as P doped samples. This is an alternative explanation and is different from the single particle density of states explanation of optical absorption, in which a-Si:H is assumed to be homogeneous. We find that α_{pds} is larger than α_{cpm} for all the samples. This result is in agreement with the literature. In the potential fluctuations model, this difference is explained as follows:

In CPM, we measure α from photoconductivity. In undoped and n type doped a-Si:H, at room temperatures and higher only electron conduction is important. This is because the hole mobility is about an order of magnitude lower [20]. Also in CPM, the photogenerated carriers must be able to conduct in order to contribute to α_{cpm}. On the other hand, PDS measures the absorption coefficient by measuring the heat produced when the sample absorbs light. Thus, only the transitions of the type marked 1 (Fig 6.3) contribute to CPM, but all the transitions marked 1 to 3 contribute to PDS. This explains the experimentally observed result ($\alpha_{pds} > \alpha_{cpm}$) qualitatively. However, it is difficult to obtain α_{cpm} theoretically. Therefore, for calculations of the width of short range potential fluctuations, we use only the PDS data, which is easier to handle.

We have estimated the width of potential fluctuations in undoped a-Si:H and a-Si:H doped with various amounts of phosphorous (P), using optical sub-gap absorption measurements and transport measurements, viz conductivity and thermopower as functions of temperature. Both measurements show that the width of the potential fluctuations increases upon increasing the phosphorous doping. We find that the width of the potential fluctuation measured by optical measurements is larger than that measured by

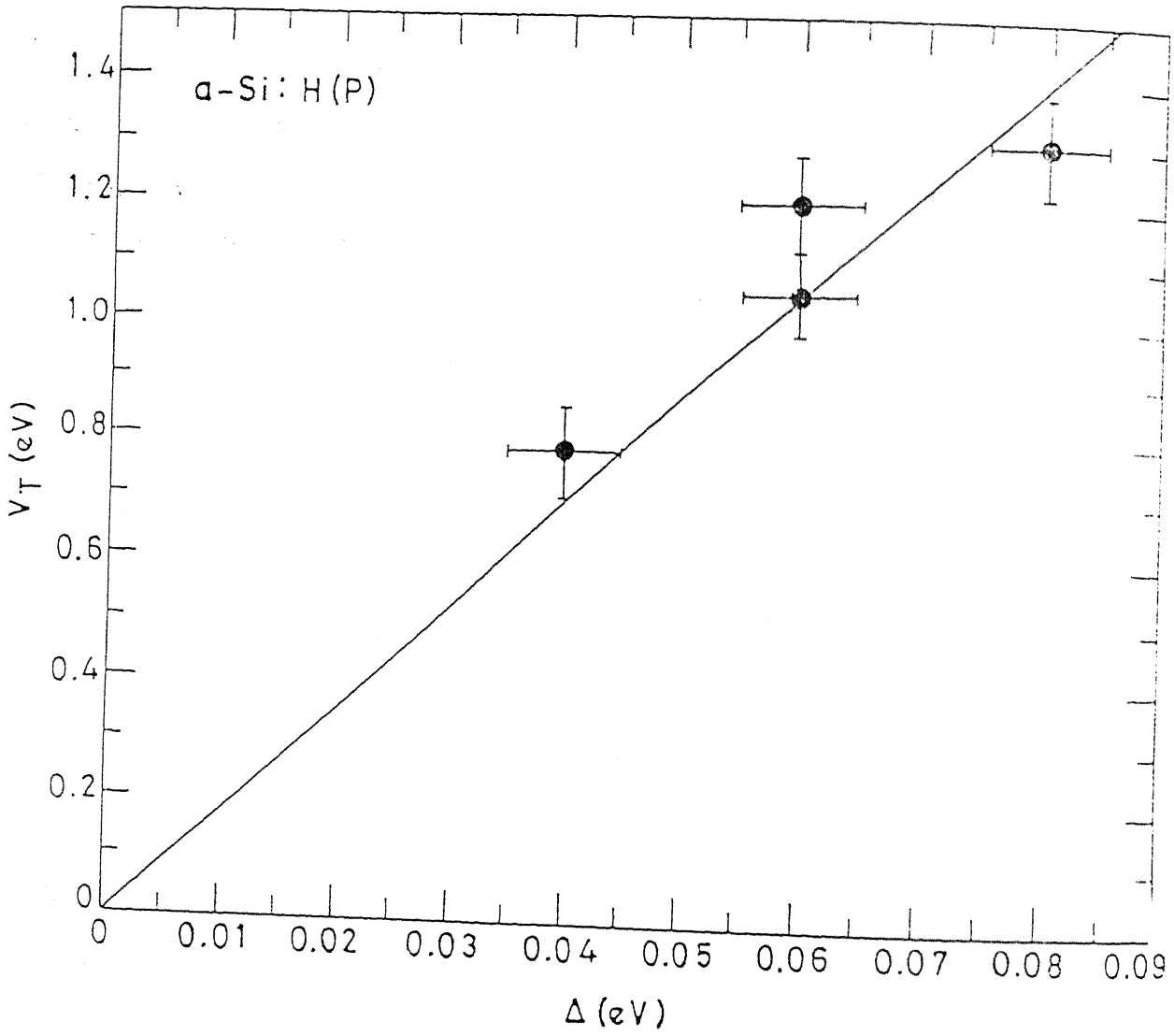

Figure 6.5: Width(V_T) of short range potential fluctuations plotted as a function of the width of long range potential fluctuations(Δ). The straight line fits the equation $V_T \approx 20\ \Delta$.

transport measurements (Δ) by a factor of ≈ 20, for all the samples. This discrepancy is explained by noting that in transport measurements, carriers are likely to overlook sharp fluctuations in the potential because of quantum mechanical tunneling, as these fluctuations are short ranged, of the order of inter atomic distances. Thus, transport measurements see long range potential fluctuations whose width may be smaller than that of the short range fluctuations. On the other hand, optical absorption is a local process and is likely to be sensitive to the short range potential fluctuations inherent in the material. We find empirically that the averaging decreases the width of the potential fluctuations as seen by the transport measurement by a factor of ≈ 20. It is also interesting to note that $V_T/\Delta \approx L/L'$, where L and L' are the ranges of the long range and short range potential fluctuations. Therefore, we conclude that the transport measurement see a potential fluctuation which gets averaged by a factor of L/L'. This, however, needs to be justified theoretically.

Bibliography

1. R. A. Reimer, R. W. Vaughan and J. C. Knights, Phys. Rev. Lett. **44**, 193 (1980).

2. H. Fritzsche, J. Non Cryst. Solids, **6**, 49 (1971).

3. S. C. Agarwal, Bull. Mater. Sci. **18**, 669 (1995).

4. H. Fritzsche, Solid State Commn. **94**, 953 (1995).

5. S. John, C. M. Soukoulis, M. H. Cohen and E. N. Economou, Phys. Rev. Lett. **57**, 1777 (1986).

6. H. Overhof and W. Beyer, Phil. Mag. **B 43**, 433 (1981).

7. H. Overhof and W. Beyer, Phil. Mag. **B 47**, 377 (1983).

8. P. Agarwal, Ph. D. thesis, "Thermal and Light Induced Metastabilities in Phosphorus and Lithium Doped Hydrogenated Amorphous Silicon", I. I. T. Kanpur, 1995 (Unpublished).

9. C. M. Soukoulis, M. H. Cohen and E. N. Economou, Phys. Rev. Lett. **53**, 616 (1984).

10. L. Borch-Brucvich and A. G. Mironov, Sov. Phys. Solid State, **3**, 2194 (1962).

11. B. I. Halprin and M. Lax, Phys. Rev. **148**, 722 (1966).

12. D. Hauschildt, W. Fuhs and H. Mell, Phys. Stat. Sol. **111**, 171 (1982).

13. M. Vanecek, J. Kocka, J. Stuchlik, Z. Koicek, O. Stika, and A. Triska, Solar Energy Materials, **8**, 411 (1983).

14. A. K. Sinha, M. Malhotra, S. Kumar, E. Bhattacharya and S. C. Agarwal, Ind. J. Pure & Appl. Phys. **31**, 548 (1993).

15. W. B. Jackson and N. M. Amer, Phys. Rev. **B25**, 5559 (1982).

16. W. B. Jackson, N. M. Amer, A. C. Boccara, and D. Fournier, Appl.Optics, **20**, 1333 (1981).

17. S. C. Agarwal, Ind. J. Pure and Appl. Phys., **34** , 597 (1996).

18. D. L. Staebler and C. R. Wronski, J. Appl. Phys. **51**, 3262 (1980).

19. K. Pierz, B. Hilgenberg, H. Mell and G. Weiser, J. Non-Cryst. Solids, **97-98**. 63(1987).

20. J. A. Howard and R. A. Street, Phys. Rev. **B44**, 7935 (1982).

Chapter 7

Summary and Conclusions

We have setup constant photocurrent measurement (CPM) [1] and photothermal deflection spectroscopy (PDS) [2]. Complete automation of the measurement have been done to get reliable set of data. Sub-gap absorption (α), for undoped hydrogenated amorphous silicon (a-Si:H) and a-Si:H doped with various concentrations of phosphorous and lithium, has been measured using PDS and CPM. We find [3], in agreement with the literature [4], that α measured by PDS is always greater than that measured by CPM on the same sample. This is explained by arguing that PDS is a photothermal effect and hence is sensitive to all the transitions. On the other hand, CPM sees only those transitions which terminate in the conduction band (CB) extended states. Further, unlike PDS, CPM is not sensitive to the transitions involving surface states because the carriers generated at surface and interface region quickly recombine [5] without contributing to the photocurrent.

In the present work, α measured by CPM and PDS on a given sample of given thickness is analysed to get bulk states in the entire mobility gap as well as surface states [3]. This method obviates the problem of making identical samples with different thicknesses as required by the other methods of measuring surface states [6-8]. However, the shape of distribution of DOS needs to be known for the analysis. Various shapes of the mid-gap states like Gaussian [9] and exponential [10] have been suggested. We find that CPM data can not distinguish between various shapes of the mid-gap states [1]. This conclusion was drawn by Payson et al [11] for their PDS data. We show that

this ambiguity can be resolved using dual beam constant photocurrent measurement (DBCPM) [12]. We find that the anomalous hump appearing in the DBCPM spectrum at lower chopping frequencies, can be fitted only if we assume the Gaussian distribution for the mid gap states and not the exponential. Thus, we conclude that the mid gap states are most likely distributed as a Gaussian. Further, we have also calculated the correlation energy (U) between electrons occupying the same defect site for undoped a-Si:H, using the DBCPM spectrum at a high chopping frequency (333Hz) and DC CPM data. We get U = 0.15eV, in agreement with the literature [12]. By plotting $\log(\alpha_{pds} - \alpha_{cpm})$ as a function of hν in the Urbach edge region, we get E_{oc}, the slope of the conduction band Urbach edge [3], which is not possible using α_{pds} or α_{cpm} data alone.

We have calculated the bulk states in the case of undoped, lithium (Li) doped and phosphorous (P) doped a-Si:H, using sub-gap absorption data. Li is an interstitial n type dopant in a-Si:H [13], unlike P, which is substitutional. We find [14] that the slope of the valance band Urbach edge (E_{ov}) increases with the increasing P concentration as well as Li concentrations. The slope of conduction band Urbach edge (E_{oc}), however, is found to 30$\pm$5 meV, independent of P or Li concentrations. Also, the density of mid-gap states are found to increase with the increasing P or Li concentrations. Our results for P doped samples are in agreement with the literature [15,16]. No results are available, in the literature for Li doped samples, at present. Our findings show that P and Li dopants give similar results.

By combining the sub-gap absorption and the activation energy data, we have obtained the energy position of the D^- in a-Si:H(Li) [17]. Two distinct models for the position of dangling bond states in doped a-Si:H have been proposed. According to Street et al [9], position of D^- in doped a-Si:H is identical with that in undoped a-Si:H. Kocka et al [18], on the other hand, propose that the position of D^- in doped a-Si:H moves deeper in band gap, moving away from the CB edge, because of the intimate bond formation between the dopant and the dangling bond states. We find that even after careful analysis of the CPM spectra, the two models are within the experimental error. But on using the conductivity data along with the α_{cpm} data, we find that our data prefer the Street's model in a-Si:H(Li) [17]. This may be because Li is an intersti-

tial dopant and may not form intimate pairs with the dangling bonds for Kocka's model to be valid.

One of the inputs required for the analysis for determination of surface states is the shape of distribution. Since this is not known, we have taken three shapes of the surface states namely delta function, Gaussian and rectangular. The density of surface states for undoped a-Si:H is found to be $(4 \pm 1)10^{12} cm^{-2}$ for all the three shapes. Therefore, we conclude that the density of surface states is not very sensitive to its distribution [3].

The surface states in a-Si:H(Li) has been measured for the first time and compared with a-Si:H(P) for various concentrations of Li and P. We find [14] that the density of the surface states in a-Si:H(Li) is $((5 \pm 1)\ 10^{12} cm^{-2})$, independent of the shape of their distribution, and is about 20% larger than that in undoped a-Si:H. It is found to be independent of the concentration of Li, for the two concentrations used in this study. The density of surface states in a-Si:H(P) is found to be about the same as a-Si:H(Li). This shows that density of surface states in the two dopings are similar.

Further, we have measured the density of bulk and surface states, after exposing undoped a-Si:H sample to light and various surface treatments. These are etching the surface oxide with dilute hydrofluoric acid, growth of oxide layer by treating the sample with concentrated sulfuric acid and subsequent annealing and exposure to nitrogen and hydrogen plasma. We find that upon light soaking, the density of the bulk states increases by a factor of 2, without much change in the surface states. This is in agreement with the common conviction [19], that light soaking is a bulk effect. Etching of native oxide with hydrofluoric acid, increases N_s by a factor of about 1.5. This shows that the surface devoid of the native oxide have a higher density of surface states. Treating the etched sample with concentrated H_2SO_4 to grow oxide again and annealing brings back the density of surface states to its value in annealed state.

In addition, we find that nitrogen plasma treatment increases the density of surface states slightly. This small change is within the errors of measurement. Hydrogen plasma, however, passivates the surface by decreasing the surface states by about 50%. This may be because surface etching and the Si bond termination by H atoms in the plasma. This might explain why the interfacial surfaces are exposed to hydrogen

plasma, while making a-Si:H based devices.

Finally, we have explained sub-gap absorption results using potential fluctuations [20]. This is an alternative explanation, different from the single particle density of states explanation, in which a-Si:H is assumed to be homogeneous. The total width of potential fluctuations (V_T) is estimated by optical absorption measurements, using PDS. The two regions (Urbach edge region and mid-gap absorption region) of the optical absorption curve have been explained by proposing two Gaussian terms in the potential fluctuations. Also, the width of long range potential fluctuations (Δ) is calculated from transport measurements, for the same samples. We find [20] that the width of the potential fluctuations obtained from optical as well as from transport measurements increases with the increasing phosphorous concentration, as expected. Also, we find that V_T is larger than Δ by a factor of ≈ 20, for all the samples. This discrepancy is explained by arguing that optical and transport measurements are sensitive to different ranges of the potential fluctuations. This is in line with the argument of Fritzsche [21] explaining the difference between electrical and optical gaps in amorphous semiconductors. We find an empirical relationship ($V_T \approx K\Delta$) between the long range and the short range potential fluctuations, where, K = 20±5. This shows that the transport measurements see potential fluctuations, which are some kind of average of the short range potential fluctuations, seen by the optical absorption measurements. This emperical results, however, needs to be verified theoretically.

Scope for Future Work

This work demonstrates the utility of the sub gap absorption measurements for obtaining information about the bulk as well as the surface states. An obvious extension of the present work is to use the technique in the case of boron doped a-Si:H. Studies of the surface states after various treatments might give the reason for lower density of surface states in a-Si:H (B) compared to that in undoped a-Si:H. Similar studies on compensated a-Si:H should be interesting. Also, effect on density of surface states of alloying a-Si:H with other materials like germanium, carbon, tin etc. Some of these materials are useful for devices and studies of their electronic properties are desirable. We have explained

the difference in α_{cam} and α_{pds} in terms of the optical transitions not seen by CPM but seen by PDS. We find that in a chalcogenide glass ($Se_{80}Te_{20}$), both α_{cpm} and α_{pds} are the same [2]. Further experimental work and analysis is necessary to explore and explain this observation in chalcogenide glasses. PDS is a unique tool for probing non radiative transitions. Luminescence, on the other hand, gives the radiative transitions. When these two techniques are applied on the same sample, a more complete picture of the branching ratios of radiative and nonradiative transitions in the material under study, may emerge.

$\alpha_{cpm}(h\nu)$ have only been explained qualitatively in this work, using potential fluctuation model. CPM requires knowledge of both optical absorption and transport of carriers through the potential fluctuations, for explanation. This requires a better theoretical understanding of these ideas. This also is a possible direction for the future research.

This work is only an initial effort in explaining sub gap absorption using potential fluctuations. Many problems remain to be solved. For example, the relation between the long range and short range potential fluctuations, found in this work, is only emperical. A theoretical justification of this relation requires the understanding of the averaging processes, when we visualise the long range potential fluctuations as an average of the short range potential fluctuations. If achieved, this will allow the model to produce transport properties, from the optical absorption data. This would be of fundamental as well as practical interest. In conclusion we can say that a lot of unsolved problems. controversies, issues and ideas remain to be explored in a-Si:H and its alloys.

Bibliography

1. A. K. Sinha, M. Malhotra, S. Kumar, E. Bhattacharya and S. C. Agarwal, Ind.J.Pure & Appl. Phys. **31**, 548 (1993).

2. A. K. Sinha and S. C. Agarwal, Ind. J. Pure & Appl. Phys. (1998), (in Press).

3 A. K. Sinha and S. C. Agarwal, Phil. Mag. B (1998), (in Press).

4. G. Amato, G. Bendetto, L. Boarino, and R. Spagnolo, Solid State comm., **77**, 177 (1991).

5. E. Bustarret, D. Jousse, C. Chaussal and F. Boulitrop, J. Non-Cryst. Solids, **77&78**, 295 (1985).

6. W. B. Jackson, D. K. Biegelsen, R. J. Nemanich, and J. C. Knights, Appl. Phys. Lett. **42**,105 (1983).

7. H. Curtnis, N. Wyrsch and A. V. Shah, Electronics Lett. **23**, 228 (1987).

8. M. Favre, H. Curtnis and A. V. Shah, J. Non-Cryst. Solids, **97 & 98**, 731 (1987).

9. R. A. Street, J. Zesch and M. J. Thompson, Appl. Phys. Lett. **43**(7), 672(1983).

10. M. Hack and M. Shur, J. Appl. Phys. **54**, 5858 (1983); S. Guha, J.Non.Cryst. Solids, **77&78**, 1451 (1985).

11. J. S. Payson and S. Guha, Phys. Rev. **B32**, 1326 (1987).

12. J. Z. Liu, G. Lewen, J. P. Conde and P. Roca i Cabarrocas, J. Non-Cryst. Solids **164 & 165**, 383 (1993).

13. W. Beyer and R. Fischer, Appl. Phys. Lett. **31**, 850 (1977).

14. A. K. Sinha, G. S. Narayana, S. K. Tripathi and S. C. Agarwal, J. Non-Cryst. Solids, 1998 (communicated).

15. H. Fritzsche, Solar Energy Mater. **3**, 447 (1980).

16. T. Tiedje in Semiconductors and Semimetals Vol. 21c (ed. J.I. Pankove, Academic Press, London 1984)

17. A. K. Sinha, S. K. Tripathi, G. S. Narayana and S. C. Agarwal, Solid State Phenomena, (Scitec Publications, Switzerland) **55**, 137 (1997).

18. J.Kocka, Proc. III winter European Course on Amorphous Silicon, Folgaria(Italy) 1989 (Task, Ispara,1989).

19. S. Guha, J. Non-Cryst. Solids, **77** & **78**, 1451 (1985).

20 A. K. Sinha and S. C. Agarwal, Phys. Rev. B, (1998), (communicated).

21. H. Fritzsche, J. Non Cryst. Solids, **6**, 49 (1971).

Appendix A

Transmission Measurement

Under the assumption of : (a) non absorbing substrate and (b) K=0 which is true for most part of the spectrum

$$T = Ax/(B - Cx.cos\phi + Dx^2), \tag{A.1}$$

where,

$$A = 16n^2s \tag{A.2}$$

$$B = (n+1)^3(n+s^2) \tag{A.3}$$

$$C = 2(n^2-1)(n^2-s^2) \tag{A.4}$$

$$D = (n-1)^3(n-s^2) \tag{A.5}$$

$$\Phi = 4\pi nd/\lambda \tag{A.6}$$

$$x = exp(-\alpha d) \tag{A.7}$$

The symbols are defined in the Fig. A1. Fig. A2 Shows the transmission spectrum of a-Si:H thin film. T_M and T_m are envelopes of maxima and minima of the interference

fringes. The spectrum is divided into three regions : transparent region ($T_M \geq 0.91$), weak and medium absorption region ($0.91 \geq T_M \geq 0.5$) and strong absorption region ($T_M \geq 0.5$). In these regions; n and α are given in the closed form [1].

(a) **Transparent region:**

$$n = [M + (M^2 - s^2)^{1/2}]^{1/2} \tag{A.8}$$

where

$$\text{where, M} = 2s/T_m - (s^2 + 1)/2$$

$$\text{and } \alpha = 0$$

(b) **Weak and Medium Absorption Region:**

$$n = (N + (N^2 - s^2)^{1/2})^{1/2} \tag{A.9}$$

$$\text{where, N} = 2 \times s\frac{T_M - T_m}{T_M T_m} + \frac{s^2+1}{2}$$

$$and\ x = \frac{F - [F^2 - (n^2-1)^3(n^2 - s^4)]^{1/2}}{(n-1)^3(n - s^2)} \tag{A.10}$$

$$\text{where, } F = \frac{4n^2 s(T_M + T_m)}{T_M T_m}$$

(c) **Strong Absorption Region:** As seen from Fig. A2, there is no interference fringes in the transmission spectrum in this region. n(λ) is calculated by the extrapolation of n(λ) obtained in other two regions (weak and medium and transparent) using Cauchy's relation

$$n(\lambda) = A + \frac{B}{\lambda^2} \tag{A.11}$$

$$and,\ x = \frac{(n+1)^3(n+s^2)}{(16n^2 s)} T_o, \tag{A.12}$$

where, s = 1.51 is the refractive index of the 7059 glass and T_0 is the measured transmission in the interference free region (Fig. A2).

Determination Of Thickness (d):

In the transparent and medium and weak absorption regions (Fig. A2), we get interference fringes. In these regions, d is calculated using the following equation:

$$d = \frac{\lambda_1 \lambda_2}{2(\lambda_1 n_2 - \lambda_2 n_1)} \tag{A.13}$$

where (n_1, λ_1) and (n_2, λ_2) are the values of refractive index and wave length two adjacent maxima (or minima). d is calculated for various pair of maxima and minima. Average value of d($d_{av} = \Sigma d/n$) is now calculated. This average value of d is put into the equations,

$$nd_{av} = m\lambda/2 : for\ maxima, \tag{A.14}$$

$$nd_{av} = (2m+1)\lambda/4 : for\ minima, \tag{A.15}$$

where m is an integer. m calculated using Eqs. (14) and (15) is approximately an integer. This is made an integer and the new values of n(λ) are calculated using Eqs. (14) and (15). These new values of n(λ) are put back in Eq. (13) to calculate the thickness d and d_{av} again. This gives the correct value of d.

New values of n(λ) and d are used in Eqs. (10) and (12) to calculate α in the weak - medium and strong absorption regions respectively. In the strong absorption region. where there is no interference fringes, we extrapolate the calculated n(λ) using Cauchy's equation given by Eq. (11).

To determine the optical gap of a-Si:H film $(\alpha h\nu)^{1/2}$ versus $h\nu$ is plotted for $h\nu \geq$ 1.5eV. It gives a straight line (see Fig. 2.2).

$$(\alpha h\nu)^{1/2} = A \times (h\nu - E_g), \tag{A.16}$$

E_g is obtained by the intercept of the straight line.

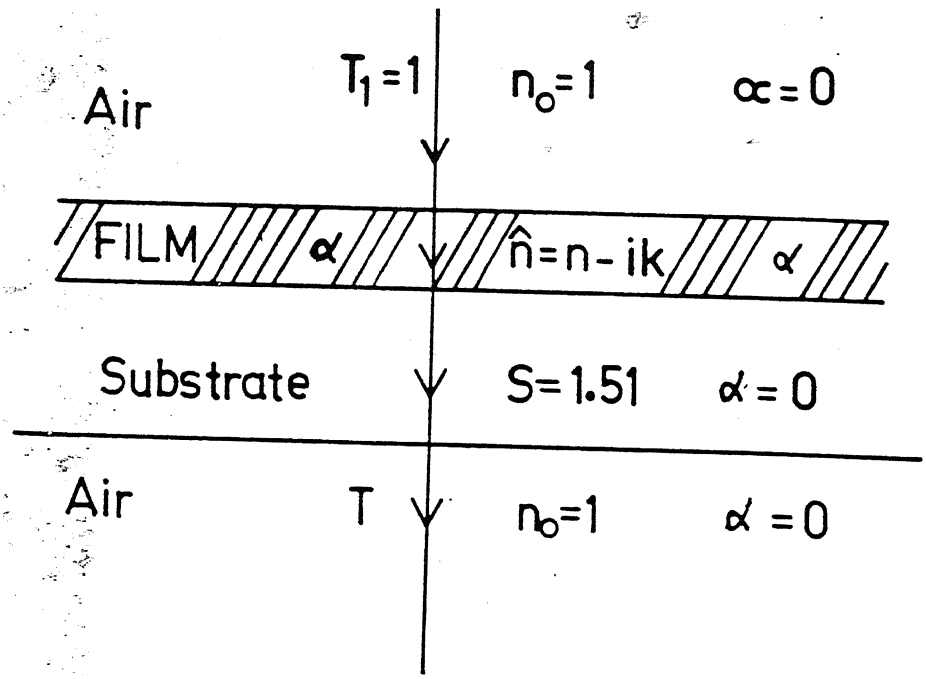

Figure A.1: Schematic showing tramission geometry of absorbing film (a-Si:H) on a non absorbing substrate (glass slide)

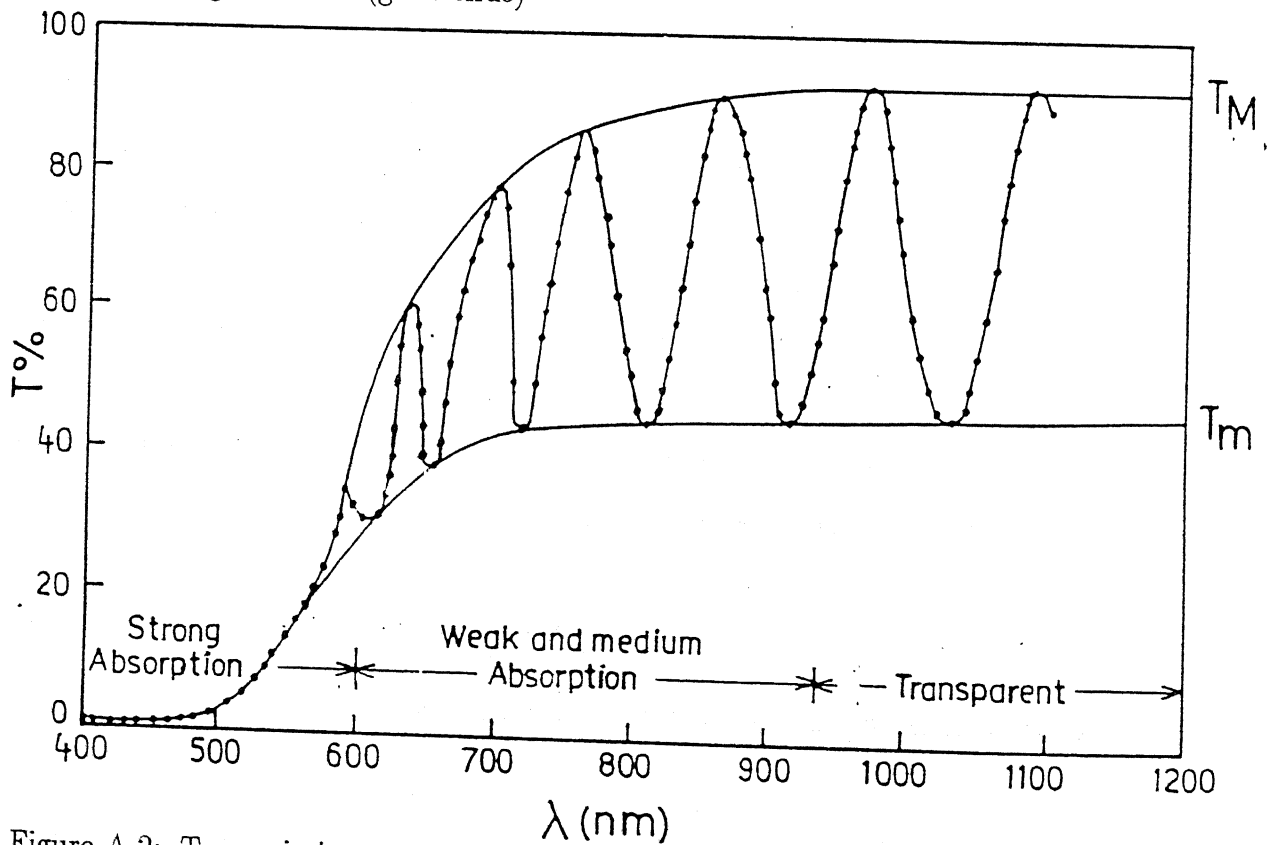

Figure A.2: Transmission spectrum of a-Si:H thin film on 7059 glass substrate. The interference fringes are because of the thin film.

Appendix B

Movement of the stepper motor

The stepper motor can be moved clockwise or anti clockwise by applying 12 volts across two of the four coils of the motor in a specific sequence. The sequence of the coil voltages for clockwise or anti clockwise rotation of the motor is given in Fig. B1. This sequencing is achieved by connecting four electronic switches to the four coils of the motor. These switches, when closed, connect a particular lead to the ground voltage and hence the current flows through the coil. When the switch is on, the current through the coil stops. The motor driver circuit is shown in Fig. B2. The circuit contains four opto-isolated relays (OIR, in Fig. B2). An optoisolated relay contains an LED which can be switched on by 5volts TTL supplied by the parallel port of the PC. This LED in turn switches on a photo transistor and a switch circuit attached with the photo transistor.

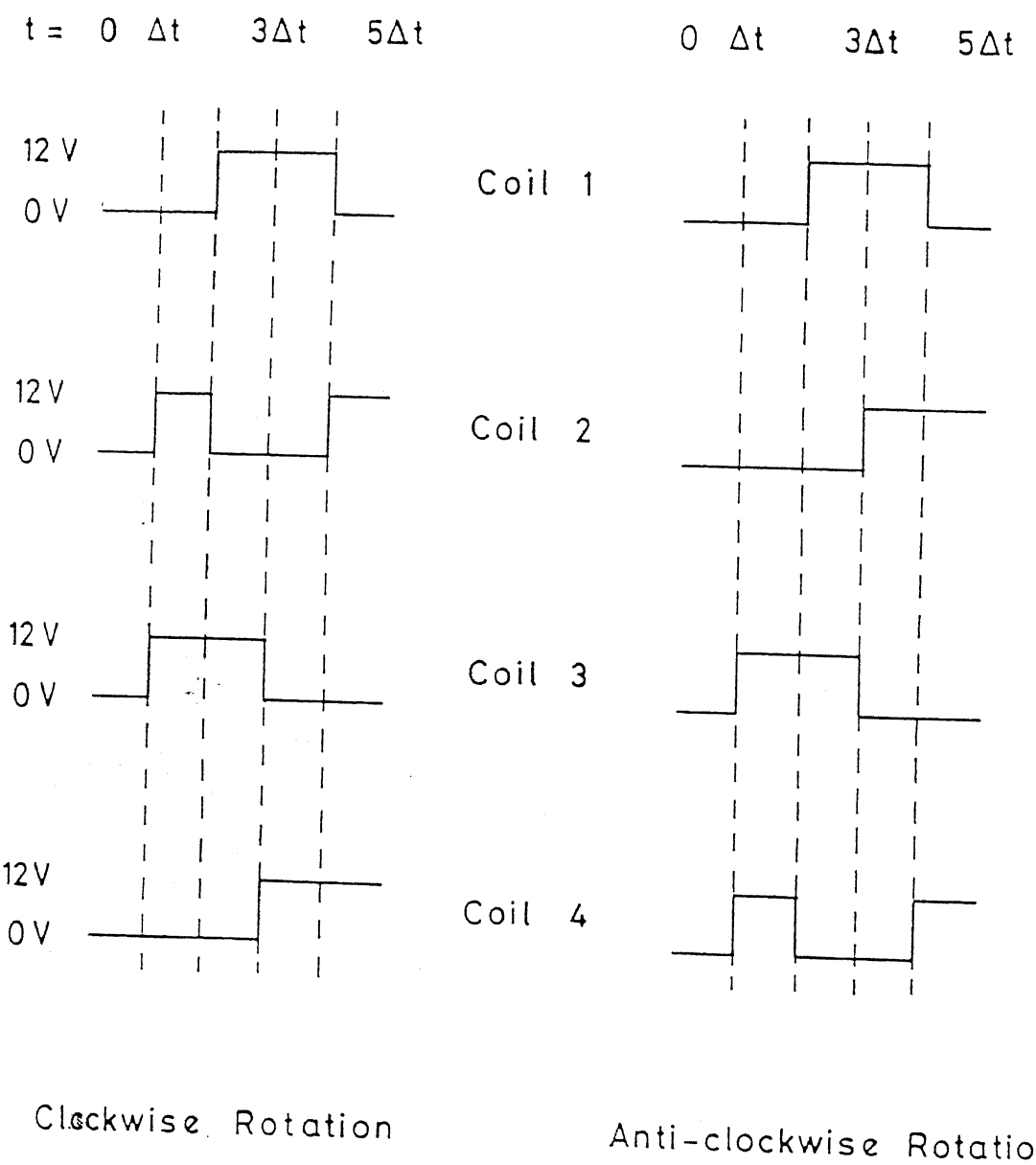

Figure B.1: Voltage sequence for the four coils of the stepper moter for clockwise and anticlockwise rotation of the motor. The sequencing is done by the parallel port of the PC by sending TTL voltage. Δt is the delay between the two steps and hence controls the speed of the motor.

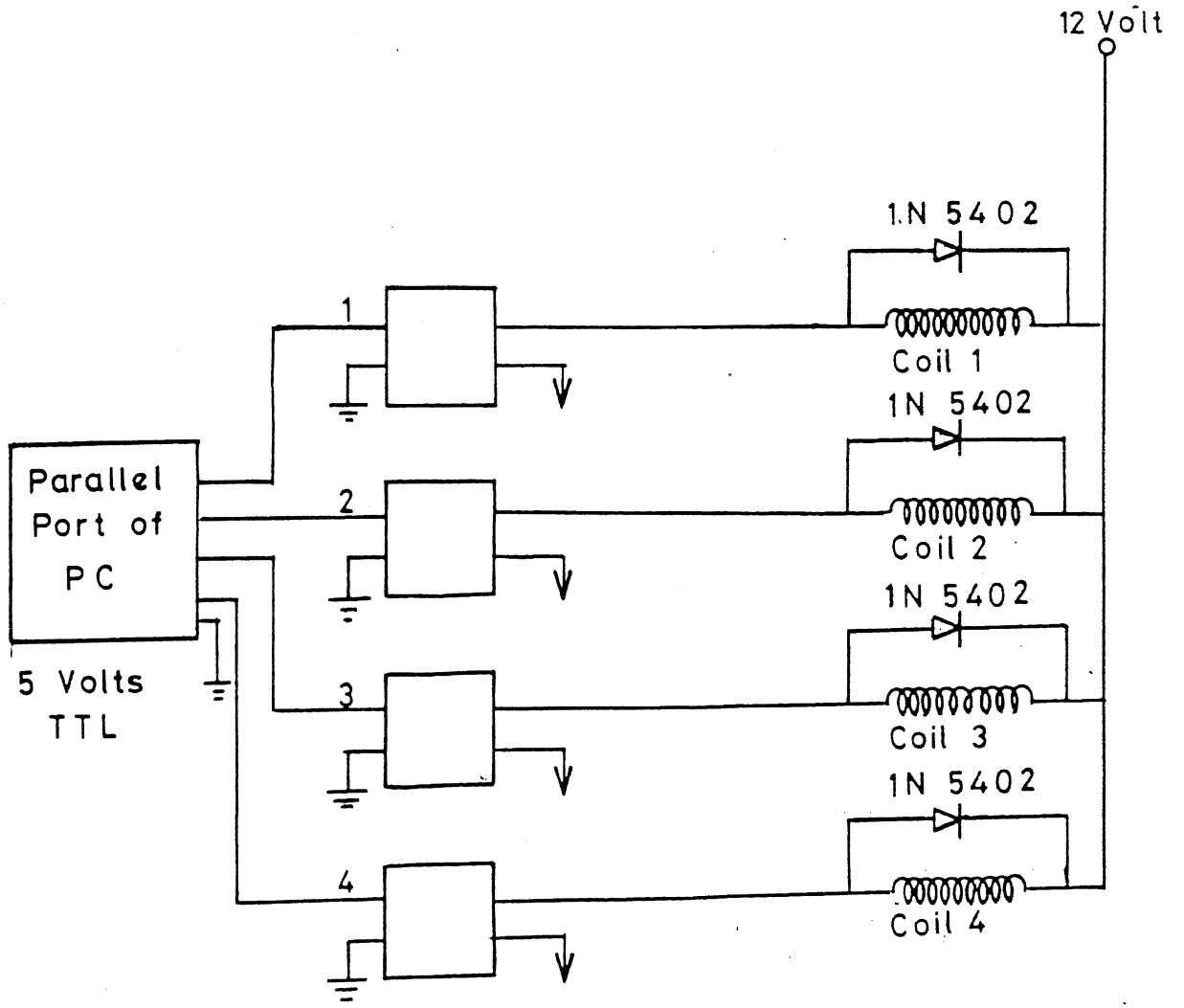

Figure B.2: The stepper motor driver circuit seperate groundings are used for the PC and the power supply to safegaurd the PC. Diodes (1N5402) are used to provide low resistance path for the quick dissipation of the energy when coil is changed from on to off position.

Appendix C

Tbasic program for Transmission and PDS

```
10 rem programme for PDS/TRANSMISSION using monochromator and motor
20 rem initialisation of monochromator
25 cls
27 input "print 1 for transmission and 2 for PDS";r
30 input " present wavelength ";a
40 input " starting wavelength ";b
45 e = b
47 t=0
50 input "final wavelength ";c
60 input " step";d
65 input "enter file.name",file.name $
67 Open file.name $ for output as #2
68 print #2. "DATE : ",DATE $,"Time : ", TIME $
70 a1 = abs (a-b)*5
75 b1 = (abs (b-c)/d)
78 b2 = abs (660-b)/d
80 if a>b then goto 1000 else goto 100
90 rem if b>c then goto 1000
```

```
100 i = 0
102 rem k = 0
105 j = 0
110 out &h378, 10
120 delay .1
130 i = i+1
140 if i> a1 then gosub 2800
141 rem if t> 0 and c¡b then goto 1420
142 if j = b2 then goto 143 else goto 146
143 input "put filter";p
144 j = j+1
146 if j>b1 then goto 2710
150 out &h378, 9
160 delay .1
170 i = i+1
180 if i>a1 then gosub 2800
181 rem if t> 0 and c¡b then goto 2610
182 if j = b2 then goto 183 else goto 186
183 j = j+1
184 input "put filter";p
186 if j>b1 then goto 2710
190 out &h378, 5
200 delay .1
210 i = i+1
220 if i>a1 then gosub 2800
221 rem if t> 0 and c¡b then goto 1820
222 if j = b2 then goto 223 else goto 226
223 j = j+1
224 input "put filter";p
226 if j>b1 then goto 2710
230 out &h378, 6
```

```
240 delay .1
250 i = i+1
260 if i>a1 then gosub 2800
261 rem if t ¿ 0 and c¡b then goto 1820
262 if j = b2 then goto 263 else goto 266
263 j = j+1
264 input "put filter";p
266 if j>b1 then goto 2710
270 goto 110
1000 i = 0
1100 out &h378, 10
1200 delay .1
1300 i = i+1
1400 if i> a1 then gosub 2800
1420 rem if t>0 and c>b then goto 141
1462 if j = b2 then goto 1464 else goto 1466
1466 if j>b1 then goto 2710
1500 out &h378, 6
1600 delay .1
1700 i = i+1
1800 if i>a1 then gosub 2800
1820 rem if t> 0 and c>b then goto 261
1862 if j = b2 then goto 1864 else goto 1866
1864 input "put filter";p
1866 if j>b1 then goto 2710
1900 out &h378, 5  2000 delay .1
2100 i = i+1
2200 if i>a1 then gosub 2800
2220 rem if t>0 and c>b then goto 221
2262 if j = b2 then goto 2264 else goto 2266
2264 input "put filter";p
```

```
2266 if j>b1 then goto 2710
2300 out &h378, 9
2400 delay .1
2500 i = i+1
2600 if i>a1 then gosub 2800
2610 rem if t> 0 and c>b then goto 181
2620 if j = b2 then goto 2640 else goto 2660
2640 input "put filter";p
2660 if j>b1 then goto 2710
2670 goto 1100
2680 rem t = t+1
2710 if r = 2 then goto 2790
2715 input "remove sample and reset the monochromator or print 1 to end";q
2720 if q = 1 then goto 2790
2725 j = 0
2730 e = b
2735 rem t = t+1
2740 goto 70
2790 end
2795 goto 5010
2800 open "com2:9600,N,8,2,cs,ds,cd" as #1
2810 print " "
2815 for i = 1 to 200
2816 next i
2817 j = j+1
2828 delay 30
2820 Print #1,"q"
2830 input #1,v1
2832 if v1 > 2e-1 then print #1,"g 24":goto 3000
2834 if v1< 2e-1 and v1> 2e-2 then print #1,"g 23" :goto 3000
2835 if v1<1e-1 and v1>1e-2 then print #1,"g 22":goto 3000
```

```
2836 if v1< 5e-2 and v1> 5e-3 then print #1,"g 21":goto 3000
2838 if v1<2e-2 and v1> 2e-3 then print #1,"g 20" :goto 3000
2840 if v1< 1e-2 and v1> 1e-3 then print #1,"g 19" :goto 3000
2850 if v1<5e-3 and v1> 5e-4 then print #1,"g 18" :goto 3000
2852 if v1< 2e-3 and v1> 2e-4 then print #1,"g 17":goto 3000
2854 if v1<1e-3 and v1> 1e-4 then print #1,"g 16" :goto 3000
2856 if v1< 5e-4 and v1> 5e-5 then print #1,"g 15":goto 3000
2858 if v1<2e-4 and v1> 2e-5 then print #1,"g 14" :goto 3000
2860 if v1< 1e-4 and v1> 1e-5 then print #1,"g 13":goto 3000
2862 if v1<5e-5 and v1> 5e-6 then print #1,"g 12":goto 3000
2864 if v1< 1e-4 and v1> 1e-5 then print #1,"g 11":goto 3000
2866 if v1<5e-5 and v1> 5e-6 then print #1,"g 10":goto 3000
2868 if v1< 2e-5 and v1> 2e-6 then print #1,"g 9":goto 3000
2870 if v1<1e-5 and v1 >1e-6 then print #1,"g 8" :goto 3000
2880 if v1<5e-6 and v1> 5e-7 then print #1,"g 7" :goto 3000
2890 if v1< 2e-7 then print #1, "g 6"
3000 if v1>2e-1 then print #1,"t1 7"
3010 if v1<= 2e-1 and v1> 2e-3 then print #1, "t1 8"
3020 if v1<= 2e-3 and v1> 2e-6 then print #1,"t1 9"
3030 if v1<= 2e-6 then print #1,"t1 10"
3040 delay 30
3050 print #1,"q"
3060 input #1,v2:delay 30
3070 print #1,"q"
3080 input #1,v3
3090 rem print #1,"q"
4000 rem input #1,v4
4005 close #1
4006 rem k = k+
4010 s = (v2+v3)/2
4020 print "output at lamda"; s, e
```

```
4022 rem Open file.name $ for output as #2
4025 rem Open file.name $ for output as #2
4030 rem Open file.name $ for output as #2
4045 rem if j = b1 then goto 4050 else goto 4060
4050 rem close #2
4060 e = e+d
4070 rem if j = abs((640-b)/d) then goto 4090
4080 a = b
4090 i = 1 :a1 = d*5
5000 return
5010 close #2
6000 stop
7000 end
```

Appendix D

Position sensitive detector (PSD)

Fig. D1 shows the equivalent circuit diagram of PSD. We use quadrant Si Photodiode as PSD. In illuminated condition, a parasitic resistance (R_P) is found between the two diode pairs because the diodes are made on the same photosensitive Si wafer. Two shunt resistances (R_{sh}) are used as current to voltage converter as shown in Fig. D1. Voltage signals A and B are obtained through these two diode pairs.

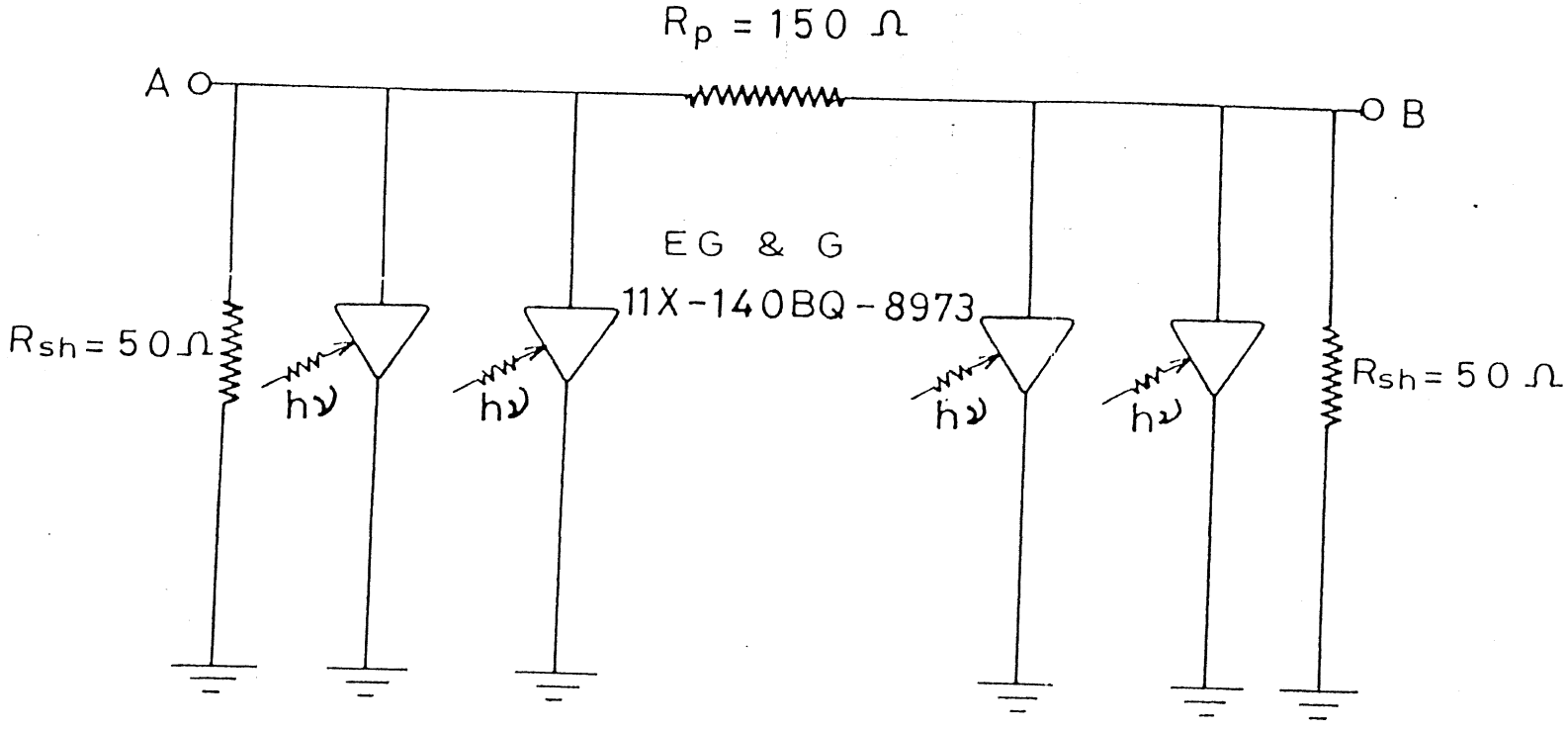

Figure D.1: equivalent circuit diagramme of the position sensitive detector in the light on condition. R_p is the parasitic resistance. For our PSD R_p is found to be 150Ω with 2mW laser illumination. The output (A and B) are the inputs to the analogue circuit shown figure E1

Appendix E

Analog circuit

Fig. E1 shows the circuit which amplifies and does the operation (A-B)/(A+B) on the outputs A & B of the PSD.The main part of the circuit consists of two differential amplifiers. Output of PSD, A & B are given in input of one of the differential amplifiers. The input of the other differential amplifier is A & (-B). So the signal B is passed through an Operational amplifier in the inverter mode as shown in the Fig. A6. Outputs of the two differential amplifiers are (A-B) and (A+B) respectively. These signals are now passed through Buffer circuits and are fed to a divider IC. Output of the divider (A-B)/(A+B) is the PDS signal. Actual components used by us are as indicated in Fig. E1.

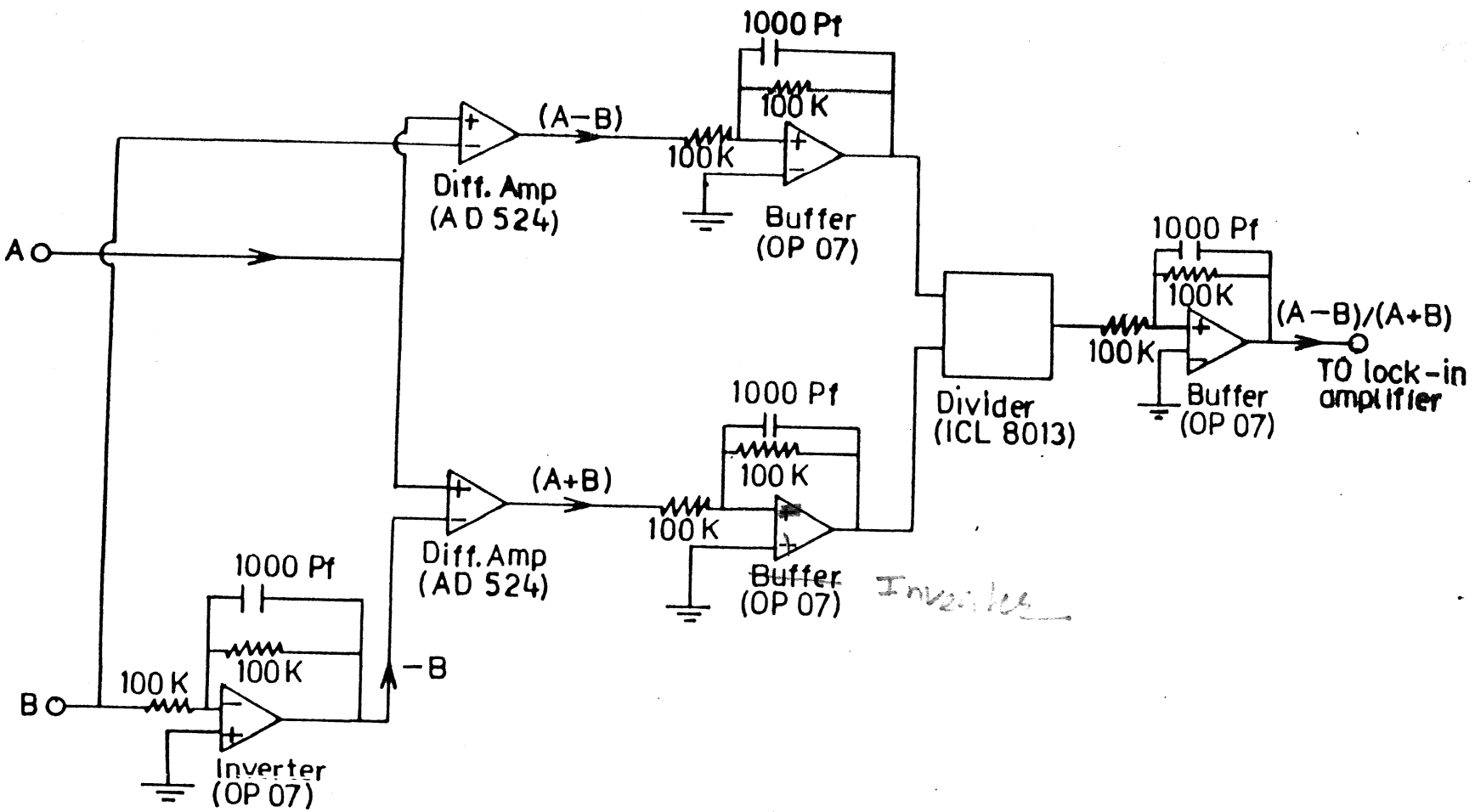

Figure E.1: Analogue circuit for amplification and processing of PDS signal. The circuit reduces signal to noise ratio

Appendix F

Tbasic program for CPM

```
10 cls
12 rem user input parameters
14 rem
20 print "input parameters"
30 input "file name", file.name $
40 input "value of constant photocurrent";cpc
50 input "present value of lamda";a1
60 input "initial value of lamda";a2
70 input "final value of lamda";a3
80 input "step";A4
90 rem open file.name $ for append as #1
95 rem j = 0 to abs(a3-a2)/a4
100 gosub 500
102 rem print "ok"
105 rem end
107 print "ok"
110 for j = 0 to abs(a3-a2)/a4
120 gosub 1100
122 print "back after reading lock in"
125 rem end
```

```
150 gosub 1500
155 rem end
170 gosub 2000
175 open file.name $ for append as #1  190 close #1
200 s = a4*5 : i = 0
210 gosub 502
215 a2 = a2+a4
217 rem end
220 next j
240 rem close #1
250 end
400 rem subroutine for the motor with monochromator
401 rem
500 s = abs(a2-a1)*5 :i = 0
502 if a = 10 then goto 540
503 if a = 9 then goto 570
504 if a = 5 then goto 600
505 if a = 6 then goto 510
510 out &h378,(10+b)
515 a = 10
520 delay .1 : i = i+1
530 if i> s then goto 1000
540 out &h378,(9+b)
545 a = 9
550 delay .1 : i = i+1
560 if i> s then goto 1000
570 out &h378,(5+b)
575 a = 5
580 delay .1 : i = i+1
590 if i > s then goto 1000
600 out &h378,(6+b)
```

```
605 a = 6
610 delay .1 : i = i+1
620 if i > s then goto 1000 else goto 510
1000 return
1100 rem subroutine for reading the analog lock in amplifier
1101 rem
1105 dim dta % (10000)
1110 port % = &h220
1120 out port % +11,1
1130 dummy = inp(port %+4)
1140 ch % = 0
1150 rem for lp1 = 0 to 2
1155 delay 10
1160 out port % +10, ch %
1170 for wait1 = 0 to 25: next wait1
1180 out port % +12,
1190 dh % = inp (port % +5)
1200 if dh %>15 then goto 1190
1210 dl % = inp(port % +4)
1220 dta % = ((dh %*256 +dl % - 2048)*50)/10.23
1125 print "data = "; dta %
1230 rem next lp1
1240 rem dta % = (dta %(0) + dta %(1) +dta %(2))/3
1250 out port % +11,0
1260 return
1500 rem comparison with cpm
1501 rem
1510 if abs(dta %) ¡ 1.02*cpc and abs(dta %)¿.98*cpc then goto 1900
1520 if abs(dta %) ¡ cpc then goto 1700 else goto 1530
1530 if b = 160 then goto 1570
1535 if b = 96 then goto 1600
```

```
1540 if b = 80 then goto 1630
1545 if b = 144 then goto 1550
1550 out &h378, (160+a) :b = 160
1560 delay 1 : gosub 1100
1562 rem print "hello"
1565 goto 1510
1567 rem print "done
1570 out &h378, (96+a) :b = 96
1580 delay 1 : gosub 1100
1585 goto 1510
1600 out &h378, (80+a) :b = 80
1610 delay 1 : gosub 1100
1620 goto 1510
1630 out &h378, (144+a) :b = 144
1640 delay 1 : gosub 1100
1650 goto 1510
1700 rem if dta %> cpc then goto 1530 else goto 1700
1710 if b = 160 then goto 1760
1715 if b = 144 then goto 1790
1720 if b = 80 then goto 1820
1725 if b = 96 then goto 1730
1730 out &h378, (160+a) :b = 160
1740 delay 1 : gosub 1100
1750 goto 1510
1760 out &h378, (144+a) :b = 144
1770 delay 1 : gosub 1100
1780 goto 1510
1790 out &h378, (80+a) :b = 80
1800 delay 1 : gosub 1100
1810 goto 1510
1820 out &h378, (96+a) :b = 96
```

```
1830 delay 1 : gosub 1100
1850 goto 1510
1900 return
2000 rem subroutine to read SR510
2001 rem
2010 open "com2:9600,n,8,2,cs,ds,cd" as #2
2020 print #2," "
2030 for i = 1 to 200: next i
2040 print #2, "b1":delay 1
2050 print #2,"q"
2060 input #2,v1
2065 rem print #2,"e 1" :delay 1
2070 if v1< 2e-1 and v1>2e-2 then print #2,"g 23" :goto 2270
2080 if v1< 1e-1 and v1> 1e-2 then print #2,"g 22" :goto 2270
2090 if v1< 5e-2 and v1> 5e-3 then print #2,"g 21" :goto 2270
2100 if v1< 2e-2 and v1> 2e-3 then print #2,"g 20" :goto 2270
2110 if v1< 1e-2 and v1> 1e-3 then print #2,"g 19" :goto 2270
2120 if v1< 5e-3 and v1> 5e-4 then print #2,"g 18" :goto 2270
2130 if v1< 2e-3 and v1> 2e-4 then print #2,"g 17" :goto 2270
2140 if v1< 1e-3 and v1>1e-4 then print #2,"g 16" :goto 2270
2150 if v1< 5e-4 and v1> 5e-5 then print #2,"g 15" :goto 2270
2160 if v1< 2e-4 and v1> 2e-5 then print #2,"g 14" :goto 2270
2170 if v1< 1e-4 and v1> 1e-5 then print #2,"g 13" :goto 2270
2180 if v1< 5e-5 and v1> 5e-6 then print #2,"g 12" :goto 2270
2190 if v1< 2e-5 and v1> 2e-6 then print #2,"g 11" :goto 2270
2200 if v1< 1e-5 and v1> 1e-6 then print #2,"g 10" :goto 2270
2210 if v1< 5e-6 and v1> 5e-7 then print #2,"g 9" :goto 2270
2220 if v1< 2e-6 and v1> 2e-7 then print #2,"g 8" :goto 2270
2230 if v1< 1e-6 and v1> 1e-7 then print #2,"g 7" :goto 2270
2240 if v1< 5e-7 and v1> 5e-8 then print #2,"g 6" :goto 2270
2250 if v1< 2e-7 and v1> 2e-8 then print #2,"g 5" :goto 2270
```

```
2260 rem if v1< 2e-1 and v1> 2e-2 then print #2,"g 23"
2270 rem if v1< 2e-1 and v1> 2e-2 then print #2,"g 23"
2280 if v1>= 1e-2 then print #2,"t1, 8"
2290 if v1< 1e-2 and v1>= 1e-3 then print #2,"t1, 8"
2300 if v1< 1e-3 and v1>= 1e-5 then print #2,"t1, 9"
2310 if v1< 1e-5 then print #2,"t1, 9"
2320 delay 15
2330 print #2,"q"
2340 input #2, v2
2350 delay 5
2360 print #2,"q"
2370 input #2, v3
2380 delay 5
2390 d = (v2 + v3)/2
2400 rem input #1,d
3000 close #2
3100 e = a2
3200 print "output at lamda ";d, e
4000 return
```

List of Publications

In Journals

1. "Sub-gap absorption measurement using constant photocurrent measurements in hydrogenated amorphous silicon"
   A. K. Sinha, M. Malhotra, S. Kumar, E. Bhattacharya and S. C. Agarwal, Ind. J. Pure & Appl. Phys. **31**, 548 (1993).

2. "Position of dangling bond states in doped a-Si:H."
   A.K. Sinha, S.K. Tripathi, G. S. Narayana and S.C. Agarwal, Solid State Phenomena, **55** 137 (1997).

3. "Photothermal deflection spectroscopy and Constant photocurrent measurements for sub-gap absorption in thin films."
   A. K. Sinha and S. C. Agarwal, Ind. J. Pure & Appl. Phys. (1998) (Accepted for publication).

4. "Determination of surface states by sub-gap absorption measurements."
   A. K. Sinha and S. C. Agarwal, Phil. Mag. B (1998), (Accepted for publication)

5. "Density of surface states in lithium doped a-Si:H."
   A.K. Sinha, G. S. Narayana, S.K. Tripathi and S.C. Agarwal, J. Non-Crystalline Solids, (1998) (communicated).

6. "Determination of potential fluctuations in a-Si:H"
   A. K. Sinha and S. C. Agarwal, Phys. Rev. B, (1998), (communicated).

In Conferences

1. "Metastabilities in undoped a-$Si_{1-x}Ge_x$ alloys."
   A. K. Sinha, P. Agarwal, S. Kumar, S. C. Agarwal, P. N. Dixit, O. S. Panwar, Tanay Seth and R. Bhattacharya, Proceedings of VIIth International Conference on Physics of semiconductor devices(New Delhi), Dec. 14-18, 1993, page 598.

2. Effect of Li doping on sub-gap absorption of hydrogenated amorphous silicon."
   S. K. Tripathi, A. K. Sinha, S. Kumar, and S. C. Agarwal, Proceedings of VIIth International Conference on Physics of semiconductor devices(New Delhi), Dec. 14-18, 1993, page 589.

3. "Temperature dependence of Sub-bandgap absorption in hydrogenated amorphous silicon"
   A. K. Sinha and S. C. Agarwal, Proceedings of VIIIth International Conference on Physics of semiconductor devices(New Delhi), Dec. 11-14, 1995, page 614.

4. "Dual beam CPM studies on Li doped a-Si:H,"
   A.K. Sinha, G. S. Narayana, S.K. Tripathi and S.C. Agarwal, Solid State Physics Symposium(DAE)-1996, IACS, Calcutta(Dec. 27-31, 1995) page 216.

5. "Bulk and surface states in a-Si:H."
A.K. Sinha, S.K. Tripathi, G. S. Narayana and S.C. Agarwal, Solid State Physics Symposium(DAE)-1996, BARC, Mumbai(Dec. 27-31, 1996) page 216

6. "Thermal Stress in Diamond films deposited by oxyacetylene flame."
G. S. Narayana, S.K. Tripathi, A.K. Sinha and S.C. Agarwal, First Meeting on "CVD diamond and diamond like carbon thin films and coatings, 10 Jan 1997, Physics department, IIT Delhi.

7. "Transport properties of a-Si:H: a theoretical approach."
A. K. Sinha and S. C. Agarwal, Proceedings of the International conference on 'The Physics of Disordered Materials', University of Rajasthan, Jaipur, Jan. 27-29, 1997, page 180.

8. "Density of surface states in lithium doped a-Si:H."
A.K. Sinha, G. S. Narayana, S.K. Tripathi and S.C. Agarwal, Proceedings of the International conference on 'The Physics of Disordered Materials', University of Rajasthan, Jaipur, Jan. 27-29, 1997, page 193.

9. "Sub-gap absorption in thin films of $Ge_{20}Se_{80-x}As_x$ using PDS."
A.K. Sinha, P. K. Dwivedi, S.K. Tripathi, S. Kumar and S.C. Agarwal, Solid State Physics Symposium(DAE)-1997, Cochin University of Science and Technology(Dec. 27-31, 1997).

10. "Residual Stress in diamond films using Raman spectroscopy."
G. S. Narayana, S.K. Tripathi, A.K. Sinha and S.C. Agarwal, National Symposium on Recent Trends in Fullerene Research(DMSRDE, Dec 1-2, 1997) Kanpur.

A 131096

Date Slip

This book is to be returned on the date last stamped.
